

# **Ocean of Sound: Underwater gliders observing the oceanic environment**

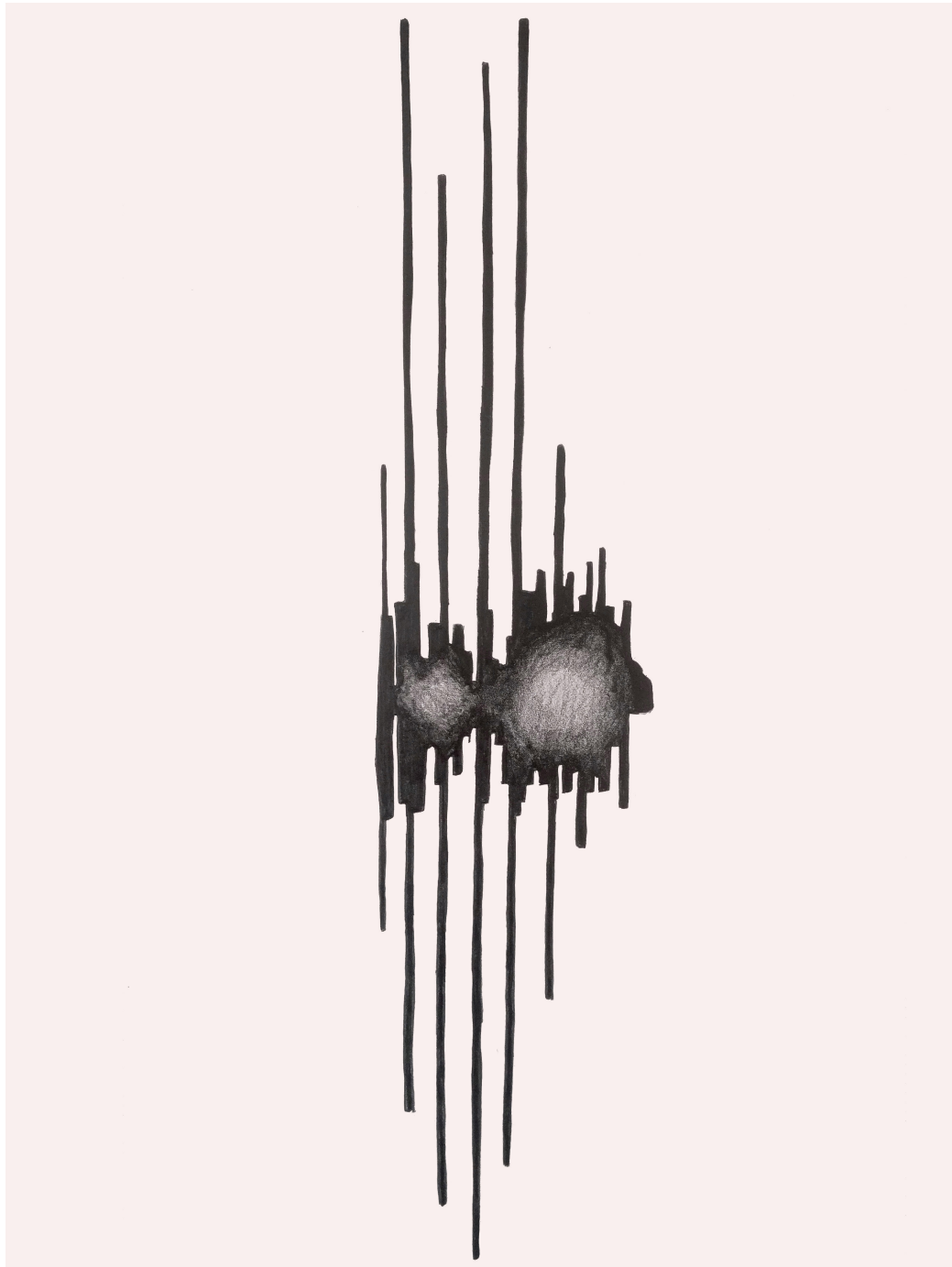
A thesis submitted to the School of Environmental Sciences of the  
University of East Anglia in partial fulfilment of the requirements for the  
degree of Doctor of Philosophy

By Pierre Cauchy

February 2021

© The author 2021 . Open Access under Creative Commons by Attribution Licence. Use, distribution and reproduction are unrestricted. Authors and original publication must be credited.





Pencil on paper

*Pod of Sperm Whales*

by Holly Drewett



# Abstract

Ocean gliders play an increasingly important role in the Global Ocean Observing System. They are now routinely used to monitor the ocean, along repeated transect lines from the coast to the open ocean, in remote locations and during severe weather events. They offer persistent presence at sea, collecting high-resolution scientific measurements during months- to year-long missions and over thousands of kilometres. The ocean glider community continuously develops new sensors, new navigation capabilities and new usage for underwater gliders, increasing their observation range.

This thesis investigates the opportunity offered by addition of passive acoustic monitoring (PAM) capability on ocean gliders and the associated technical challenges. Ocean gliders' specificities, such as quiet propulsion, low speed and vertical profiling make them highly suitable for PAM applications. Ocean gliders were equipped with PAM systems during 12 missions in different conditions, in polar regions, in open ocean remote locations and along routine coastal transect lines. This thesis reviews the currently available PAM glider solutions, identifies technical challenges and desirable developments and presents pathways to improved scientific PAM glider observations. Intense ocean glider presence in the northwestern Mediterranean basin provided an experimental framework to demonstrate the ability to collect valuable scientific information from PAM glider surveys. Wind speed measurements obtained from glider-borne acoustic recordings, up to  $20 \text{ m s}^{-1}$ , colocated with collection of oceanographic profiles, can improve air-sea interaction studies. Sperm whale acoustic activity detected on PAM glider recordings provides information on population distribution and behaviour along the glider tracks. Wide addition of PAM systems on the ocean glider fleet would benefit for its global time and space coverage, enabling long-term observations in key areas, critical for conservation, monitoring of anthropogenic pressure and assessment of ecosystems health.



## **Access Condition and Agreement**

Each deposit in UEA Digital Repository is protected by copyright and other intellectual property rights, and duplication or sale of all or part of any of the Data Collections is not permitted, except that material may be duplicated by you for your research use or for educational purposes in electronic or print form. You must obtain permission from the copyright holder, usually the author, for any other use. Exceptions only apply where a deposit may be explicitly provided under a stated licence, such as a Creative Commons licence or Open Government licence.

Electronic or print copies may not be offered, whether for sale or otherwise to anyone, unless explicitly stated under a Creative Commons or Open Government license. Unauthorised reproduction, editing or reformatting for resale purposes is explicitly prohibited (except where approved by the copyright holder themselves) and UEA reserves the right to take immediate 'take down' action on behalf of the copyright and/or rights holder if this Access condition of the UEA Digital Repository is breached. Any material in this database has been supplied on the understanding that it is copyright material and that no quotation from the material may be published without proper acknowledgement.

# Acknowledgements

First of all, I would like to thank Karen Heywood for offering me the opportunity to carry out this project, for her constant availability during these years, and for gathering a great team of supervisors, Denise Risch, Bastien Queste and Nathan Merchant, supporting, motivating and patient.

I would also like to thank all the people I met during this journey, who made me enjoy it: The UEA glider group, COAS and ENV for contributing to a great research environment and providing exciting and entertaining coffee break chats. Marcos Cobas and Gareth Lee for making things happen, for always taking the time to try and strap a last minute hydrophone on a busy glider. Bastien, for the friendly supervision, the honest translations and for helping me settle at UEA and in Norwich. Marina, of course, for sending me to Antarctica, a fantastic break before the writing effort. Ange and her Wednesday Posses, with special mention to Jan and Rich for always leading the way. Nans, Ben and Bastien for the french-speaking gastronomic dinners. Marta and Rich for the intermittent but always enjoyable company at 55.

My friends and colleagues at LOCEAN, where it all started. Pierre Testor, for introducing me to the glider community and supporting me since then. My 5<sup>th</sup> floor office friends, Karine, Laurène, Sara & Jérôme. My climbing buddies Rémy, Jérôme, Vincent, Seb, Anthony, Joan and Sarah. My sailing crew, the famous "L'équipage pour". Casimir, Jérôme and Guillaume for the endless wine/beer tasting nights. My friends and colleagues at CEFREM, especially the François Bourrin Lab. My friends from ALSEAMAR, may I end up working with your gliders. All the PhD students I have seen struggling in the past 15 years, thinking I would avoid this effort. "Les sumos de satan et autres collègues Marseillais". Kerem, always available for a quick acoustic lesson. All of those who said they would come and visit me in Norwich. Jérôme, who actually did.

Finally, I would like to thank my parents and family, for doing their best to understand my job, following my adventures from the distance and even reading my papers! My grandfather François, who showed me no one is ever too old to start a PhD.

Thank you Suzanne, bien sûr, for the always positive coaching and support, for making exciting plans and for James, hardest deadline ever, who will be here soon.



# Contents

	iii
<b>Abstract</b>	<b>v</b>
<b>Acknowledgements</b>	<b>vii</b>
<b>1 Introduction</b>	<b>1</b>
1.1 Ocean monitoring . . . . .	1
1.2 Underwater acoustics . . . . .	2
1.2.1 Physics of underwater sounds . . . . .	2
1.2.2 Applications . . . . .	5
1.2.3 Sources of sounds . . . . .	7
1.3 Ocean observing platforms . . . . .	9
1.3.1 Oceanographic research vessels . . . . .	9
1.3.2 Fixed-point observatories . . . . .	10
1.3.3 Profiling floats . . . . .	12
1.3.4 Ocean gliders . . . . .	13
1.3.5 Other marine autonomous systems . . . . .	15
1.4 Aim of the thesis . . . . .	16
<b>2 Wind speed measured from underwater gliders using passive acoustics</b>	<b>19</b>
2.1 Abstract . . . . .	19
2.2 Introduction . . . . .	20
2.3 Instrumentation and field measurements . . . . .	24
2.4 Acoustic data sampling and pre-processing procedures . . . . .	28
2.5 Wind speed derivation . . . . .	31

2.5.1	Wind speed derivation model . . . . .	31
2.5.2	Performance of the wind speed derivation model . . . . .	35
2.6	Application to other glider campaigns and implications . . . . .	36
2.7	Discussion . . . . .	40
2.8	Conclusion . . . . .	42

**3 Sperm whale presence observed using passive acoustic monitoring from gliders of opportunity 43**

3.1	Abstract . . . . .	43
3.2	Introduction . . . . .	44
3.3	Materials and Methods . . . . .	46
3.3.1	Instrumentation and field operations . . . . .	46
3.3.2	Acoustic data sampling and processing procedure . . . . .	49
3.3.3	Estimation of the mixed layer depth . . . . .	53
3.3.4	Definition of detection ratios . . . . .	54
3.3.5	Statistical analysis . . . . .	55
3.3.6	Glider mission SoS . . . . .	55
3.4	Results . . . . .	56
3.4.1	Opportunistic observations . . . . .	56
3.4.2	Repeated glider transects . . . . .	58
3.4.3	Temporal patterns . . . . .	59
3.4.4	Large scale monitoring . . . . .	60
3.4.5	Collocated oceanographic measurements . . . . .	60
3.4.6	Observation from varying depth . . . . .	61
3.5	Discussion . . . . .	63
3.5.1	Sperm whale observation from opportunistic glider surveys . . . . .	63
3.5.2	Collocated oceanographic measurements . . . . .	63
3.5.3	Spatial distribution . . . . .	64
3.5.4	Circadian pattern . . . . .	64
3.5.5	Seasonal to inter-annual variations . . . . .	65
3.5.6	Depth distribution . . . . .	66
3.5.7	Sampling strategy . . . . .	66

3.5.8	Acoustic detection . . . . .	67
3.6	Conclusion . . . . .	67
<b>4</b>	<b>Use of ocean gliders for passive acoustic monitoring applications</b>	<b>69</b>
4.1	Platform noise, limitations . . . . .	69
4.1.1	Profiling phases . . . . .	70
4.1.2	Apogee . . . . .	75
4.1.3	Surface . . . . .	75
4.1.4	Influence of profiling depth . . . . .	76
4.2	PAM systems . . . . .	77
4.2.1	Self-contained PAM systems . . . . .	77
4.2.2	Integrated PAM systems . . . . .	81
4.2.3	Desirable hardware developments . . . . .	82
<b>5</b>	<b>Conclusion</b>	<b>85</b>
5.1	Lessons learnt - Going further . . . . .	85
5.1.1	Weather observation . . . . .	85
5.1.2	Marine life monitoring . . . . .	87
5.2	Absolute sound level measurements . . . . .	88
5.2.1	Challenge . . . . .	88
5.2.2	Outcomes . . . . .	89
5.3	Take home messages . . . . .	90
5.3.1	Recommendations for a first PAM glider deployment . . . . .	90
5.3.2	Key successes of the project . . . . .	91
<b>A</b>	<b>Supplementary Material</b>	<b>93</b>



# Chapter 1

## Introduction

### 1.1 Ocean monitoring

Oceans are a key component of the global earth system, playing a central role in many aspects of our society. They regulate the climate and weather systems, absorbing heat and CO<sub>2</sub> from the atmosphere, and provide resources critical to many industrial activities such as shipping, energy, mineral extraction and aquaculture (Hoegh-Guldberg *et al.*, 0014). They host complex ecosystems and a large biodiversity, supporting fisheries and tourism (Hoegh-Guldberg *et al.*, 0014). Oceans are also under threat from permanent and global anthropogenic pressure (e.g. carbon emissions, global warming, pollution, fisheries, shipping, noise) (Hoegh-Guldberg *et al.*, 0014; Van der Graaf *et al.*, 2012). Sustainable management of the oceanic environment is considered critical to address some of the most pressing global challenges, such as climate change, poverty and food accessibility (Van der Graaf *et al.*, 2012). Accurate and timely information about marine resources and ecosystems is needed, to achieve good environmental status (Van der Graaf *et al.*, 2012).

The Global Ocean Observing System ([www.goosocean.org](http://www.goosocean.org)) was established in 1991 to develop and coordinate ocean observations for effective and sustainable management of the oceans (IOC, 2019), providing an operational framework with global coverage combining in-situ observations carried out from ships, fixed point observing systems and autonomous platforms (Fig. 1.1). In the first decades, it was targeted at supporting climate science and operational forecast systems, providing observations of oceanographic parameters describing ocean circulation, heat and carbon transfer and primary production.

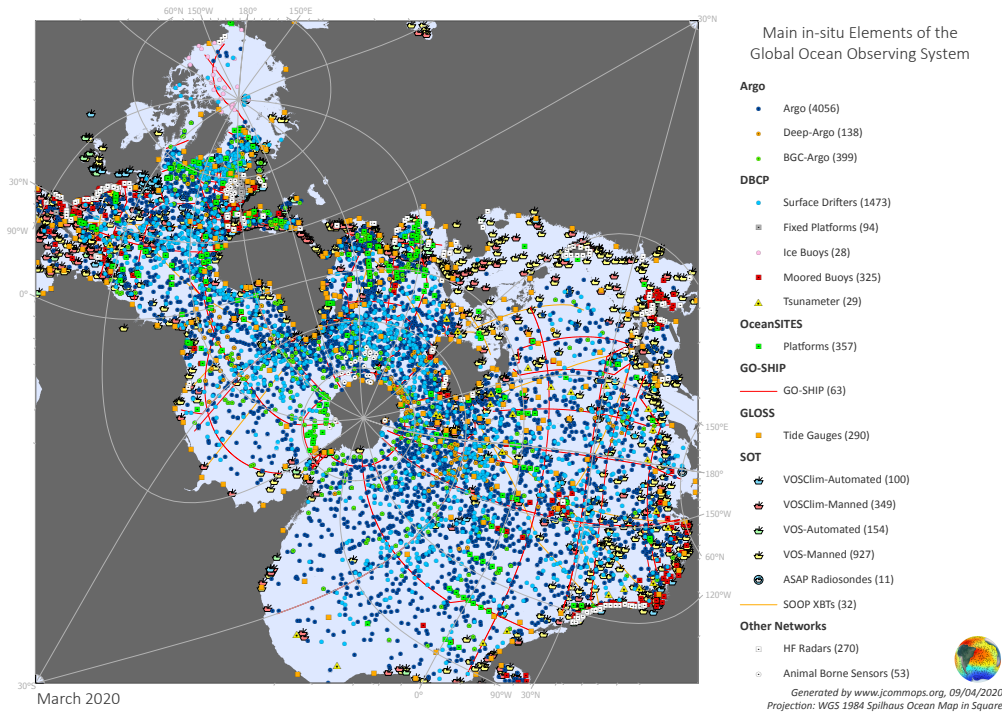


**Figure 1.1:** Spatial coverage of the Global Ocean Observing System (GOOS) in March 2020. WGS 1984 Spilhaus projection. From [www.jcommops.org](http://www.jcommops.org), accessed 9<sup>th</sup> Apr 2020.

In the past decade, growing concerns about the health of the oceans have led to widening of the observation efforts to better monitor ecosystems, biodiversity and anthropogenic pressures (IOC, 2019), now including the use of passive acoustic monitoring techniques (Van der Graaf *et al.*, 2012).

## 1.2 Underwater acoustics

### 1.2.1 Physics of underwater sounds

#### 1.2.1.1 Sonar equation

Propagation of a signal emitted from a source at source level  $SL$  and received at level  $RL$  can be simply summarised using the sonar equation (all units are in dB):

$$RL = SL - TL, \quad (1.1)$$

where  $TL$  is the transmission loss during the sound travel, from the source to the receiver.  $TL$  is the sum of multiple effects contributing to sound attenuation:

$$TL = L_{GS} + L_{VA} + L_R. \quad (1.2)$$

$L_{GS}$  represents the loss due to geometrical spreading of the signal. The most common example of geometrical spreading in the ocean is spherical spreading, a sound propagating uniformly in all directions away from a point source. The sound level received in one specific direction decreases by  $20\log(r)$  with distance  $r$ . Volume attenuation,  $L_{VA}$ , represents the loss when travelling through the medium. It depends on the physical properties of the medium and the distance travelled from the source to the receiver. If the path from the source to the receiver includes reflections,  $L_R$  accounts for the reflexion loss by scattering or attenuation, dependent respectively on the roughness and reflectivity of the interface.

The opportunity to detect a sound depends on the signal to noise ratio,  $SNR$ , the difference between the received level,  $RL$ , and the noise level  $N$ :

$$SNR = RL - N, \quad (1.3)$$

where  $N$  is the combination of the instrument noise  $N_i$  and the ambient noise at the receiver's location  $N_a$ :

$$N = 10\log(10^{\frac{N_i}{10}} + 10^{\frac{N_a}{10}}). \quad (1.4)$$

A signal is considered detectable when its  $SNR$  is greater than a detection threshold. Loud sounds in low background noise have a high  $SNR$  and are easy to detect. Presence of sources of noise can introduce a masking effect by increasing  $N_a$ , reducing  $SNR$  and the detectability of the targeted signal. For detection of low  $SNR$  signal, using an array of hydrophones allows enhancement of the  $SNR$  through a beamforming process, using the directivity of the array to enhance sounds received from the direction of the source. This array gain,  $AG$  is added to the  $SNR$ :

$$SNR_{Array} = RL - N + AG. \quad (1.5)$$

The performance (e.g. sensitivity, directivity, gain, resolution) of such arrays are dependent on the size of the array and the geometrical arrangement of the hydrophones. Best results are obtained using complex arrays of controlled shape and large dimensions, with a large number of closely spaced hydrophones (Butler and Sherman, 2016).

### 1.2.1.2 Absorption

Volume attenuation in the ocean depends on the length of the path  $r$  (in m) and the absorption of seawater,  $\alpha$  (in dB km<sup>-1</sup>). The absorption of sound in seawater is the combined effects of pure water viscosity and chemical relaxation of boric acid and magnesium sulfate (Francois and Garrison, 1982):

$$\alpha = \frac{A_1 f_1 f^2}{f_1^2 + f^2} + \frac{A_2 f_2 f^2}{f_2^2 + f^2} + A_3 f_3 f^2, \quad (1.6)$$

where  $A_1$  and  $A_2$  (in dB km<sup>-1</sup> kHz<sup>-1</sup>) are the relaxation coefficients and  $f_1$  and  $f_2$  (in kHz) the relaxation frequencies of boric acid and magnesium sulfate respectively and  $A_3$  (in dB km<sup>-1</sup> kHz<sup>-2</sup>) the absorption coefficient of pure water. The coefficients  $A_1$ ,  $A_2$  and  $A_3$ , dependent on temperature, salinity, pH and pressure, have been empirically determined (Francois and Garrison, 1982). The absorption of sound in seawater increases with frequency, as shown in Fig. 1.2, letting low frequency sounds travel on far greater distances than high frequency sounds. As a consequence, sperm whale echolocation clicks ( $\sim 5$  kHz,  $\sim 180$  dB re 1  $\mu$ Pa @ 1 m) cannot be detected further than 20 km away, whereas blue whale calls ( $\sim 20$  Hz,  $\sim 180$  dB re 1  $\mu$ Pa @ 1 m) have been shown to propagate over hundreds of kilometres.

### 1.2.1.3 Refraction

Sound velocity in the ocean varies from 1450 to 1550 m s<sup>-1</sup>, affected by pressure, temperature and salinity (Kuperman, 2001):

$$c = 14449.2 + 4.6T - 0.055T^2 + 0.00029T^3 + (1.34 - 0.01T)(S - 35) + 0.016z, \quad (1.7)$$

where  $c$  (in m s<sup>-1</sup>) is the sound velocity,  $T$  (in °C) the temperature,  $S$  the salinity and  $z$  (in m) the depth. The vertical gradient of sound velocity, called sound velocity profile, varies

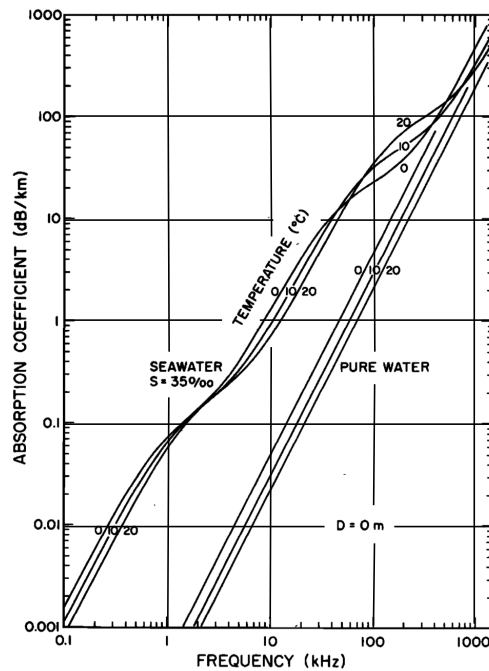


**Figure 1.2:** Seawater absorption for frequencies from 100 Hz to 1 MHz, at  $S = 35$  psu,  $T = 0, 10$  and  $20$  °C and  $pH = 8$ . Adapted from (Francois and Garrison, 1982)

with location and seasons, due to variations of the water column properties (Fig. 1.3).

Sounds travelling through such sound velocity gradients are refracted, following Snell's Law, causing sounds to propagate along complex paths (Fig. 1.4). Sounds emitted at the surface in A radiate at depth following divergent trajectories. Sounds emitted in B are focused along the mid-water column sound velocity minimum acting as a waveguide, called SOFAR channel. They propagate without reflections and with reduced loss due to geometrical spreading, enhancing the sound propagation range (Northrop and Colborn, 1975).

### 1.2.2 Applications

Underwater acoustic technologies have been developed from World War I, with the increasing importance of submarine warfare. Active sonar technology analyses propagation and reflections of an emitted sound to detect and identify targets (e.g. submarine, mine). Active acoustic technologies are now commonly used for ocean monitoring applications. Echo-sounders are used for seabed imaging, fish and plankton detection and biomass estimation (Benoit-Bird and Lawson, 2016). Acoustic doppler current profilers are used for currents (Visbeck, 2002) and turbidity profiling (Many *et al.*, 2018). Acoustic tomography

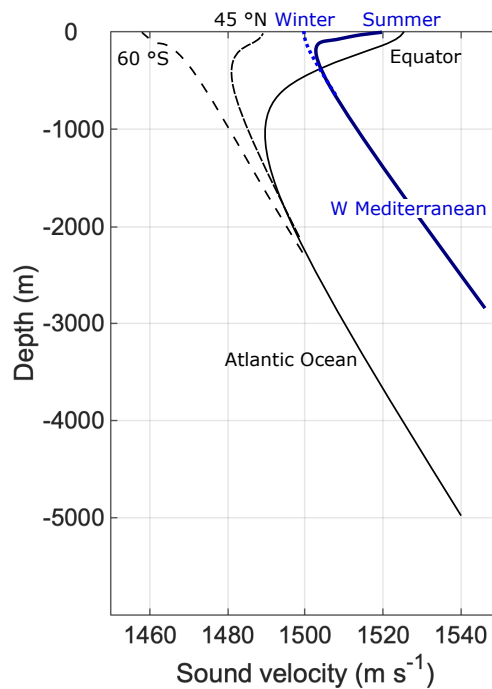


**Figure 1.3:** Usual sound velocity profiles at 60 °S, equator and 45 °N in the Atlantic and during winter and summer in the western Mediterranean Sea. Adapted from (Munk *et al.*, 1995; Salon *et al.*, 2003)

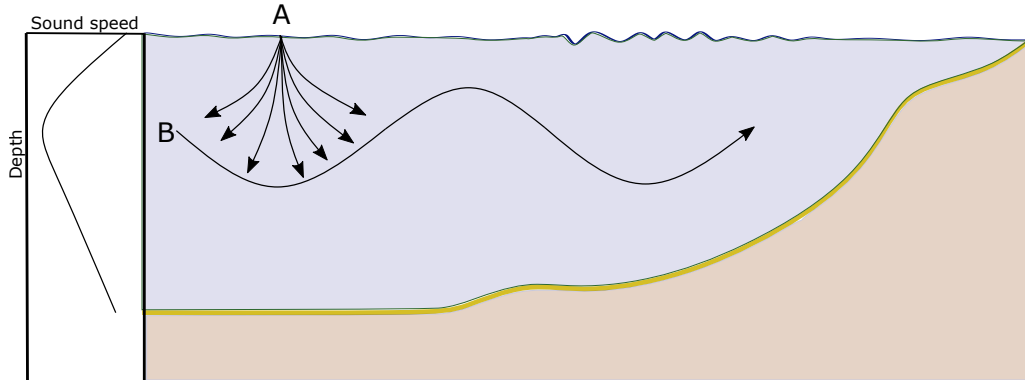


**Figure 1.4:** Sound propagation paths, radiating from the surface (A) and emitted near the deep sound velocity minimum (B).

provides measurements of the ocean heat content on a very large scale (Malanotte-Rizzoli, 1985). Acoustic modems are used for underwater communication and acoustic networks are used for underwater positioning (Milne, 1983).

Passive sonar technology detects and identifies submarines and ships by simply recording and analysing their own engine and propeller noise. The strategic advantage of passive acoustic technology for military applications is that it is impossible to detect. Passive acoustic monitoring (hereafter PAM), as simply recording and analysing soundscapes to

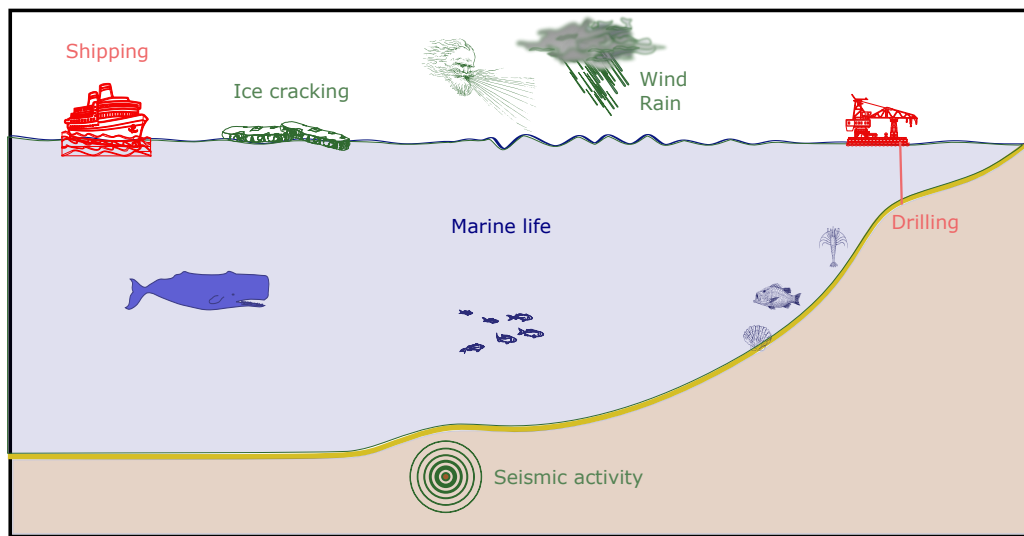


**Figure 1.5:** Schematic summarising sound sources contributing to the underwater soundscape. Sources contributing to anthropophony, biophony and geophony are respectively represented in red, blue and green.

collect information about sound sources, is a powerful and non-invasive way to monitor the ocean. Analysis of the underwater soundscape allows detection, identification and localisation of a wide variety of sound sources, therefore observation and monitoring of the associated activities summarised in Figure 1.5. Whether they purposefully emit sounds or not, most marine anthropic and biological activities, as well as some natural processes, generate sounds (Fig. 1.5), respectively classified as anthropophony, biophony and geophony (Krause, 2008).

### 1.2.3 Sources of sounds

#### 1.2.3.1 Anthropophony

Anthrophony is composed of sound contributions from industrial, military and leisure activities such as shipping (Merchant *et al.*, 2012), seismic surveys (Guan *et al.*, 2015; Guerra *et al.*, 2011; Nowacek *et al.*, 2015), pile driving (Bailey *et al.*, 2010; Thompson *et al.*, 2013), anti-submarine warfare (Ricks *et al.*, 2012), seabed characterisation (Harrison and Simons, 2002; Quijano *et al.*, 2012), active sonar (Dolman *et al.*, 2011) and whale watching (Erbe, 2002), causing anthropogenic underwater noise pollution (Williams *et al.*, 2015; Haver *et al.*, 2017; Merchant *et al.*, 2018). Most marine animals rely on acoustics for navigation, foraging, mating and communicating (Simmonds *et al.*, 2014). Anthropogenic noise is now identified as a source of pressure of anthropic activities on the

oceanic environment (Van der Graaf *et al.*, 2012), widely affecting marine life. Two descriptors have been defined in the European Marine Strategy Framework Directive Good Environmental Status (MSFD-GES), to monitor anthropic pressure on the oceans through noise. Descriptor 11.1.1 focuses on impulsive noise, identified as short and intense sounds and likely to cause serious adverse impacts on the marine environment, ranging from avoidance to death. Potentially lethal effects of impulsive noise on cetacean populations, such as seismic prospection airguns and military sonars causing stranding events, are publicly known (Weilgart, 2007). Descriptor 11.2.1 focuses on ambient noise, mostly due to shipping and likely to cause physiological and behavioural stress. Anthropogenic noise pollution affects all types of animals, reducing their ability to communicate and hunt or avoid predators, modifying soundscapes they rely on for habitat selection and inducing stress. Marine mammals show vigilance, escaping and avoidance behaviours (Tyack, 2008). Fish show behaviour change, such as habitat avoidance and spawning and migration disruption (Hawkins *et al.*, 2014). Knowledge gaps remain regarding our understanding of the effects of noise on invertebrates (Hawkins *et al.*, 2014), but multiple studies have shown effects on marine invertebrates, from scallop larvae to giant squid (Aguilar de Soto, 2016).

### 1.2.3.2 Biophony

Biophony is composed of various sounds emitted by marine life. Toothed whales produce echolocation clicks at high frequency (5 – 150 kHz) to sense their surroundings and find and track prey (Jensen *et al.*, 2018). The most powerful, from sperm whales, can be detected as far as 20 km away (Miller and Miller, 2018). Sperm whales (Weilgart and Whitehead, 1993) and porpoises (Clausen *et al.*, 2011) communicate using sequences of clicks, other toothed whales using whistles (Weilgart and Whitehead, 1990; Riesch *et al.*, 2008). Baleen whales communicate using calls and songs (Watkins *et al.*, 2000; Širović *et al.*, 2004). Blue whale low frequency calls (~20 Hz) can be detected several hundreds of kilometres away (Stafford *et al.*, 1998). Seals communicate using calls (Cleator *et al.*, 1989; Moors and Terhune, 2004; Rosson and Terhune, 2009). Some species of fish produce sounds using their swim bladder or rubbing skeletal elements (Parmentier and Fine, 2016; Bolgan *et al.*, 2020). Invertebrates mainly produce sounds from rubbing,

tapping or clacking together calcareous parts (Coquereau *et al.*, 2016). Many species are not purposefully acoustically active, but make noise when foraging, such as snapping shrimp, spider crab and sea urchin or moving, such as sea urchin and scallops (Di Iorio *et al.*, 2012; Coquereau *et al.*, 2016).

PAM techniques allow estimation of whale population density (Marques *et al.*, 2013), population abundance (Lewis *et al.*, 2018), seasonality (Stafford *et al.*, 2007) and behaviour (Wahlberg, 2002; Miller and Miller, 2018). Seal calls present individual signatures enabling individual identification (Charrier *et al.*, 2017). Analysis of sounds from fish (Bolgan *et al.*, 2018; Di Iorio *et al.*, 2018), shrimps (Everest, 1947; Johnson *et al.*, 1947) and sea urchins (Radford *et al.*, 2008a) provides valuable information about habitats and ecosystems health (Radford *et al.*, 2008b; Harris *et al.*, 2016).

### 1.2.3.3 Geophony

Geophony is composed of sounds generated by physical processes occurring naturally. Wind, rainfall and breaking waves generate surface noise that radiates as deep as 6000 m in the ocean (Barclay and Buckingham, 2013) and dominates underwater ambient noise in the 500 Hz – 50 kHz frequency range (Wenz, 1962; Vagle *et al.*, 1990; Black *et al.*, 1997). Wind noise during storms significantly raises the background noise, affecting animal communication (Ladich, 2013) and sonar performance (Ainslie, 2010). Analysis of the underwater ambient noise provides information about sea surface wind speed and rainfall rate (Vagle *et al.*, 1990; Nystuen, 1996). Seismic activity generates low frequency sounds that can be detected over thousands of kilometres away (McGuire *et al.*, 2005) and can disturb marine life (Gallo-Reynoso *et al.*, 2011). Submarine volcanoes (Matsumoto *et al.*, 2011), large ice shelf calving events (Dziak *et al.*, 2019) and turbidity currents (Hatcher, 2017) can be monitored through their contribution to the underwater soundscape.

## 1.3 Ocean observing platforms

### 1.3.1 Oceanographic research vessels

Oceanographic research vessels offer high spatial resolution observations. They can carry unrestricted range of instruments without weight, size or energy constraints. Human

presence onboard allows for real-time adaptation of the mission to the conditions (e.g. weather, ice conditions, scientific observations) and operation of non-automated instruments (e.g. collection of water, biological and litter samples, filtration, chemical reactions, visual surveys). For obvious economic and logistical reasons, ship-based observations are mainly limited to large scale hydrographic sections, with a yearly to decadal repeat rate, such as the Global Ocean Ship-based Hydrographic Investigations Program (GO-SHIP), or smaller scale process studies, such as the yearly snapshot of the NW Mediterranean Sea provided by the MOOSE oceanographic cruise ([www.moose-network.fr](http://www.moose-network.fr)).

PAM techniques are commonly used from ships, using PAM systems towed behind the ship to limit engine, propeller and hull-radiated noise (Lasky *et al.*, 2004). Towed systems are powered from the ship and provide a real-time data stream that can be analysed onboard by acoustic experts. Multiple sensors can be used to enable source localisation and tracking (Thode, 2004) and complex hydrophone arrays can be used, up to 1000 m long, forming high-sensitivity antennas to detect weak signals and collect robust source localisation information (Lemon, 2004).

Towed PAM systems are routinely used for military application, such as anti-submarine warfare (Lemon, 2004), and for monitoring of cetacean population. The example of the ACCOBAMS Survey Initiative ([www.accobams.org](http://www.accobams.org)) illustrates the use of towed PAM surveys for cetacean population abundance, density and distribution estimation. Combined towed PAM surveys and air- and ship-borne visual surveys, provided a snapshot of the cetacean population in June – July 2018 over the Mediterranean Sea. Such large-scale survey effort is the result of unprecedented international collaboration and funding. At the time of writing, funding for future repetition of this survey is not yet secured (Accobams, 2019).

### 1.3.2 Fixed-point observatories

Fixed-point observatories are composed of collections of sensors mounted on a bottom lander on the seabed, on a mooring line at various depths in the water column or on an instrumented buoy at the surface. They offer oceanographic measurements at a high temporal resolution over long periods. Arrays of moorings, such as the Global Tropical Moored Buoy Array monitoring the tropical oceans around the globe for about 30 years

(McPhaden *et al.*, 2010), provide sustained real-time observations allowing for monitoring, understanding and prediction of the impacts of ocean variability on weather events. Sophisticated fixed-point observatories are costly and require complicated maintenance operations that limit the number of components available in an array. Therefore, such arrays of moorings are limited to a very coarse spatial resolution. Moored systems can be damaged by storms, vandalism and fishing activities, with possible loss of instruments and data.

A wide range of autonomous recorders is commercially available, for moored PAM applications, offering long-term (months to years) observation capability. Moored PAM systems are commonly used for underwater noise monitoring (Merchant *et al.*, 2016) and observation of cetacean presence (Miller and Miller, 2018). They are particularly adapted to monitor evolutions of the soundscape (Erbe *et al.*, 2015). Multiple PAM systems can be deployed to allow source localisation and tracking, critical for monitoring animal behaviour (e.g. diving dynamics, foraging behaviour, swimming) (Wiggins *et al.*, 2012). Data from autonomous recorders are only accessed at the end of the deployment, when the PAM system is recovered. There are examples of cabled observatories, usually developed for unique applications such as the deep sea neutrino telescope at ANTARES in the northwestern Mediterranean Sea (Ageron *et al.*, 2011) and the NEPTUNE observatory, built from decommissioned submarine telecommunication cables, to monitor a critical seismic activity hotspot, off the west coast of Canada (Barnes *et al.*, 2010). Cabled PAM systems provide sustained, continuous, real-time observations with high temporal resolution, enabling inter-seasonal and annual trends and daily patterns in cetacean populations and anthropogenic noise to be studied (André *et al.*, 2011, 2017) and to explore acoustic activity of deep sea marine life (Wall *et al.*, 2014). Such observatories are unfortunately very complex and expensive to maintain, therefore remain very rare. Interaction with waves and currents can generate noise, through vibration and movement of the mooring's components (e.g. rope, chain). For PAM applications, specific mooring design can be used to significantly reduce such mooring noise. In strong currents, flow noise can be observed, affecting measurements in the 1 – 100 Hz frequency band (Erbe *et al.*, 2015).

### 1.3.3 Profiling floats

Profiling floats were developed in the 1950s (Davis *et al.*, 1992, 2001), to carry out ocean observations during long autonomous missions. They consist of a 1 – 2 m long cylindrical body containing batteries, sensors and a buoyancy engine. The buoyancy engine, by pumping air or oil into and out of an external swim bladder, allows variations of the float's average density from negative to positive values inducing vertical motion through the water column, from the surface to a predefined depth (Fig. 1.6). They follow subsurface currents at their predefined parking depth and collect recurrent temperature and salinity measurement along vertical profiles (Davis *et al.*, 2001). Observations from profiling floats are coordinated by the Argo Program, implemented in 1999, and now a significant part of the Global Ocean Observing System. As defined by the Argo Program specifications, profiling floats drift at a parking depth of 1000 m and collect hydrographic temperature and salinity profiles every 10 days, with an expected lifetime of 4 years (Roemmich *et al.*, 2019). The Argo Program has been providing sustained ocean observation for 20 years, from currently (March 2020) ~4000 floats transmitting temperature and salinity profile in real time. The Argo Program is now developing its observation capabilities, extending to full ocean depth (~6000 m) and expanding the sensor suite (e.g. biogeochemistry, optical sensors, passive acoustics) (Roemmich *et al.*, 2019). Location of drifting platforms is dependent on the currents only, resulting in inhomogeneous coverage and too sparse observation in some areas (e.g. western boundary currents, shelf-open ocean interface).

PAM systems have been integrated on profiling floats for monitoring of seismic activity (Sukhovich *et al.*, 2015), observing the effects of monsoon in the Bay of Bengal through wind and rain measurements (Riser *et al.*, 2008) and beaked whale tracking (Matsumoto *et al.*, 2013). At the time of writing, there is one commercially available system, PABLO ([www.metocean.com](http://www.metocean.com)) not mentioned in the peer reviewed literature. Profiling floats are particularly adapted to PAM applications, emitting no engine nor flow noise. However, profiling floats are usually not recovered at the end of their life, due to having drifted to remote locations, which prevents access to raw acoustic data.

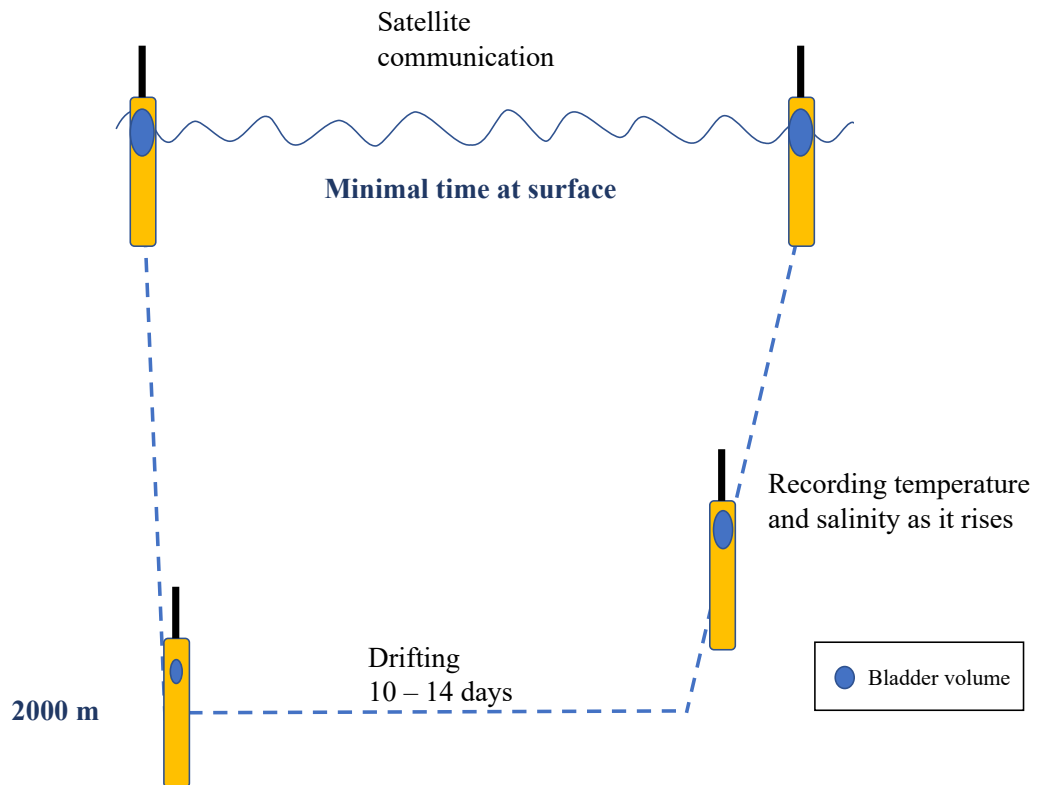
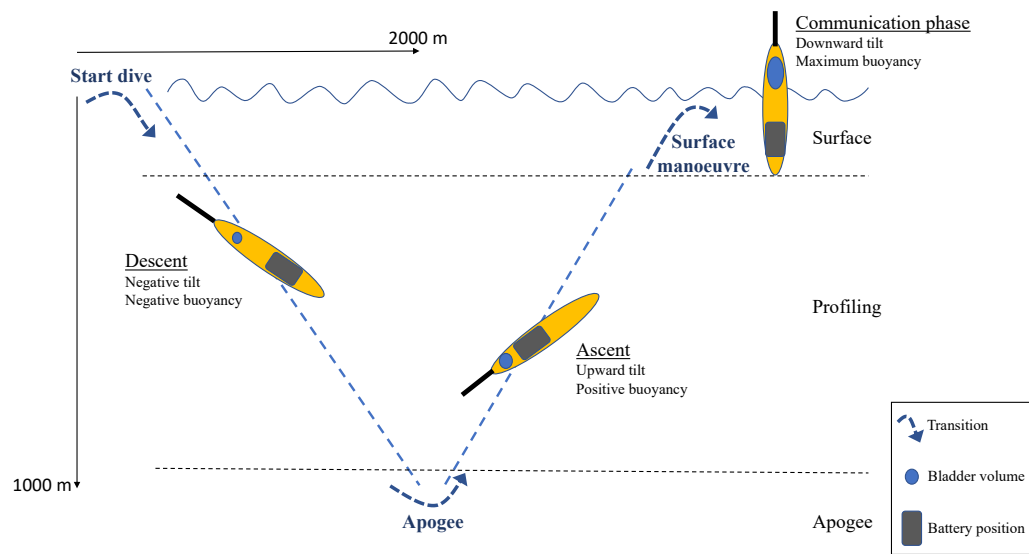


Figure 1.6: ARGO float cycle, reproduced from (Roemmich *et al.*, 2019)

### 1.3.4 Ocean gliders

Ocean gliders have similar profiling ability to that of profiling floats, with additional navigation capabilities. They use a buoyancy engine to move vertically through the water column, from the surface to 1000 m deep. Fixed wings, fins and a specifically profiled body convert their vertical velocity ( $\sim 0.1 \text{ m s}^{-1}$ ) into horizontal velocity ( $\sim 0.2 \text{ m s}^{-1}$ ), following V-shape pseudo-vertical profiles (Fig. 1.7). Internal battery displacements control pitch and roll changes. Roll adjustments or a rudder are used for steering and a compass for underwater navigation. They perform successive dives along a predefined trajectory, using satellite positioning and communication when at surface to transfer data back to shore and update their mission plan (Fig. 1.7). At the time of writing, three types of ocean gliders are commercially available: Seaglider is developed by the University of Washington and commercialised by Hydroid, Slocum is developed by Teledyne and Sea-Explorer is developed by Alseamar. Scripps Institution for Oceanography develops and operates its own glider Spray, that is no longer commercially available. They share similar shape and dimensions, 1.5 – 2 m long, 0.5 – 1 m wingspan, 50 – 60 kg in air (Fig.



**Figure 1.7:** Schematic diagram of an ocean glider dive cycle.

1.8). They are easily handheld, deployed and recovered by two people and from small boats. Their unique propulsion system, necessitating engine effort during short periods at the beginning and end of long effortless profiles, allows ocean gliders to reach great endurance (Rudnick *et al.*, 2004). When performing 1000 m dives, each gliding profile lasts for approximately 2 hours and the glider can reach an overall autonomy of up to a year, covering thousands of kilometres. They collect high resolution profiles ( $\sim 2$  km,  $\sim 2$  h) and can carry a wide range of sensors measuring physical, chemical and biological properties of the water column. Ocean gliders have the demonstrated capacity to fill gaps in the global ocean observing systems (Testor *et al.*, 2019). They can navigate along a pre-defined trajectory to target identified geographical areas where coverage from Argo floats is insufficient (e.g. coastal regions, boundary currents). They provide high-resolution measurements that allow observation of mesoscale (10 – 100 km) processes, difficult to resolve with traditional observing platforms. They are unaffected by storms and are used to provide prediction and observation of tropical storms (Glenn *et al.*, 2016). They can travel near and under ice (Lee *et al.*, 2017).

Ocean gliders are highly suitable for PAM applications. They glide quietly through water, without any propulsion noise; they collect hydrographic profiles, from which sound velocity profiles can be calculated; raw acoustic data can be accessed after recovery of the glider; they can carry one or several hydrophones, offering multiple acoustic monitoring possibilities. Flow noise, generated by turbulent water flow around the glider's hull, is



**Figure 1.8:** From left to right, Slocum glider (taken from [www.auvac.org](http://www.auvac.org)), Seaglider (UEA picture) and SeaExplorer (picture courtesy ALSEAMAR).

of similar magnitude to flow noise observed on moored PAM systems (Dos Santos *et al.*, 2016; Erbe *et al.*, 2015). Ocean gliders have been equipped with custom-built PAM systems and on-board processing capability for near real-time detection of beaked whales (Klinck *et al.*, 2012) and baleen whales (Baumgartner *et al.*, 2013), demonstrating the opportunity to use PAM gliders as a component of operational whale monitoring observatories. Multi-channel systems have been used to demonstrate the ability to track sperm whales (Kusel *et al.*, 2017) and perform tactical maritime surveillance operations (Tesei *et al.*, 2015). Autonomous PAM systems have been successfully attached on gliders, to observe soundscape variability along the glider's track (Wall *et al.*, 2017) and map fish activity along cross-shelf transects in the Gulf of Mexico (Wall *et al.*, 2012). Sensor integration on ocean gliders is challenging, due to drastic limitations in size, weight and power consumption. At the time of writing, glider manufacturers have recently started to provide integrated PAM systems, expensive and with high power consumption, shortening the glider's autonomy. Most PAM glider experiments to date have been carried out with custom-built sensors or externally attached third-party autonomous PAM systems.

### 1.3.5 Other marine autonomous systems

In the last decade, many marine autonomous systems have been developed to improve unmanned ocean observation. They enable ocean monitoring with reduced costs, manpower and pollution, allowing for improved mission safety and increased repeatability. They are not limited by crew safety issues and can therefore operate in remote and dangerous locations (e.g. storms, polar regions, near or under ice). Most of them have not shown any particular advantage for PAM applications, due to reduced autonomy (hours to days) and constant engine and propeller noise. However, new surface vehicles, wind (Saildrone,

Sailbuoy) or wave (Autonaut, Waveglider) propelled, are highly suited for PAM applications. They offer long-range observations similar to ocean gliders and profiling floats (months to years) and reduced platform-generated noise. They benefit from access to solar energy and large payload capacity. Towed PAM systems have been developed specifically to be used on such autonomous surface vehicles. PAM applications from such vehicles are still in their infancy, but highly promising. Some challenges, such as onboard processing and real-time communication of summarised observations, are similar to PAM gliders and PAM profiling floats.

## 1.4 Aim of the thesis

This PhD project: *Sounds in the sea: How can we listen from ocean gliders?* was part of the Next-Generation Unmanned System Science (NEXUSS) Centre for Doctoral Training, which aims at training doctoral students in the development and application of Smart and Autonomous Observation Systems (SAOS) for Environmental Sciences. From the first developments of ocean gliders in the 1990s to their technological maturation in the 2000s, ocean gliders were only used by glider enthusiasts, mostly physical oceanographers, demonstrating their ocean observing capabilities. In the last decade, the reliability and ease of use of ocean gliders as a platform increased. They can now be used as a data collection tool in operational observing systems and by non-specialist scientists, like ships, buoys, moorings and satellites. Ocean gliders also offer the opportunity to host experimental sensors, to develop new usage and ocean monitoring solutions. Acoustic recording from ocean gliders is a recent development, already very promising. This project aimed at investigating and demonstrating new ways of observing the oceanic environment, using PAM gliders. I considered the multidisciplinary aspect of PAM sensors, well known to marine biologists and fairly new to physical oceanographers, as a vector of promotion of glider observations to new scientific communities and a way to broaden the spectrum of glider users and usage.

In Chapter 2, I investigate the opportunity to adapt the WOTAN (Weather observation through ambient noise) technique (Vagle *et al.*, 1990) to vertically profiling ocean gliders. The relationship between wind speed and underwater noise has been known for decades (Vagle *et al.*, 1990) and the ability to infer wind speed from underwater ambient noise

**Table 1.1:** Details of the PAM glider missions, geographic area, type of glider and PAM system used and application of the acoustic data to WOTAN, whale monitoring, soundscape analysis or hardware trial.

Name	Location / Date	Glider	PAM system	Application
MOOSE 4 missions	NW Mediterranean 12/2012 – 04/2013	Slocum	Acousonde +alkaline pack	WOTAN Whale
MED-REP14	NW Mediterranean 06/2014	Seaglider	Integrated PAM	Whale
MASSMO4	N Atlantic 06/2017	Seaglider	Integrated PAM	Trial
Orchestra	Southern Ocean 12/2017 – 01/2018	Seaglider	Acousonde	WOTAN
MASSMO5	N Atlantic 10/2018	Seaglider	Acousonde	Trial
ELO 2 missions	Indian Ocean 01/2019 – 04/2019	Seaglider	Acousonde Integrated PAM	WOTAN
PERLE	E Mediterranean 01/2020 – 03/2020	Seaglider	Acousonde +lithium pack	WOTAN
PROVOCCAR	Southern Ocean 02/2020	Seaglider	Acousonde	Soundscape

has been demonstrated (Nystuen and Ma, 2002). Adapting this technique to glider-borne recordings widens the scope of ocean glider observations. The collection of wind speed measurements, collocated with the usual glider oceanographic profiles, has the potential to significantly improve observation of air-sea interaction processes. In Chapter 3, I investigate the benefits of PAM glider observations for marine biology applications. Sperm whale echolocation clicks can be detected on glider-borne recordings, enabling observation of sperm whale presence and behaviour along the track of the glider. Such observation has the potential to improve monitoring of cetacean populations, increasing the observation effort and providing high spatial-temporal resolution along their track. Many PAM glider experiments were involved in this project, mapped in Figure 1.9 and listed in Table 1.1, generating large amounts of data recorded using different PAM systems, gliders and setups. I review in Chapter 4 the commercially available PAM systems and their desirable future developments, I discuss piloting, sampling and data processing good practices. Chapter 5 summarises the lessons learnt from this project, presents the main challenge identified, pathways to improvement, and tools for successful PAM glider deployments.

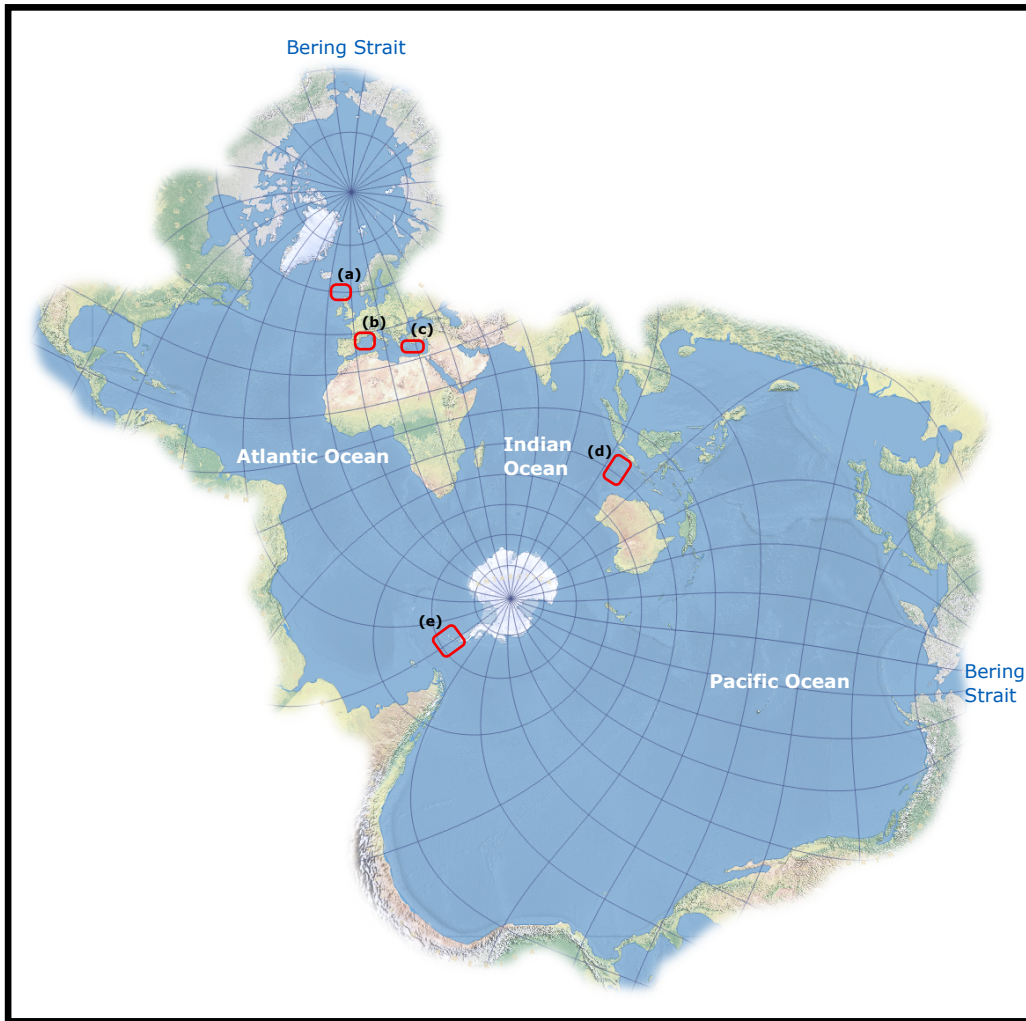


**Figure 1.9:** Areas covered by the glider missions mentioned in this thesis. (a) North Atlantic, (b) Northwestern Mediterranean Sea, (c) Eastern Mediterranean Sea, (d) Tropical Indian Ocean and (e) Southern Ocean – Spilhaus map.

## Chapter 2

# Wind speed measured from underwater gliders using passive acoustics

This section was published in in a peer-reviewed journal prior to the submission of the thesis. No changes have been made but re-formatting in a thesis format.

Cauchy, P., K. J. Heywood, N. D. Merchant, B. Y. Queste, and P. Testor (2018), *Wind Speed Measured from Underwater Gliders Using Passive Acoustics*, *Journal of Atmospheric and Oceanic Technology*, 35(12), 2305–2321. <https://doi.org/10.1175/JTECH-D-17-0209.1>

PC carried out the research and prepared the paper. KJH, NDM, BYQ and PT supported the research, provided feedback on earlier drafts of the paper and approved the final version to be published.

### 2.1 Abstract

Wind speed measurements are needed to understand ocean – atmosphere coupling processes and their effects on climate. Satellite observations provide some spatial and temporal coverage but are lacking adequate calibration, while ship- and mooring-based observations are spatially limited and have technical shortcomings. However, wind-generated

underwater noise can be used to measure wind speed, a method known as Weather Observations Through Ambient Noise (WOTAN). Here, we adapt the WOTAN technique for application to ocean gliders, enabling calibrated wind speed measurements to be combined with contemporaneous oceanographic profiles over extended spatial and temporal scales. We demonstrate the methodology in three glider surveys in the Mediterranean Sea during winter 2012/13. Wind speeds ranged from 2 to 21.5 m s<sup>-1</sup>, and the relationship to underwater ambient noise measured from the glider was quantified. A two-regime linear model is proposed, which validates a previous linear model for light winds (below 12 m s<sup>-1</sup>) and identifies a regime change in the noise generation mechanism at higher wind speeds. This proposed model improves on previous work by extending the validated model range to strong winds of up to 21.5 m s<sup>-1</sup>. The acquisition, data processing, and calibration steps are described. Future applications for glider-based wind speed observations and the development of a global wind speed estimation model are discussed.

## 2.2 Introduction

Quantifying air-sea fluxes is critical in understanding the weather – ocean – climate system. Numerical models need forcing by in situ measurements at an increasingly higher spatial and temporal resolution (Zhang *et al.*, 2006). Sea surface wind speed is a key parameter in forcing numerical models, as well as in quantifying turbulent air-sea fluxes and gas exchanges (Wanninkhof, 2014).

Observations made from satellites can provide wind speed data with near-global coverage over the ice-free oceans with a spatial and temporal resolution of about 0.25 ° and 24 h (e.g. QuickScat, ASCAT), respectively. However, there is a lack of calibration of in situ observations outside the tropics and away from coasts, or in high wind speed (>18 m s<sup>-1</sup>) conditions (Bourassa *et al.*, 2010). In situ monitoring of weather conditions over the ocean is difficult to achieve. Ship-based observations are affected by airflow distortion (Moat *et al.*, 2005) and are sparse (Kent, 1998). Making observations from moored meteorological buoys in the long term (years to decades) presents difficulties, such as damage or loss caused by the roughness of the sea surface environment (storms, ice, fishing activity, vandalism, etc.). The spatial coverage offered by moored meteorological buoys and ship-based observations remains limited, as is their ability to provide observations of

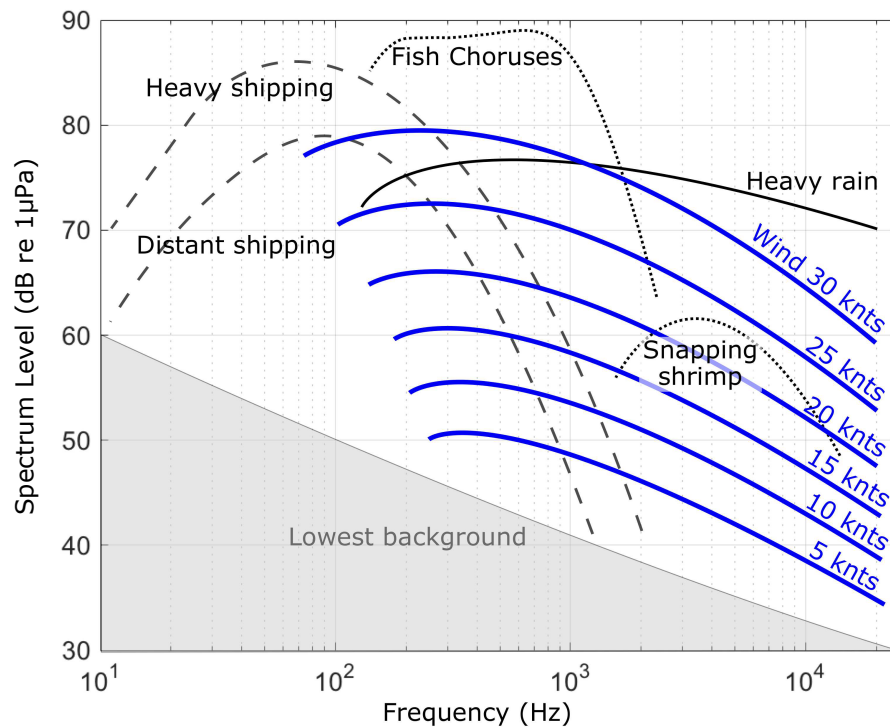


**Figure 2.1:** Spectra of the typical contributions to underwater ambient noise in the open ocean, from anthropogenic (dashed), biotic (dotted), and abiotic (continuous) sources (adapted from (Wenz, 1962)). In the absence of heavy rain events or nearby biotic activity, wind-generated noise is predominant in the 500 Hz – 20 kHz frequency range.

extreme wind events, because of sensor and platform limitations (Weller *et al.*, 2008).

The Weather Observations Through Ambient Noise (WOTAN) technique (Vagle *et al.*, 1990) enables monitoring of the sea surface weather conditions from underwater, away from the rough sea-air interface, with no difficulties induced by extreme weather events. This approach relies on the analysis of underwater ambient noise, generated by the excitation of the sea surface by the weather conditions. Surface-generated noise can be recorded up to at least 6 km deep (Barclay and Buckingham, 2013). The unique characteristics of the main underwater sound sources (e.g., spectrum shape, time variability) allow wind-generated noise to be isolated and quantified (Fig. 2.1).

Underwater noise generated by surface weather conditions was first studied in the mid-twentieth century, because of its effect on the performance of submarine detection systems (Urick and Kuperman, 1989). In the open ocean, and in the absence of sound from marine life or nearby ships, the main source contributing to underwater sound in the frequency band from 500 Hz to 50 kHz is the sound produced by surface weather conditions (Black *et al.*, 1997; Vagle *et al.*, 1990; Wenz, 1962). The action of the wind on

the surface of the ocean induces air bubbles, spray, splash, and turbulence noise, which contribute to underwater ambient noise (Carey *et al.*, 1993). These complex surface processes are influenced by multiple parameters, such as wind speed, wind duration, fetch, and marine atmospheric boundary layer (MABL) stability. In this study, we will focus on the instantaneous wind speed only, as a first-order approximation. A linear relationship between the logarithm of the surface wind speed and the sound pressure level (decibels) was first reported in shallow water ( $\sim 40$  m) (Piggott, 1964), and then extended to deep water (5000 m) in the 1 – 10 kHz frequency range (Crouch, 1972; Shaw *et al.*, 1978). An empirical linear relationship between the surface wind speed and the sound pressure ( $\mu\text{Pa}$ ) was then proposed in the 4 – 15  $\text{m s}^{-1}$  wind speed range (Vagle *et al.*, 1990), which is now widely used (Nystuen and Ma, 2002; Riser *et al.*, 2008; Vakkayil *et al.*, 1996).

The wind speed measured using this technique is relative to the sea surface, so it is applicable to estimation of heat and moisture fluxes and wind stress (Bourassa *et al.*, 2010). The WOTAN technique spatially averages over an area dependent on the frequency used, the depth of the measurement, and the sound speed profile at the measurement site. At 3 kHz, it varies from 0.1  $\text{km}^2$  for a measurement depth of 100 m to 10  $\text{km}^2$  for a measurement depth of 1000 m (Vagle *et al.*, 1990). For increasing frequencies, the sound absorption coefficient increases, thus the listening area decreases. This spatial scale corresponds to the scales considered in interaction studies (Bourassa *et al.*, 2010). The linear relationship

$$p = b + sU \quad (2.1)$$

between the sound pressure  $p$  ( $\mu\text{Pa}$ ) and the surface wind speed  $U$  ( $\text{m s}^{-1}$ ), where  $b$  ( $\mu\text{Pa}$ ) and  $s$  ( $\mu\text{Pa m}^{-1} \text{s}$ ) are respectively the offset and slope of the linear regression, is widely used in most recent studies (Nystuen and Ma, 2002; Riser *et al.*, 2008; Vakkayil *et al.*, 1996). These studies agree on a low wind speed limit of around 2  $\text{m s}^{-1}$ , below which the wind-generated sound is below the background noise level. They also agree on a high wind speed limit around 15  $\text{m s}^{-1}$ , above which measurements are scattered and the correlations are poor, and propose an explanation based on the hypothesis of bubble-layer attenuation of surf noise (Black *et al.*, 1997; Farmer and Lemon, 1984). It is worth noting that these previous studies contained few observations of high wind speeds.

Ocean gliders are autonomous underwater vehicles, carrying sensors to monitor the

ocean. They perform long autonomous missions (several months to a year, and several thousand kilometres) and provide high-resolution ( $\sim 2$  h,  $\sim 2$  km) hydrographic profiles (Testor *et al.*, 2010; Rudnick, 2016). Glider measurements are not affected by extreme weather events. Their unique way of moving through the water column (buoyancy driven with no propellers) makes them extremely quiet and therefore very suitable for passive acoustic monitoring. Gliders also measure temperature and salinity profiles, from which sound velocity profiles can be derived. This collocated information on the acoustical properties of the water column is of considerable value for soundscape studies. Passive acoustic monitoring (PAM) sensors have been successfully deployed on ocean gliders for cetacean monitoring purposes (Baumgartner and Fratantoni, 2008; Baumgartner *et al.*, 2013; Klinck *et al.*, 2012; Moore *et al.*, 2007). The combination of hydrographic profiles with surface weather measurements on submesoscales (i.e., kilometre scale), tracking a weather event or monitoring a selected area for many months, would be highly valuable for interaction studies.

This paper presents a novel method for measuring surface wind speed using glider-borne underwater ambient noise measurements, from the subsurface to 1 km deep. We deployed gliders equipped with PAM sensors in the Mediterranean Sea during winter 2012/13 in the framework of the Deep Water formation Experiment (DEWEX) experiment (Testor *et al.*, 2018). The gliders recorded 4 months of acoustic data, with recurring opportunities to compare our wind speed estimates with Météo-France meteorological buoys in the area. Focusing on the sound pressure level in the 3 kHz third octave band, which shows the most dynamic response to wind speed, we estimate the surface wind speed around the glider's position ( $0.1 - 10$  km<sup>2</sup>) throughout the  $2 - 21.5$  m s<sup>-1</sup> wind speed range. Section 2.3 describes the experiment and the associated datasets. Section 2.4 presents the data acquisition and processing methods, and the results. Section 2.5 presents the wind speed derivation model and its performance. In section 2.6, we consider the broader application of the model to different experiments or regions, and we discuss future improvements and the contribution to wider monitoring activities.

### 2.3 Instrumentation and field measurements

Passive acoustic measurements were made using an Acousonde B003A-HF datalogger (Fig. 2.2), developed by Greeneridge Sciences, Inc. The Acousonde is a self-contained underwater acoustic recorder comprising two hydrophones, sensors for attitude, orientation, depth, and temperature, a digital recorder, and a field-replaceable battery (Burgess, 2010). The core of the sensor consists of a high-frequency hydrophone (capable of sampling up to 232 kHz), with a sensitivity of  $-204$  dB re  $1\text{ V } \mu\text{Pa}^{-1}$ . A 6-pole linear-phase anti-aliasing filter is used, with  $-3$  dB passband ( $12.5$  kHz –  $42$  kHz) and  $-22$  dB at  $100$  kHz (Fig. A.2a). Data are stored on a 128 GB flash memory, with a 16-bit sampling resolution. An external three-D-cell tethered battery pack allows up to 200 h of recording. The Acousonde operates autonomously, and has its own battery, memory, and programmed mission. Data processing is undertaken after the sensor is recovered. Initially developed to be attached to marine mammals (Cazau *et al.*, 2017), it has also been used on ocean gliders (Nott, 2015). Details of the sampling method used in this study are given in Section 2.4.

The platform we used in this study is the Slocum glider, developed by Teledyne Webb Research. It is driven by buoyancy changes, controlled by  $500\text{ cm}^3$  of oil pumped into or out of a swim bladder, inducing a vertical motion in the water column, from the surface down to 1000 m depth. Fixed wings convert the vertical velocity into forward velocity, internal battery displacements enable pitch and roll management, and a moving rudder enables direction changes. This novel way of propulsion makes it a very quiet platform between the oil pumping phases that occur at the apogee and perigee of each dive ( $\sim 2$  h for 1000 m dives). Water turbulence around the sensor induces flow noise, proportional to the glider's speed in the  $5 - 50$  Hz frequency band (Dos Santos *et al.* 2016; Erbe *et al.* 2015), with no effects regarding the wind generated sound levels over 1 kHz. The version of the Slocum gliders we used can complete autonomous missions up to 3 months and 1000 km long. Along with the external PAM sensor, the gliders were equipped with integrated temperature, salinity, and pressure sensors.

The experiment took place within the Mediterranean Ocean Observing System for

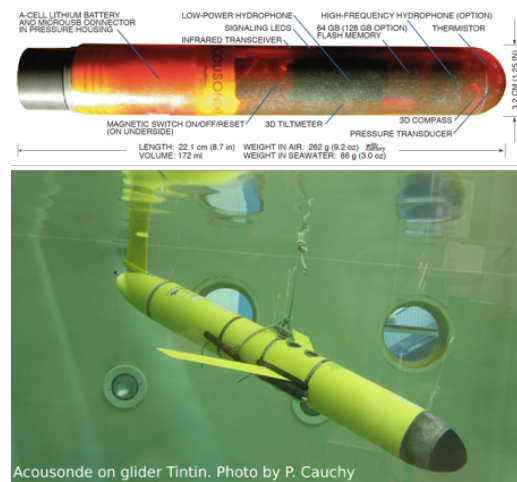


**Figure 2.2:** Model B003A Acousonde (reproduced with permission of Greeneridge Sciences, Inc.) (top) layout and (bottom) assembled with a B003-XHD external three-D-cell alkaline battery (4.5 V, 15 Ah) housing mounted on a Slocum glider.

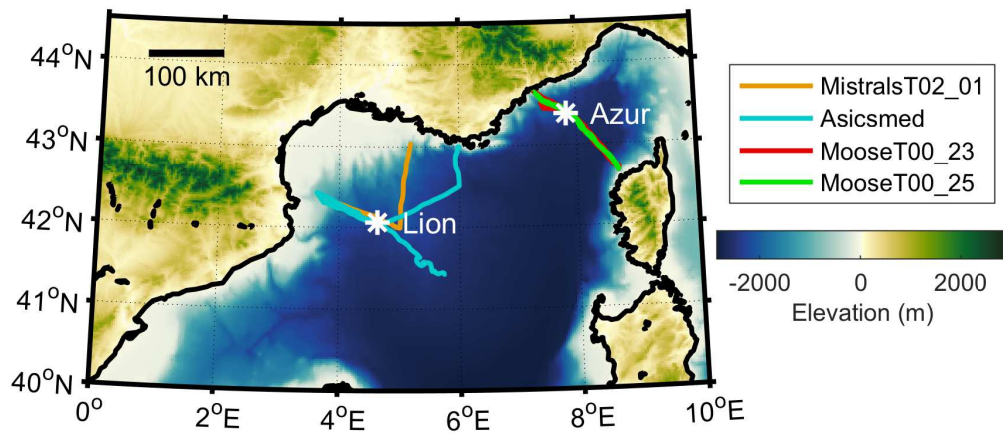


**Figure 2.3:** Map of the Gulf of Lion (Lambert projection), tracks of the four glider missions, and location of the two Météo-France meteorological buoys, Lion and Azur.

the Environment (MOOSE) framework, which aims to monitor the oceanographic variability of the northwestern Mediterranean Basin over a continuum of spatial and temporal scales (<http://www.moose-network.fr>), and the DEWEX experiment (Testor *et al.*, 2018). From December 2012 to May 2013, PAM equipped gliders were deployed along the MOOSET00 [Nice, France – Calvi (Ligurian Sea), France] and MOOSET02 [Marseille, France – Menorca, Spain (Gulf of Lion)] glider endurance lines (Fig. 2.3). These lines closely pass the two Météo-France meteorological buoys Azur and Lion respectively, defining two distinct experiment sites in which continuous in situ surface wind measurements are available, thus allowing recurring calibration and validation of the glider measurements.

These two experiment sites present different geographical characteristics, hence different spatial variability scales in their wind fields. The Lion buoy (42.06 °N, 4.64 °E) is in the middle of the Gulf of Lion, 100 km from the nearest shore, in waters 2300 m deep, in an open sea area affected by the mistral and tramontane winds, and away from the main shipping lanes. The Azur buoy (43.38 °N, 7.83 °E) is 50 km from the shore, in waters 2300 m deep, in an area affected by cyclogenesis in the Gulf of Genoa (Rainaud *et al.*, 2016), and close to the alongshore shipping lanes. Each buoy measurement is considered to represent the conditions for an area around the buoy's position, whose size depends on the spatial variability of the measured parameters and the geographical position of the buoy. To better estimate the area represented by each buoy wind speed measurement, we used output from the atmospheric model Application of Research to Operations at Mesoscale – Western Mediterranean (AROME-WMED; (Nuret and Fourri , 2011)) to compare the wind speed at the buoy position with the wind speed for the rest of the Gulf of Lion, for the two sites, Lion and Azur (Fig. 2.4). Around the Lion buoy, the correlation (0.93), root-mean-square (RMS) difference ( $2.1 \text{ m s}^{-1}$ ), and mean difference ( $0.2 \text{ m s}^{-1}$ ) with the wind speed at the buoy position are good within 80 km of the buoy, with a rapid deterioration outside. We define this as the Lion confidence area, in which we use the buoy 1-min average measurements of wind speed at 10 m as ground truth. Around the Azur buoy, this radius decreases to 40 km. We defined the Azur confidence area as a 40-km radius around the Azur buoy that provides hourly average measurements of wind speed at 10 m, with mean correlation, RMS difference, and difference of 0.86,  $2.5 \text{ m s}^{-1}$ , and  $0.2 \text{ m s}^{-1}$ , respectively (Fig. 2.4).

We undertook four PAM glider deployments around the two sites, Lion (missions Asicsmed and MistralT02.01) and Azur (missions MooseT00.23 and Moose T00.25). These cover 138 days of data, 37 of which are within the confidence area of one of the buoys and can be used to derive a relationship between sound pressure and surface wind speed (Table 2.1). Multiple factors can induce differences between our measurements in the different experiments: the two buoys have different measurement sampling frequencies; shipping activity, and therefore its generated noise, is different at the two sites; and our PAM sensors have different sensitivities per experiment, because of the varying mounting position on the glider, and the difficulty of using Acousonde to produce absolute

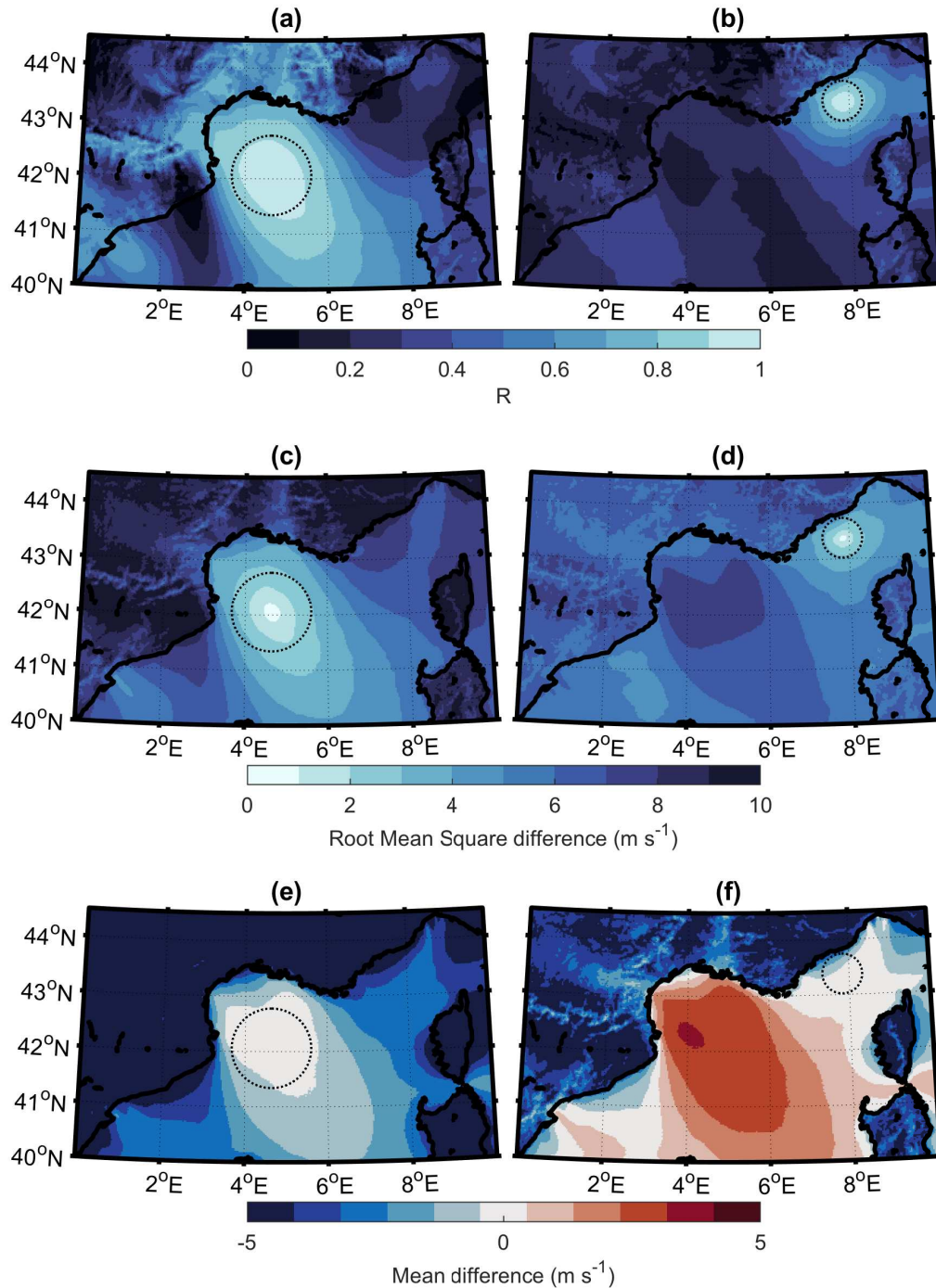


**Figure 2.4:** Maps (Lambert projection) of the (a), (b) correlation, (c), (d) RMS difference, and (e), (f) mean difference ( $U_{buoy} = U$ ) of the wind speed at the sites (a), (c), (e) Lion and (b), (d), (e) Azur with the wind speed on the Gulf of Lion. The maps are computed using hourly averages of wind speed at 10 m, from the atmospheric model AROME\_WMED analysis, over the time of the glider deployments, November 2012 – March 2013. The dashed circles of radius 80 km around the Lion buoy and 40 km around the Azur buoy represent the confidence areas in which we use the buoy measurements as ground truth. The mean values in the confidence areas are ( $R = 0.93$ ,  $RMSE = 2.1 \text{ m s}^{-1}$ ,  $\text{error} = -0.2 \text{ m s}^{-1}$ ), and ( $R = 0.86$ ,  $RMSE = 2.5 \text{ m s}^{-1}$ ,  $\text{error} = -0.2 \text{ m s}^{-1}$ ) around the sites Lion and Azur, respectively.

**Table 2.1:** Amount of PAM sensor data at each step of the preprocessing, for the three datasets (GB, days, and 1-min samples).

Dataset	Lion	MooseT00_23	MooseT00_25
Raw data	45 GB	48 GB	33 GB
	51 days	54 days	38 days
	7371 samples	7802 samples	5444 samples
Quiet gliding phase	40 days	50 days	14 days
	4021 samples	4938 samples	1553 samples
Within the confidence area	15 days	17 days	5 days
	2081 samples	2365 samples	707 samples

sound level measurements (Wiggins 2013). For these reasons, we decided to process each experiment separately. We merged the two Lion datasets, Asicsmed and MistralsT02\_01 (referred to as Lion dataset), as both deployments used the same setup in the same area without any maintenance operations in between.

## 2.4 Acoustic data sampling and pre-processing procedures

We designed the data acquisition protocol to evenly distribute the 200 h of recording time over the 3-month glider mission. The shortest sample allowed by the PAM sensor, 1 min, is sufficient for analysis of wind-generated noise (Nystuen and Ma, 2002). The PAM sensor recorded 1 min every 10 min, to allow a mission duration of 80 days. The sampling rate was set at 50 kHz, constrained by the PAM sensor’s onboard memory capacity. This sampling method produces 27 GB of data every month. We adapted the WOTAN technique (Vagle *et al.*, 1990). We processed each 1-min sample individually, extracting the sound level on third octave frequency bands [third octave level (TOL)], according to the standards [American National Standards Institute (ANSI) S1.11–2004] and using the software PAMGuide (Merchant *et al.*, 2015) on 1-s-long non overlapping Hanning windows. To focus on the wind contribution to the underwater ambient noise, any other sound sources have to be detected and removed from the dataset. The noise generated by the glider’s oil pump is a loud broadband signal, lasting for several minutes. Slocum gliders generally activate their pump only during the apogee (surfacing) and perigee (bottom inflexion) phases of a dive. As we programmed only 1000-m-deep dives, we removed data acquired during apogee (depth <20 m) and perigee (depth >950 m) to focus on the

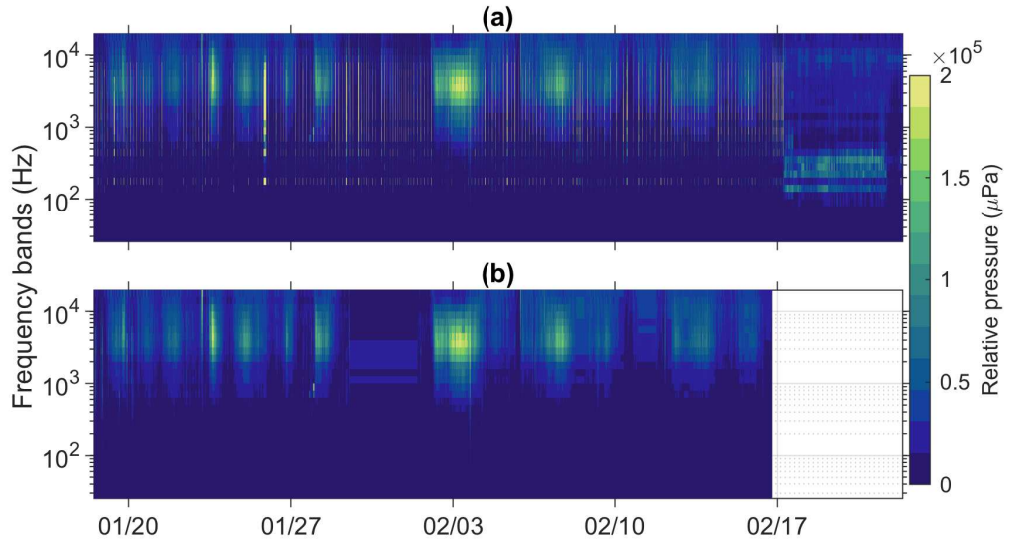


**Figure 2.5:** (a) Raw spectrogram of the sound recorded during the Lion–Asicsmed mission and (b) after removal of the main-glider-generated noises during the apogee (depth <20 m) and perigee (depth >950 m) phases.

quiet gliding phase of each dive (Fig. 2.5). The Lion dataset contains 4021 remaining 1-min samples, the equivalent of 40 days (Table 2.1).

To eliminate transient sounds (e.g., clicks, whistles, and glider’s motors), we assumed that wind speed is constant over a 1-min sample and kept only the minimum TOL values. We therefore condense a 1-min sample spectrogram to a single spectrum in which remains no signal of the transient sounds (Fig. 2.6). The pitch of the glider varies significantly between ascending (approximately  $26^\circ$ ) and descending (approximately  $-26^\circ$ ) phases. To assess the effects of this variation on the measurements, we compared the estimated wind speed during climbing and diving profiles. There is an average overestimation from the ascending profiles of  $0.3 \text{ m s}^{-1}$ . An ANOVA test on these time series gives a p value of 0.3. Therefore, we neglected the effect of the variation of the pitch in this study.

The glider profiling behaviour implies significant variations in the depth of the measurements, which affect the received sound level. The effects of refraction, attenuation, spreading loss, and directionality of the sound sources are accounted for, for each depth and frequency, depending on the sound attenuation and velocity profile (Vagle *et al.*, 1990). Therefore,  $TOL(h, f)$ , measured at depth  $h$  and frequency  $f$ , can be corrected to an equivalent  $TOL_0(f)$  at the surface:

$$TOL_0(f) = TOL(h, f) + \beta(h, f), \quad (2.2)$$

**Table 2.2:** Depth, frequency, and wind speed ranges of previous studies.

Reference	Depth (m)	Frequency range	Wind speed range (m s <sup>-1</sup> )
(Piggott, 1964)	40	8.4 Hz–3.1 kHz	1–20
(Wenz, 1962)		500 Hz–5 kHz	1.2–20
(Crouch, 1972)	800–5000	10 Hz–3 kHz	2.5–25
(Shaw <i>et al.</i> , 1978)	5000	1–10 kHz	2.5–12.5
(Vagle <i>et al.</i> , 1990)	100–300	3–25 kHz	4–15
(Vakkayil <i>et al.</i> , 1996)	500–2600	3–25 kHz	4–16
(Black <i>et al.</i> , 1997)	1.8–46	10–30 kHz	1.3–13.9
(Nystuen and Ma, 2002)	38	100 Hz–50 kHz	2–12
(Riser <i>et al.</i> , 2008)	600	8 kHz	2.3–10

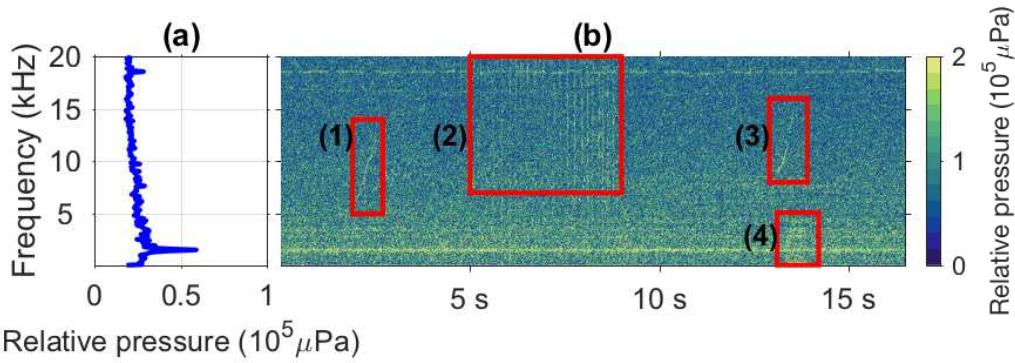


**Figure 2.6:** (b) Spectrogram with examples of transient noises, such as 2: biological echolocation clicks, 1 and 3: whistles, and 4: glider’s fin movement noise. (a) The associated extracted minimum spectrum shows no remaining signal of any of the identified transient sounds. The Acousonde self noise, at 2 and 18 kHz, is not removed but the affected frequencies are not used in our analysis.

where

$$\beta(h, f) = -10 \log \left( 2 \int_0^\infty \frac{r \sin^2 \theta_{h,f} e^{-\alpha_f l_{h,f}}}{l_{h,f}^2} dr \right), \quad (2.3)$$

where  $r$  is the horizontal distance from the source to the point directly above a hydrophone at  $h$ ;  $l$  is the path length from the source to the receiver, including refraction effects;  $\theta$  is the angle between the surface and the path to the receiver;  $\alpha$  is the frequency-dependent attenuation coefficient for bubble-free water. For each deployment, we calculated the  $\beta$  profile using the average sound velocity profile, and attenuation, obtained from the glider’s temperature and salinity measurements. The average sound velocity and  $\beta$  profiles are shown in Fig. A.1 in the online supplement.

The applied correction for a depth of 1000 m is 1.3 dB, which means that the received sound pressure ( $\mu\text{Pa}$ ) is 14 % lower than the sound pressure at the surface. The associated

wind speed estimation correction varies from 0 to  $2.5 \text{ m s}^{-1}$  with the sound speed in the  $0\text{--}25 \text{ m s}^{-1}$  range. The nonlinearity observed at  $9\text{--}10 \text{ m s}^{-1}$  is due to the regime change. Because of the change of the derivation slope, a similar sound pressure correction will lead to a wind speed correction divided by 4 in the high wind speed regime than in the low wind speed regime.

## 2.5 Wind speed derivation

### 2.5.1 Wind speed derivation model

Previous studies (Lemon *et al.*, 1984; Nystuen and Ma, 2002; Vagle *et al.*, 1990; Vakkayil *et al.*, 1996) were conducted on wind speeds limited to the  $3\text{--}15 \text{ m s}^{-1}$  range (Table 2.2). These studies found a linear relationship [eq. 2.1] between sound pressure at 8 kHz ( $p_{8kHz}$ ,  $\mu\text{Pa}$ ) and 10-m wind speed ( $U_{10}$ ,  $\text{m s}^{-1}$ ). They discussed limitations at high wind speeds (Vagle *et al.*, 1990). In this study, we use

$$p_{f_c} = 10^{\frac{TOL_0(f_c)}{20}} - p_{min}(f_c), \quad (2.4)$$

where  $p_{f_c}$  is the sound pressure for the third octave band of central frequency  $f_c$ , relative to the minimal pressure  $p_{min}(f_c)$  observed on the deployment. The correlation between  $p_{f_c}$  measured by the glider and  $U_{10}$  measured by the buoy depends on  $f_c$ . The best correlations are in the  $2\text{--}10 \text{ kHz}$  frequency band, where the wind-generated sound is predominant (Fig. 2.7). The poor correlations in frequency bands below  $1 \text{ kHz}$  is due to the predominance of non-wind-dependent sound sources (e.g., distant shipping). The poor correlations in frequency bands above  $10 \text{ kHz}$  can be explained by the attenuation of sound in the high-frequency bands observed during high wind speed events ( $>15 \text{ m s}^{-1}$ ) (Fig. 2.7). We chose to use the relative pressure in the  $3 \text{ kHz}$  third octave band, which shows the most dynamic response to wind speed and shows no attenuation effect during high wind speed events (Fig. 2.7). Similar results are obtained if other frequency bands (within  $2\text{--}10 \text{ kHz}$  range) are used.

To train our wind speed derivation model, we consider the median values of the acoustic parameter and the measured wind speed over each glider profile. As a result, contaminating sounds of duration of several 1-min samples (e.g., nearby ship) will be filtered out,

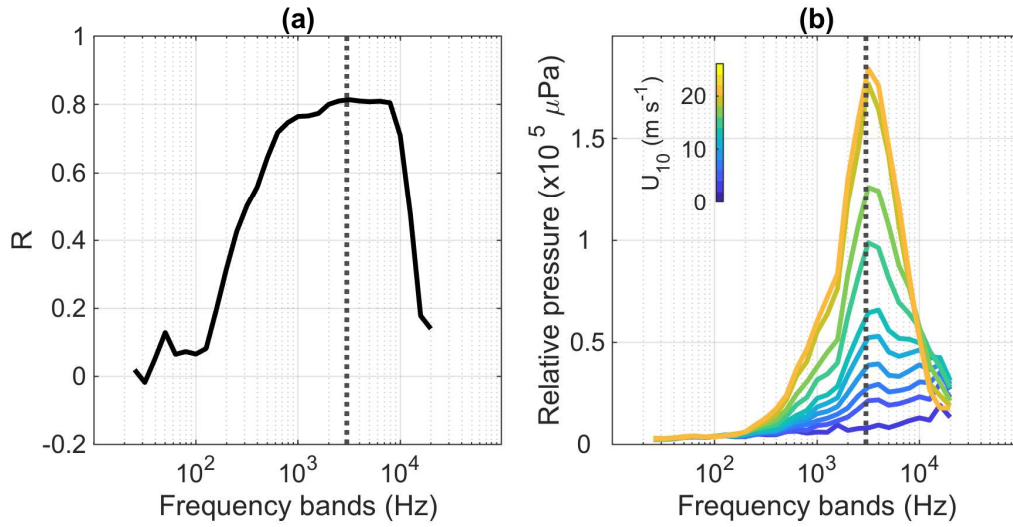


**Figure 2.7:** (a) Correlation of the surface wind speed measurements at the Lion buoy ( $U_{10}$ ) with the relative pressure in third octave frequency bands recorded by the glider within 80 km from the site Lion. (b) Relative pressure spectrum for each  $2 \text{ m s}^{-1}$  wind speed bin. The black dotted line marks the 3 kHz frequency band.

**Table 2.3:** Distribution of buoy wind speed measurements in each  $2 \text{ m s}^{-1}$  wind speed bin for the Lion dataset.

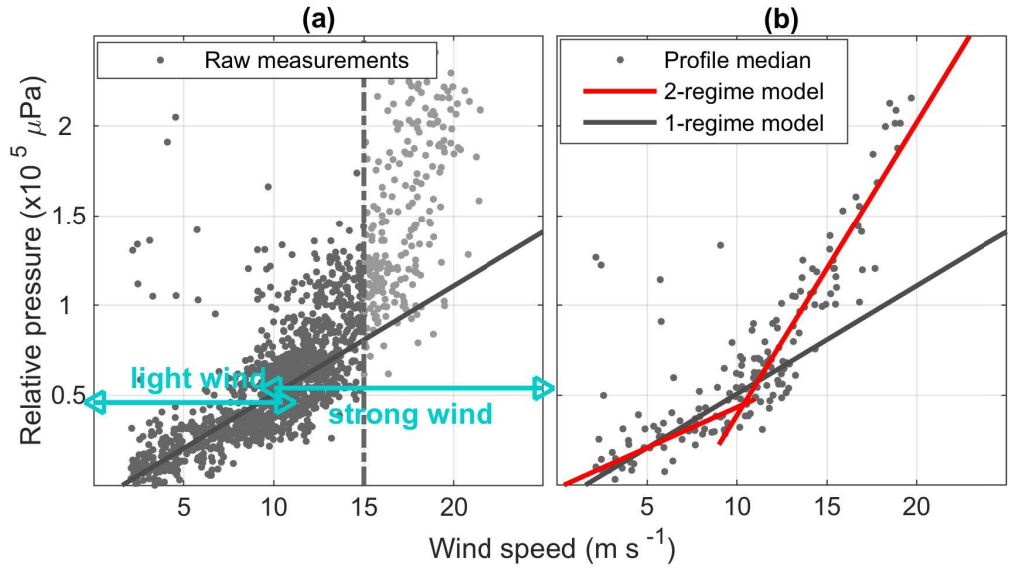
$U_{10}$ ( $\text{m s}^{-1}$ )	No. of 1-min samples	No. of profiles
2–4	105	20
4–6	90	15
6–8	120	17
8–10	197	20
10–12	317	39
12–14	257	36
14–16	147	16
16–18	93	9
18–20	52	7
20–22	12	0
22–24	0	0

and the time and length scales are the usual glider profiling scales ( $\sim 2\text{h}$ ,  $2\text{km}$  for a  $1000\text{-m}$  vertical profile). The number of observations is unevenly distributed over the wind speed range (Table 2.3). Therefore, to give an equal weight to each wind speed during the regressions between  $p_{fc}$  and  $U_{10}$ , we calculated the median sound pressure in each  $2 \text{ m s}^{-1}$  wind speed bin.

During our experiment, we observed several high wind speed events of 6–48 h of wind speed above  $15 \text{ m s}^{-1}$ , with the glider in the confidence area around the buoy. Our dataset

**Table 2.4:** Distribution of buoy wind speed measurements in each  $2 \text{ m s}^{-1}$  wind speed bin for the Lion dataset.

	Single linear model	Two-regime linear model
Low wind speed $U_{10} < 11 \text{ m s}^{-1}$	$b_{single} = -1.0 \times 10^4 \text{ (}\mu\text{Pa)}$ $s_{single} = 0.6 \times 10^4 \text{ (}\mu\text{Pa m}^{-1} \text{ s)}$ $R^2 = 0.86$	$b_{low} = -0.2 \times 10^4 \text{ (}\mu\text{Pa)}$ $s_{low} = 0.4 \times 10^4 \text{ (}\mu\text{Pa m}^{-1} \text{ s)}$ $R^2 = 0.88$
High wind speed $U_{10} > 9 \text{ m s}^{-1}$		$b_{high} = -12.5 \times 10^4 \text{ (}\mu\text{Pa)}$ $s_{high} = 1.6 \times 10^4 \text{ (}\mu\text{Pa m}^{-1} \text{ s)}$ $R^2 = 0.95$

**Figure 2.8:** (a) Variation of relative pressure at 3 kHz with surface wind speed. The historical single linear model [(1); dark line] is obtained by regression on the wind speed data below  $15 \text{ m s}^{-1}$ . The two wind speed regimes considered in this study are marked by blue arrows. (b) The two-regime linear model (red line) is obtained by regression on the median values in  $2 \text{ m s}^{-1}$  wind speed bins of the median pressure for each glider profile for the low wind speed and high wind speed subsets.

covers a broader wind range ( $2\text{--}21.5 \text{ m s}^{-1}$ ) than previous studies, allowing us to investigate the relationship between  $p_{fc}$  and  $U_{10}$  for wind speed regimes above  $15 \text{ m s}^{-1}$ . To assess the validity of the historical single linear model [eq. 2.1] for our observations, we fitted a linear model, of parameters  $b_{single}$  and  $s_{single}$  (Table 2.4), to the wind speed range below  $15 \text{ m s}^{-1}$ , simulating the wind speed range of the previous studies. Its coefficient of determination  $R^2 = 0.86$  indicates a good fit for the  $2\text{--}15 \text{ m s}^{-1}$  range. We extrapolated this to the high wind speed range and tested it against the data available in the Lion dataset, revealing a tendency of the single linear model to overestimate wind speed in the higher wind speed range ( $15\text{--}21.5 \text{ m s}^{-1}$ ) (Fig. 2.8).

To improve the agreement at high wind speed we investigated the hypothesis of two distinct sound production regimes, related to the physical processes of wind-generated underwater noise (bubbles, spray, and splash). Whitecaps can be observed on sea surface images at wind speeds as low as  $3.7 \text{ m s}^{-1}$  (Callaghan *et al.*, 2008), with this threshold varying with air and sea temperature (Monahan and O’Muircheartaigh, 1986). Previous studies using ambient noise show a low wind speed detection threshold at  $1.5\text{--}4 \text{ m s}^{-1}$  (Table 2.2). A wind speed threshold in the range of  $9\text{--}11 \text{ m s}^{-1}$  is commonly used in the description of physical sea surface processes, such as the generation of spume drops, torn off wave crests by high winds (Monahan *et al.*, 1983, 2017), spray generation function (Large and Pond, 1981), and drag coefficient (Foreman and Emeis, 2010). As these processes all impact wind noise production, it is likely we will observe regime change in the underwater noise production at wind speeds above this threshold. We therefore defined a low wind speed range ( $U_{10} < 11 \text{ m s}^{-1}$ ), where whitecaps are solely for the sound production, and a high wind speed range ( $U_{10} > 9 \text{ m s}^{-1}$ ), where additional physical processes contribute to the sound production. We fitted two linear regressions for low wind speed parameters  $b_{low}$  and  $s_{low}$ , and for high wind speed parameters  $b_{high}$  and  $s_{high}$  (Table 2.4). The low wind speed model is very close to the single linear model, despite being fitted on a dataset of narrower wind speed range. The two-regime linear model allows a good description of the observations for the complete measured wind speed range (Fig. 2.8). As an alternative to the two-regime linear model, we investigated the possibility of fitting a power-law ( $p = a + U^b$ ) relation. We obtained good results with the quadratic model —  $p = 459.6U^2$  — but with a tendency to overestimate low wind speeds. We elected to use a two-regime model instead, as the fit was better and can be explained by a change in physical processes at elevated wind speeds.

The physical processes explaining the regime change appear in a continuous and smooth way, around a wind speed limit that is believed to depend on multiple parameters (sea state, current, fetch, temperature,...). To better describe this smooth transition between two different linear relationships on both sides of an undetermined joint point, we can use a hyperbola as a transition model (Watts and Bacon, 1974). Therefore, we

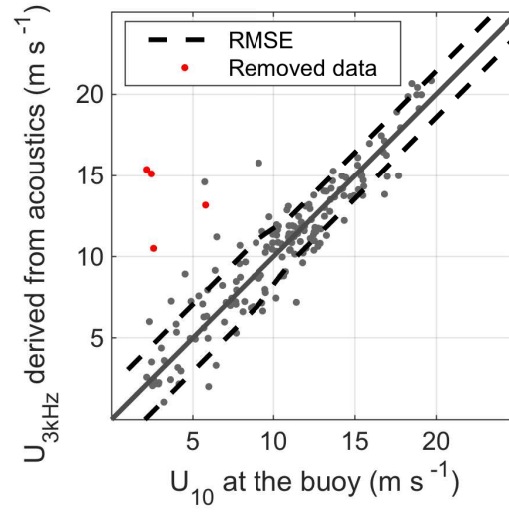


**Figure 2.9:** Wind speed  $U_{10}$  measured at the buoy vs  $U_{3kHz}$  derived from acoustic measurements using the two-regime linear model with hyperbolic transition [2.3]. The RMSE is calculated on the low and high wind speed regimes. Corrupted data points, excluded from the analysis, are shown in red.

estimate  $U_{3kHz}$ , the wind speed derived from the sound pressure  $p_{3kHz}$ , as

$$U_{3kHz} = U_{lim} + \frac{s_{low} \times s_{high}}{2(s_{high} + s_{low})} (p_{3kHz} - p_{lim}) + \frac{s_{low} \times s_{high}}{2(s_{high} - s_{low})} \sqrt{(p_{3kHz} - p_{lim})^2 + \frac{\delta^2}{4}}, \quad (2.5)$$

where  $\delta = 10000$  is the radius of curvature at the joint point ( $p_{lim} = 4.5 \times 10^4 \mu\text{Pa}$ ;  $U_{lim} = 10.4 \text{ m s}^{-1}$ ) between the low ( $s_{low}, b_{low}$ ) and high ( $s_{high}, b_{high}$ ) wind speed linear models.

### 2.5.2 Performance of the wind speed derivation model

Prior to the estimation of the performance of the wind speed derivation model, we detected and removed some data points from the analysis that we suspected to be corrupted by an anemometer failure. They all occur during the 23–28 January 2013 period, during which the buoy measurements are sparse, and disagree with both the glider estimation and the model output (Figs. 2.9, 2.10). A comparison between the wind speed derived from the sound pressure using [eq. 2.5],  $U_{3kHz}$ , and surface wind speed measured by the buoy,  $U_{10}$ , shows a good agreement for the 2–20  $\text{m s}^{-1}$  range. The root-mean-square of the error ( $U_{10} - U_{3kHz}$ ) between the estimation and the observation is 2 and 1.4  $\text{m s}^{-1}$  for the low and high wind speed regimes, respectively (Fig. 2.9).

Because the glider traveled repeatedly toward and away from the buoy, the wind speed

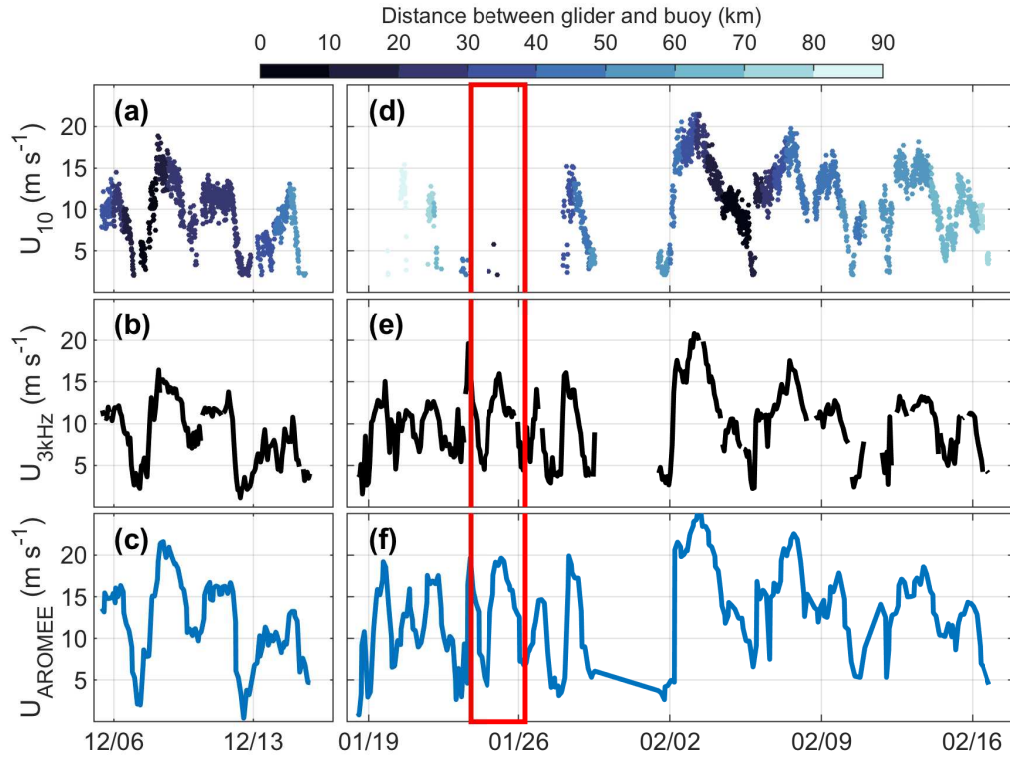


**Figure 2.10:** Wind speed (a), (d)  $U_{10}$  measured by the buoy coloured by distance to the glider position, (b), (e)  $U_{3kHz}$  derived from the glider acoustic measurements, and (c), (f)  $U_{AROME}$  from AROME\_WMED model at the glider position. The data displayed are from the (a)–(c) MistralsT02\_01 and (d)–(f) Asicsmed experiments that were merged into the Lion dataset. The red box shows the period where the measurements from the buoy have been discarded.

derivation model, calibrated against  $U_{10}$  using the data collected within the buoy’s confidence area, can be used when the glider is away from the buoy, extending the spatial coverage of the wind speed measurements. The time series of  $U_{10}$  measured at the buoy position,  $U_{3kHz}$  derived from the glider measurements, and  $U_{AROME}$  from the AROME\_WMED model output collocated with the glider position show a good fit between  $U_{3kHz}$  and  $U_{AROME}$  when the glider is away from the buoy confidence area (light blue colour coding) and when the buoy’s anemometer failed to provide data (Fig. 2.10).

## 2.6 Application to other glider campaigns and implications

The same technique was applied to the MooseT00\_23 and MooseT00\_25 campaigns, around the Azur meteorological buoy. For the MooseT00\_23 experiment, the wind speed  $U_{3kHz}$  derived using the associated hyperbolic transition model [eq. 2.3] fits  $U_{10}$  measured by the buoy throughout the 2–20  $\text{m s}^{-1}$  wind speed range, with a root-mean-square

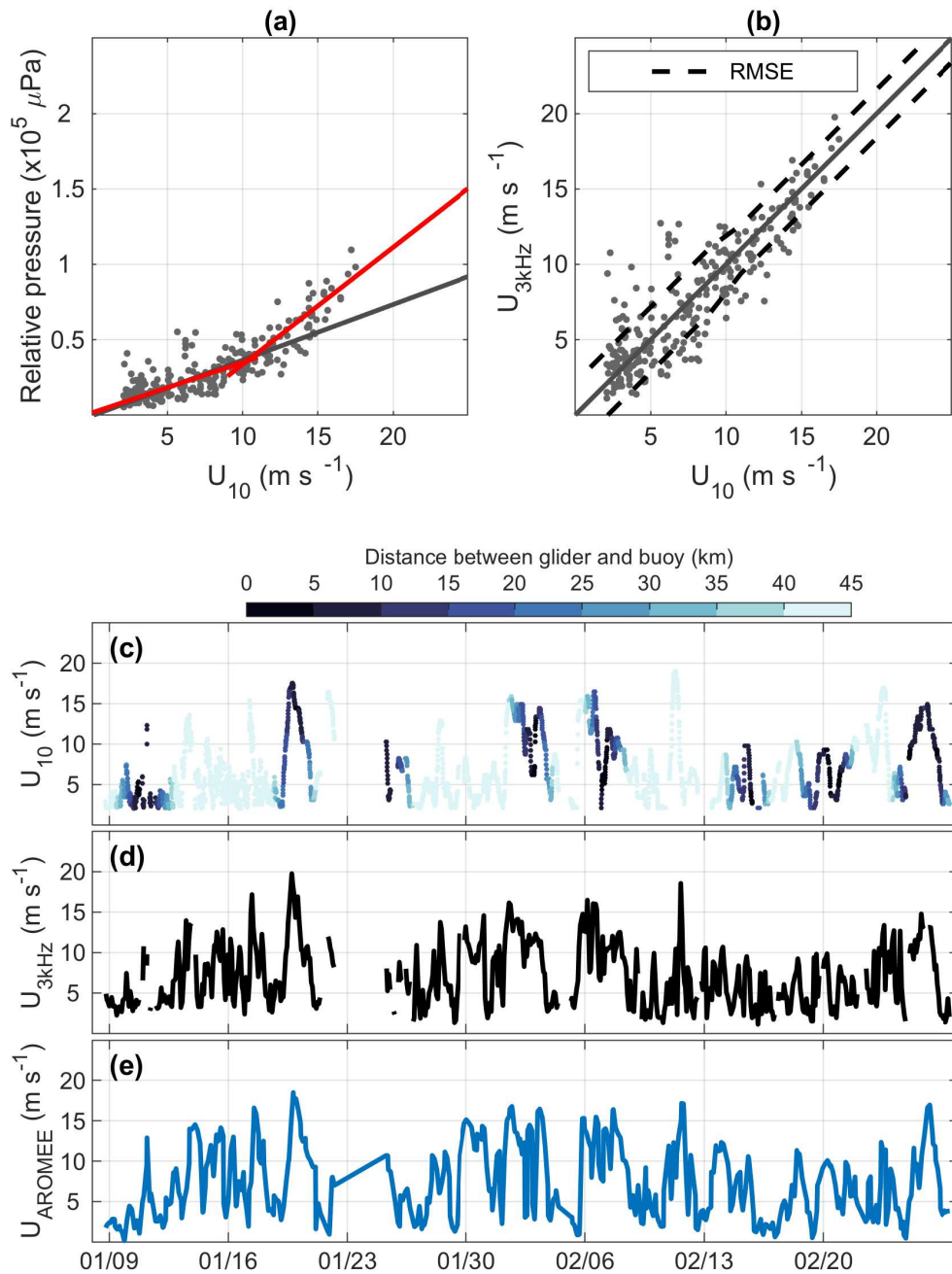


**Figure 2.11:** (a) Two-regime linear model relationship between  $p_{3\text{kHz}}$  and  $U_{10}$ ; (b) comparison between measured  $U_{10}$  and estimated  $U_{3\text{kHz}}$ ; and time series of (c)  $U_{10}$ , (d)  $U_{3\text{kHz}}$  and (e)  $U_{\text{AROME}}$  for the Azur MooseT00.23 experiment.

error of about  $2.2 \text{ m s}^{-1}$  in the low wind speed regime and  $1.6 \text{ m s}^{-1}$  in the high wind speed regime (Fig. 2.11). This long experiment (7 weeks), with eight occurrences of the glider surveying the Azur buoy area, illustrates the opportunity of repeated calibrations using the buoy measurements to estimate the surface wind speed along the glider path (Fig. 2.11).

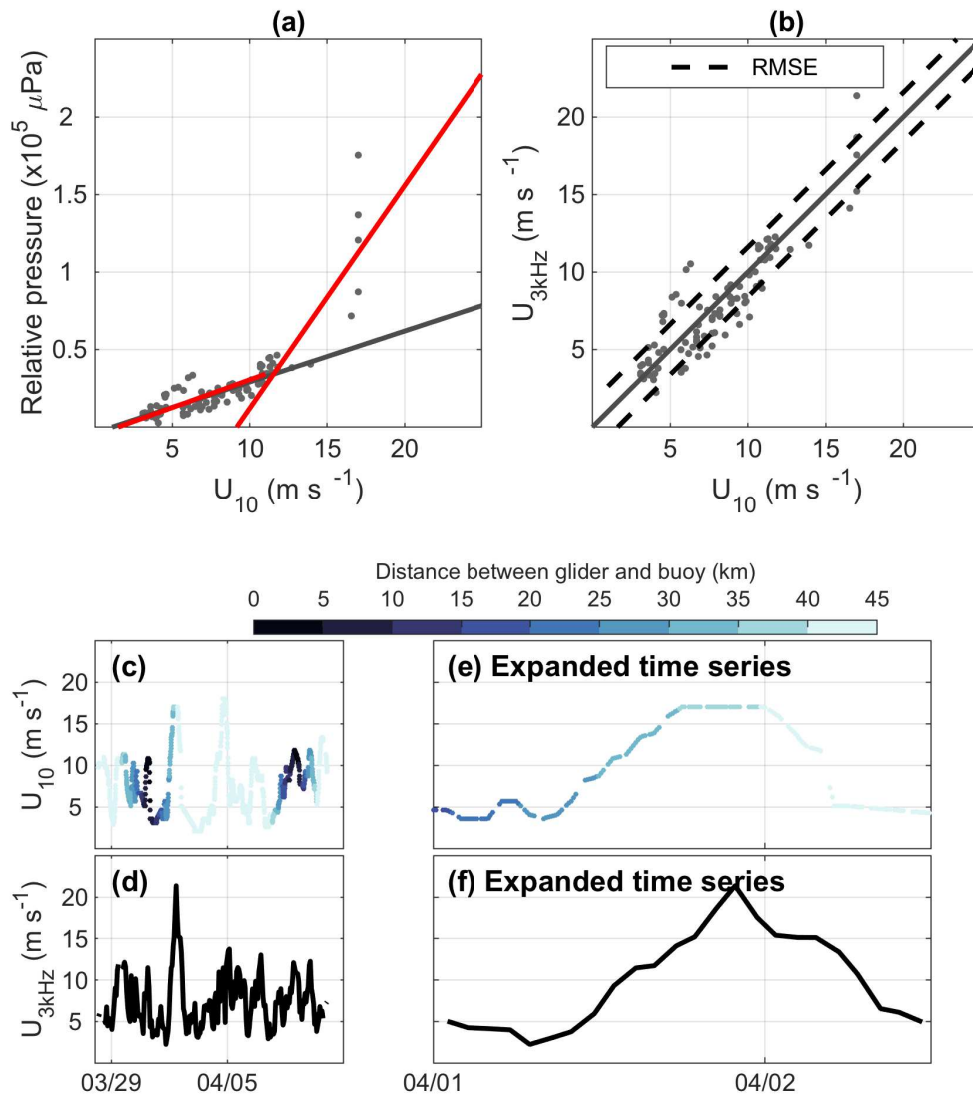


**Figure 2.12:** (a) Two-regime linear model relationship between  $p_{3kHz}$  and  $U_{10}$ ; (b) comparison between measured  $U_{10}$  and estimated  $U_{3kHz}$ ; and time series of (c)  $U_{10}$ , (d)  $U_{3kHz}$  and (e)  $U_{AROME}$  for the Azur MooseT00.25 experiment. (e),(f) Expanded time series for 1 Apr reveal a dubious  $U_{10}$  plateau. No output from the AROME\_WMED model are available for this experiment, which took place after the end of the Hydrological Cycle in the Mediterranean Experiment (HyMeX) exercise.

For the MooseT00.25 experiment, the wind speed  $U_{3kHz}$  derived using the associated hyperbolic transition model [eq. 2.3] fits  $U_{10}$  measured by the buoy throughout the 2–17 m s<sup>-1</sup> wind speed range, with a root-mean-square error of about 1.6 m s<sup>-1</sup> (Fig. 2.12). The poor results in the 16–18 m s<sup>-1</sup> wind speed bin can be explained by the low amount of data (six dives), all of which were recorded during one single event on 1 April. The buoy measurements during this event show a 6-h-long plateau at 17.0 m s<sup>-1</sup> exactly that could suggest an anemometer failure (Fig. 2.12).

**Table 2.5:** Parameters of the wind speed derivation two-regime linear models for the Lion, MooseT00\_23, and MooseT00\_25 datasets.

	Lion	MooseT00_23	MooseT00_25
For $U_{10} < 11 \text{ m s}^{-1}$			
$b_{low}$ ( $\mu\text{Pa}$ )	$-0.2 \times 10^4$	$0.2 \times 10^4$	$-0.5 \times 10^4$
$s_{low}$ ( $\mu\text{Pa m}^{-1} \text{ s}$ )	$0.4 \times 10^4$	$0.3 \times 10^4$	$0.4 \times 10^4$
$R^2$	0.88	0.85	0.88
For $U_{10} > 9 \text{ m s}^{-1}$			
$b_{high}$ ( $\mu\text{Pa}$ )	$-12.5 \times 10^4$	$-4.4 \times 10^4$	$-13.1 \times 10^4$
$s_{high}$ ( $\mu\text{Pa m}^{-1} \text{ s}$ )	$1.6 \times 10^4$	$0.8 \times 10^4$	$1.4 \times 10^4$
$R^2$	0.95	0.96	0.97
$U_{lim}$ ( $\text{m s}^{-1}$ )	10.4	10.3	11.7
$p_{lim}$ ( $\mu\text{Pa}$ )	$4.5 \times 10^4$	$3.6 \times 10^4$	$3.7 \times 10^4$

The noticeable differences in the absolute values of the parameters (Table 2.5) can be explained by differences between the two Acousonde sensors used, and by the unavoidable variation in sound level with the orientation of the recorder in each deployment. The internal layout of the Acousonde makes it asymmetrical, with the electronic board likely to affect the measurements of the sounds coming from one side. Its cylindrical shape makes it difficult to accurately position the electronic board between the transducer and the glider’s hull. This inter-deployment sensitivity variability is believed to be responsible for the quantitative differences between our three experiments. Despite this variability in absolute sound level, these results show that once calibrated with buoy data, a relative sound level can be used and produces consistent results.

The recent availability of PAM sensors integrated into ocean gliders should reduce this inter-deployment sensitivity variability. Being able to calibrate the whole PAM/glider system in situ once, knowing that the sensitivity will be the same for each following deployment, will allow using the PAM glider for wind speed estimation in areas where in situ calibration data are not available.

The method we propose here is based on relative sound pressure levels. Building a similar model using absolute sound pressure levels would improve the method, since it would negate the need for a specific in situ calibration, although the consistency of these absolute measurements (e.g., for different sensor orientations) would need to be tested.

## 2.7 Discussion

The adaptation of the WOTAN technique (Vagle *et al.*, 1990) to recordings from ocean gliders provides wind speed measurements with long endurance, large spatial coverage, and resilience to severe weather conditions. During this study, we were able to collect data without maintaining ship presence during several high wind speed events. Previous studies were mostly limited to wind speeds below  $15 \text{ m s}^{-1}$  (Table 2.2), so they were unable to successfully characterise higher wind speeds. The significant amount of high wind speed conditions encountered during this experiment allows us to propose a model extending the WOTAN technique measurement range to strong wind conditions, up to  $21.5 \text{ m s}^{-1}$ . No evidence of an upper limit of our model, where the sound at 3 kHz would be attenuated, has been found here. Further experiments are necessary to determine whether this critical wind speed exists. The positions of the meteorological buoys relative to the coast and the direction of the main winds limits the fetch to 100 km at the Lion buoy, and 50 km at the Azur buoy. This does not allow a fully developed sea at wind speed higher than 10 and  $7 \text{ m s}^{-1}$  at the sites Lion and Azur, respectively. Future experiments in the open ocean (e.g., Southern Ocean) will provide more data at high wind speed and with unlimited fetch, which will allow studying the impact of sea state on the wind noise and assessing the validity of our model at high wind speed.

The use of sound pressure level at 3 kHz in this study was driven by the instrument self noise at  $\sim 2 \text{ kHz}$  and the possible contamination by traffic noise at lower frequencies on one side, and the limitations observed for the high frequencies at high wind speeds on the other side. It is however not necessary to focus on this specific third octave band. Moreover, monitoring higher wind speed conditions than the ones presented here may necessitate the use of multiple frequencies. At high wind speeds, lower frequencies maintain a linear response to wind speed, while higher frequencies show decreasing amplitude/intensity/power with increasing wind speed. Further work is required to constrain the relation between higher frequencies and high wind speeds in relation to sea surface physical parameters (sea state, wave age, energy flux...). In the particular case of surface wind speed estimation, the use of  $p_{3kHz}$  for wind speeds up to  $25 \text{ m s}^{-1}$ , and  $p_{500Hz}$  for higher wind speeds, when wind-generated noise is loud enough to prevent masking by shipping noise, could be considered, allowing a wide wind speed range to be monitored.

This paper focuses on providing submesoscale measurements of surface wind speed combined with oceanographic profiles. We recorded 1 min every 10 min, and considered the median of the acoustic measurements to provide a robust wind speed estimation for the duration of each glider profile — in this case measured every 2 h and 2 km. This method allows the acquisition of high-resolution in situ forcing data, in weather conditions or locations of interest (e.g., storms, remote regions) for numerical models and satellite calibration (Schmidt *et al.*, 2017). Recent progresses in the integration of PAM sensors into ocean gliders now enables continuous recording during a monthlong glider campaign (limited by the glider's battery). The variation of the listening area with the depth of measurement (Vagle *et al.*, 1990) can be used to choose to measure wind speed over different spatial scales. For example, limiting the glider measurements to the upper 100–200 m would enable monitoring of a sea surface area of 0.1–0.5 km<sup>2</sup>, hence studying of smaller-scale processes than with typical 1000 m glider dives (e.g., land sea breezes, transient events). Continuous sampling throughout the glider dive, combined with sound speed and attenuation profiles measured by the glider, will allow better evaluation of the vertical distribution of ambient noise.

The combination of surface wind speed measurements with glider oceanographic profiles allows better observation and quantification of air–sea interaction processes, and monitoring of the associated processes in the ocean. Surface wind speed measurements allow correction of the bulk SST to obtain skin SST values, which are fundamental for the quantification of air–sea interaction processes (Alappattu *et al.*, 2017). Heat and freshwater transport can be monitored from the air–sea interface to the water column, linking heat content changes in the ocean to meteorological events (Grist *et al.*, 2016).

Wind noise is caused by complex physical processes, such as wave breaking and bubble inclusion (Wenz, 1962), driven by weather, sea surface conditions, and history. As a first approximation, we estimate the instantaneous surface wind speed from measurement of wind noise. We believe that further experiments (e.g., glider campaigns together with surface processes monitoring) could improve the wind speed estimation, by accounting for more contributing parameters (wind duration, MABL stability, sea state, fetch...). Also, we could evaluate the ability to directly monitor physical parameters (whitecap coverage, bubble creation rate, airflow separation, spume drop production...) through analysis

of ambient noise recorded by gliders. Such direct measurements would significantly improve the quantification of air-sea gas exchanges (Garbe *et al.*, 2014), bubble-mediated carbon exchange (Monahan and Dam, 2001), heat and moisture fluxes (Andreas *et al.*, 2015), and sea salt aerosol production fluxes (Lewis and Schwartz, 2004).

Onboard processing (e.g., TOL extraction, event detection) and real-time transmission of the data via Iridium connection will make it possible to detect targeted events (e.g., storm, rainfall) and trigger an adaptation of the sampling behaviour to improve the observations. For example, fast and shallow dives during a storm or a rainfall event would increase the sampling resolution (Lee *et al.*, 2012) of its effects on the water column (e.g., internal waves, mixing, freshwater input). The route of the glider can also be adapted to better sample a targeted event (e.g., along-track or cross-track sampling). For future deployments, we suggest that in situ calibration of the PAM glider should be performed at the beginning of each deployment. Deploying the PAM glider at the surface from a small boat, next to a calibrated hydrophone, in various noise conditions (e.g., engine on / off) should be sufficient to allow the acquisition of absolute sound levels. Also, the use of an integrated PAM sensor will reduce the inter deployment variability in the positioning of the sensor, and therefore allow use of the same in situ calibration for multiple deployments.

## 2.8 Conclusion

Surface wind speed can be measured remotely, derived from underwater acoustic measurements. The proposed two-regime linear model yields improved results in high wind speed conditions, extending the wind speed range to 2–21.5 m s<sup>-1</sup>. The PAM sensor can be mounted on an ocean glider, diving from the surface to 1000 m deep, thus allowing the surface wind speed measurements to be combined with the oceanographic profiles (e.g., temperature, salinity). These PAM glider observations provide high-resolution, frequent, and localised in situ data for forcing numerical models and improving the understanding of the air–sea–climate system.

## **Chapter 3**

# **Sperm whale presence observed using passive acoustic monitoring from gliders of opportunity**

This section was published in in a peer-reviewed journal prior to the submission of the thesis. No changes have been made but re-formatting in a thesis format.

Cauchy, P., K. J. Heywood, D. Risch, N. D. Merchant, B. Y. Queste, and P. Testor (2020), Sperm whale presence observed using passive acoustic monitoring from gliders of opportunity, *Endangered Species Research*, 42, 133–149. <https://doi.org/10.3354/esr01044>

PC carried out the research and prepared the paper. KJH, DR, NDM, BYQ and PT supported the research, provided feedback on earlier drafts of the paper and approved the final version to be published.

### **3.1 Abstract**

Habitat use of the endangered Mediterranean sperm whale subpopulation remains poorly understood, especially in winter. The sustained presence of oceanographic autonomous underwater vehicles in the area presents an opportunity to improve observation effort, enabling collection of valuable sperm whale distribution data, which may be crucial to their conservation. Passive acoustic monitoring loggers were deployed on vertically-profiling oceanographic gliders surveying the north-western Mediterranean Sea during winter 2012

– 2013 and June 2014. Sperm whale echolocation usual click trains, characteristic of foraging activity, were detected and classified in the recordings, providing information about presence of sperm whale along the glider tracks. Widespread presence of sperm whales in the north-western Mediterranean Sea was confirmed. Winter observations suggest different foraging strategies between the Ligurian Sea, where mobile and scattered individuals forage at all times of day, and the Gulf of Lion, where larger aggregations target intense oceanographic features in the open ocean such as fronts and mixing events, with reduced acoustic presence at dawn. This study demonstrates the ability to successfully observe sperm whale behaviour from passive acoustic monitoring gliders. We identify possible mission design improvements that would lead to benefit from passive acoustic monitoring glider surveys to significantly improve sperm whale population monitoring and habitat use.

### 3.2 Introduction

Sperm whales (*Physeter macrocephalus*) are widespread across the Mediterranean Sea (Gannier *et al.*, 2002; Drouot *et al.*, 2004c; Frantzis *et al.*, 2011; Notarbartolo-Di-Sciara, 2014; Carpinelli *et al.*, 2014; Lewis *et al.*, 2018) and constitute an isolated subpopulation, genetically distinct from the Atlantic population (Drouot *et al.*, 2004a; Engelhaupt *et al.*, 2009). The Mediterranean sperm whale subpopulation contains fewer than 2500 mature individuals (Notarbartolo-Di-Sciara, 2014) and is considered as 'Endangered' by the International Union for Conservation of Nature (IUCN) (Notarbartolo-di Sciara *et al.*, 2012). Anthropogenic pressures on this subpopulation include bycatch in fishing gear (Notarbartolo-di Sciara, 1990; Notarbartolo-di Sciara *et al.*, 2004), ship strike (Carrillo and Ritter, 2010; Frantzis *et al.*, 2019), ingestion of marine debris (de Stephanis *et al.*, 2013) and disturbance by anthropogenic noise (Frantzis *et al.*, 2003; Weir, 2008) and whale watching activities (Gordon *et al.*, 1992; Notarbartolo-di Sciara *et al.*, 2008). Sperm whale distribution in the Mediterranean Sea is non-uniform (Gannier *et al.*, 2002; Boisseau *et al.*, 2010) and influenced by oceanographic (e.g. fronts, upwellings, primary production) and topographic features (e.g. steep slopes, sea mounts) (Cañadas *et al.*, 2002; Gannier *et al.*, 2002; Gannier and Praca, 2007; Praca and Gannier, 2008; Praca *et al.*, 2009; Pirota *et al.*, 2011, 2019; Frantzis *et al.*, 2014; Virgili *et al.*, 2019). Information on

the ecology of the Mediterranean sperm whale subpopulation remains sparse and does not meet the needs of conservation managers and policy makers (Pace *et al.*, 2014). Broader surveys are needed, increasing observation effort in non-summer months in particular (Mannocci *et al.*, 2018) to better understand the seasonality in habitat use, and identifying key seasonal habitats to allow appropriate management of shipping and fishing activities (Rendell and Frantzis, 2016).

Sperm whales are highly vocal, producing four distinct types of clicks both for echolocation and social interaction purposes. When socializing at the surface, they use short stereotyped sequences of clicks, called codas, to maintain cohesion in a group (Weilgart and Whitehead, 1993) and mature male sperm whales produce slow clicks of lower frequency and longer inter-click interval (Weilgart and Whitehead, 1988). When foraging, they produce extremely powerful and highly directional usual clicks (Møhl *et al.*, 2000; Wahlberg, 2002; Zimmer *et al.*, 2005) punctuated by lower intensity and shorter inter-click interval creak clicks during prey capture (Madsen *et al.*, 2002; Miller *et al.*, 2004). Sperm whales spend a substantial amount of their time foraging. When in a foraging cycle, they produce usual clicks during 60 % of the time (Watwood *et al.*, 2006; André *et al.*, 2017), starting at a depth of 100 to 200 m at the beginning of the dive, until the beginning of the ascent phase (Madsen *et al.*, 2002; Watwood *et al.*, 2006). Usual clicks are emitted in series of tens to hundreds (Wahlberg, 2002), in a 10 Hz – 30 kHz frequency band with an inter-click interval varying from 0.5 to 2 seconds (Madsen *et al.*, 2002; Møhl *et al.*, 2003). Usual clicks provide a reliable indicator of sperm whale presence and foraging activity (Whitehead, 2003; Stanistreet *et al.*, 2018) and their specific features allow them to be identified and detected up to a distance of 4 to 20 km (Gannier *et al.*, 2002; Barlow and Taylor, 2005; André *et al.*, 2017; Miller and Miller, 2018).

Passive acoustic survey methods have significantly improved over recent decades and are now commonly used in cetacean observation (Pavan *et al.*, 2008; Van Parijs *et al.*, 2009; Samaran *et al.*, 2010; Au *et al.*, 2014; Caruso *et al.*, 2015; André *et al.*, 2017; Miller and Miller, 2018). Unlike more traditional visual survey methods, passive acoustic techniques offer sustained observations during nighttime and adverse weather conditions (Barlow and Taylor, 2005; Mellinger, 2007; Van Parijs *et al.*, 2009) and when the whales are sub surface. In the specific case of sperm whale detection, highly vocal and deep

divers, combined visual and acoustic surveys found that acoustic techniques are much more efficient than visual techniques, as sperm whales were always first detected acoustically (Boisseau *et al.*, 2010).

Ocean gliders are autonomous underwater vehicles, carrying various payloads to monitor the ocean. They provide high resolution ( $\sim 2$  h,  $\sim 2$  km) hydrographic profiles (Testor *et al.*, 2010; Rudnick, 2016), performing long autonomous missions (several months to a year, and several thousand km) unaffected by extreme weather events. They are highly suitable for passive acoustic monitoring (hereafter PAM), quietly gliding unpropelled through the water column and collecting information on the acoustic properties of the water column. PAM sensors have been successfully deployed on ocean gliders for weather observation (Cazau *et al.*, 2019; Cauchy *et al.*, 2018) and for cetacean monitoring purposes (Moore *et al.*, 2007; Baumgartner and Fratantoni, 2008; Klinck *et al.*, 2012; Baumgartner *et al.*, 2013).

This paper presents a case study on the ability to use PAM glider observations as a tool to study sperm whale habitat use. We added PAM sensors to oceanographic gliders deployed in the north-western Mediterranean Sea during winter 2012 – 2013 in the framework of the DEWEX experiment (Testor *et al.*, 2018) and summer 2014 within the REP14-MED experiment (Onken *et al.*, 2018), recording a total of five months of acoustic data along 3200 km of glider tracks. We focused on the detection of sperm whale usual clicks to monitor their presence along the glider tracks. We identified 39 distinct encounter events with one or more sperm whales, along the slopes and in the open ocean, in the Ligurian Sea, the Sea of Sardinia, and the Gulf of Lion.

### **3.3 Materials and Methods**

#### **3.3.1 Instrumentation and field operations**

The platforms we used in this study are the Slocum glider, developed by Teledyne Webb Research, and the Seaglider, developed by the University of Washington and distributed by Kongsberg. They are autonomous underwater vehicles driven by buoyancy changes, controlled by pumping oil into and out of a swim bladder, inducing a vertical motion in the water column, from the surface down to 1000 m depth. Fixed wings convert the

vertical velocity into forward velocity. Internal battery displacements enable pitch and roll management for direction changes. This novel way of propulsion, performing successive V-shape dives along a pre-defined trajectory, makes it a very quiet platform between the oil pumping phases that occur at the apogee and perigee of each dive (every  $\sim 2$  h for 1000 m dives), able to cover  $\sim 20$  km per day for up to 6 months. Along with the PAM sensor, the gliders were typically equipped with integrated temperature, salinity, pressure, oxygen, turbidity and chlorophyll fluorescence sensors.

The Slocum gliders were equipped with an externally mounted Acousonde B003A-HF data logger, developed by Greenridge Sciences Inc (Fig. 3.1). The Acousonde is a self-contained underwater acoustic recorder comprising two hydrophones, sensors for attitude, orientation, depth and temperature, a digital recorder, and a field-replaceable battery (Burgess, 2010). The core of the sensor consists of a high frequency hydrophone (capable of sampling up to 232 kHz), with a sensitivity of  $-204$  dB re  $1 \text{ V } \mu\text{Pa}^{-1}$ . A 6-pole linear-phase anti-aliasing filter is used, with  $-3$  dB passband (12.5 kHz – 42 kHz) and  $-22$  dB at 100 kHz (Fig. A.2a). Data are stored on a 128 GB flash memory, with a 16-bit sampling resolution. An external 3-D-cell tethered battery pack allows up to 200 hours of recording. The Acousonde operates autonomously and has its own battery, memory and programmed mission. Data processing is undertaken after the sensor is recovered. Initially developed to be attached to marine mammals (Cazau *et al.*, 2017), it has also been used on ocean gliders (Nott, 2015; Cauchy *et al.*, 2018).

The Seaglider was equipped with an integrated Seaglider PAM system (Fig. 3.1). This acoustic data logger is made of an HTI-92-WB hydrophone, developed by High Tech Inc., with a sensitivity of  $-165$  dB re  $1 \text{ V } \mu\text{Pa}^{-1}$ , associated with a WISPR v1.1 digital signal processing board with Analog Devices BF537E Blackfin CPU and HM1 digital preamplifier developed by Embedded Ocean Systems. The frequency response of the preamplifier board is designed to be approximately equal to the inverse of typical deep-water ambient noise (Matsumoto *et al.*, 2015) (Fig. A.2b). The sampling frequency is fixed at 125 kHz, and the data are stored on a 512 GB flash memory, with a 24-bit maximum sampling resolution.

The glider missions took place in the north-western Mediterranean basin. The PAM equipped Slocum gliders were deployed within the frameworks of Mediterranean Ocean

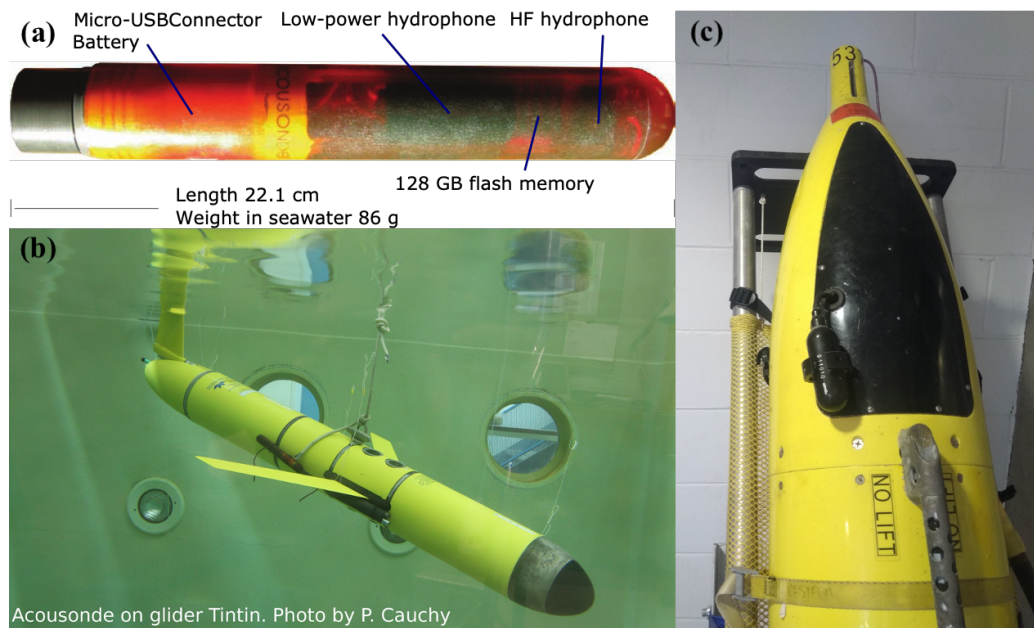


**Figure 3.1:** (a) Internal layout of the Acousonde and (b) experimental setup, externally attached on a Slocum glider in the ballasting tank. (c) Seaglider integrated PAM unit. Only the sensor can be seen outside the hull, the electronics is integrated in the glider’s pressure housing.

Observing System for the Environment (MOOSE, <http://www.moose-network.fr>) and the Deep Water Experiment (DEWEX) (Testor *et al.*, 2018). MOOSE offers year-long coverage of repeated sections to monitor oceanographic variability of the north-western Mediterranean basin over a continuum of spatial and temporal scales to assess the evolution of the oceanic circulation and the anthropogenic impacts. DEWEX was targeted at better understanding the dynamics of the vernal bloom that occurs in this region after deep convection events in winter. Slocum glider ”Tintin” was deployed twice in the middle of the Pelagos Sanctuary, a Marine Protected Area created to protect marine mammals (Notarbartolo-di Sciara *et al.*, 2008). It followed a predefined transect crossing the Ligurian Sea, (Fig. 3.2, Fig. 3.3). Slocum glider ”Hannon” was deployed twice along a predefined transect covering the open ocean across the Gulf of Lion and the westernmost slopes of the basin (Fig. 3.2, Fig. 3.3). Each of these transects includes a mooring site, DYFAMED/Azur (43.39 °N, 7.84 °E) and LION (42.06 °N, 4.64 °E) respectively, with permanent presence of a meteorological buoy and a mooring line equipped with oceanographic sensors at several depths. For consistency, these transects will be called Gulf of Lion (glider missions GoL1 and GoL2) and Ligurian Sea (glider missions LS1 and LS2), and the associated mooring sites Lion and Azur. Seaglider SG524 ”Kong” was deployed within the REP14-MED experiment, aiming to demonstrate methods for the rapid characterisation of the marine

	2012		2013					...	2014
Mission	Dec	Jan	Feb	Mar	Apr	May		Jun	
GoL1	█								
GoL2		█	█						
LS1		█	█						
LS2					█				
SoS								█	

**Figure 3.2:** Time coverage of the glider missions in the Gulf of Lion (blue), Ligurian Sea (green) and Sea of Sardinia (orange).

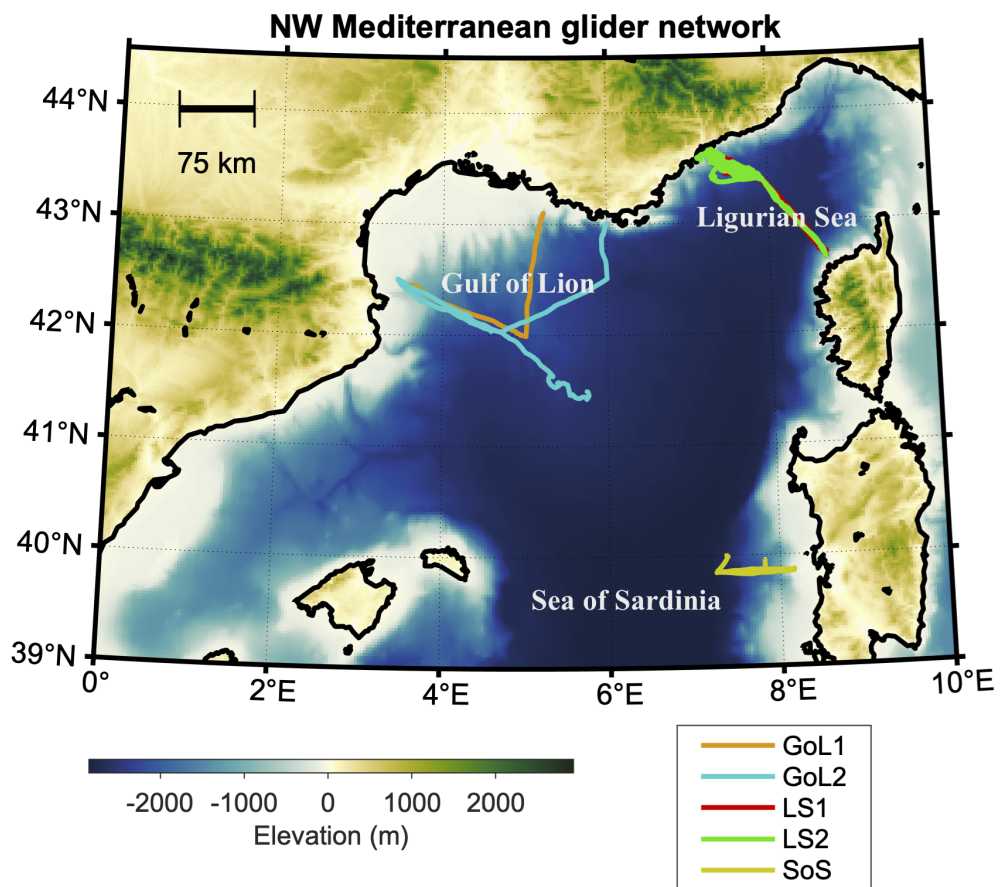


**Figure 3.3:** Map of the glider tracks. Glider missions GoL1 and GoL2 follow a predefined transect across the Gulf of Lion; Glider missions LS1 and LS2 follow a predefined transect across the Ligurian Sea; Glider mission SoS is in the Sea of Sardinia, off the Sardinian coast.

environment using a fleet of gliders (Onken *et al.*, 2018). It followed a repeated cross shelf zonal transect at latitude  $39^{\circ} 51' N$ , off the western coast of Sardinia in June 2014 (Fig. 3.2, Fig. 3.3), hereafter called Sea of Sardinia (glider mission SoS).

### 3.3.2 Acoustic data sampling and processing procedure

The four MOOSE PAM glider missions (GoL1, GoL2, LS1 and LS2) were designed for Weather Observation Through Ambient Noise (WOTAN) purposes and to optimise the

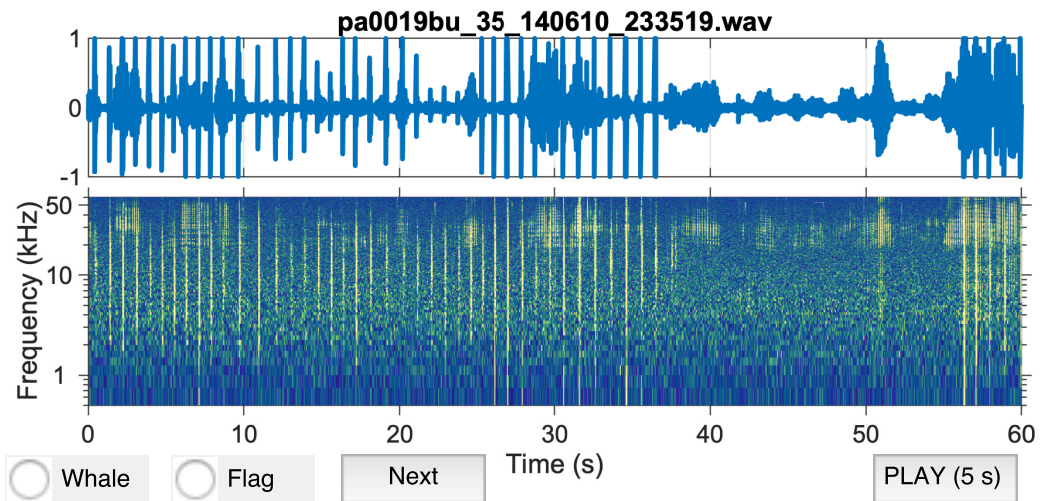
battery and memory usage (Cauchy *et al.*, 2018). The Acousonde loggers were configured to record one minute every ten minutes, at a sampling frequency of 50 kHz. This setup saved battery, enabling a tenfold increase in the monitoring duration (compared to continuous recording) to match the duration of the glider mission, and produced 27 GB of data every month. The PAM equipped Seaglider of the SoS mission was configured to record continuously throughout the glider deployment, at a sampling frequency of 125 kHz, collecting 250 GB of data in 14 days.

The recordings made when the glider is sitting at the surface are contaminated by splash sounds coming from the interaction of the glider hull with the sea surface, and the sensor oscillating between air and water. Water turbulence around the sensor induces flow noise at low frequencies, related to the glider's speed (Erbe *et al.*, 2015; Dos Santos *et al.*, 2016), with no discernible effects at the sound level and frequency range of sperm whale click trains. In addition, self-noise generated by the glider comes from four identified behaviours: adjustment of the battery position for attitude (pitch and roll) management, rudder movements for heading adjustment (Slocum glider only), modification of the bladder volume for buoyancy management, and use of the altimeter. Using the metadata provided in the glider log files, we extracted the information about noise-generating behaviours of the glider and removed the contaminated samples from the recorded acoustic data. During the missions described here, the glider spent on average 13.1 % of the time at the surface (depth <5 m). When underwater (depth >5 m), the glider was quiet 96.7 % of the time (Table 3.1). The amount of usable data, when the glider was in a quiet gliding phase, represents 84 % of the total deployment time. It is worth noting that the SoS dataset, collected using a Seaglider, presents a lower rate of quiet gliding time (74.8 %). The frequent battery movements performed during each dive for heading adjustment are the source of this increased self-noise generation. The frequency of such manoeuvres can be modified by the pilot, whether the focus is on accurate navigation or low noise emission or power consumption.

The recordings were processed manually to identify sperm whale *usual click* trains using a graphical user interface developed in Matlab (Fig. 3.4). This tool provides two visual representations of the acoustic signal, spectrogram (40 ms Hann window, 4 ms overlap, 100 Hz frequency bands) and waveform, on which to detect sperm whale *usual*

**Table 3.1:** Deployment area, platform and PAM sensor used, duration, time spent underwater and free from self-noise for glider missions GoL1, GoL2, LS1, LS2 and SoS.

Glider mission	GoL1	GoL2	LS1	LS2	SoS
Deployment area	Gulf of Lion		Ligurian Sea		Sea of Sardinia
Platform	Slocum				Seaglider
Sensor	Acousonde				Integrated
Days deployed	15.9	29.8	51.0	33.9	13.9
Days underwater (>5 m)	13.8	25.9	45.2	28.7	11.9
Days quiet	13.5	25.5	44.1	27.8	10.4
Days quiet (%)	84.9	85.6	86.5	82.0	74.8

**Figure 3.4:** Graphical user interface used for visual 2 annotation of the acoustic files. Top panel shows the acoustic signal recorded as a waveform, the bottom panel as a spectrogram (40 ms Hann window, 4 ms overlap, 100 Hz frequency bands). The operator is given the opportunity to zoom in on both panels, select and play a 5 s audio sample if needed. On this example, the wide-band high-intensity sperm whale clicks trains, at  $\sim 0.5$  s click interval, are easily identified even in the presence of dolphin sounds (narrower frequency band, higher frequency and click rate, higher time variability).

*click* trains. *Usual click* trains are wide-band, high-intensity with a regular  $\sim 0.5$  s click interval, easily identified even in the presence of other cetacean clicks (e.g. dolphin) (Fig. 3.4). The opportunity to listen to the audio was also given to the operator to dispel doubt when necessary. Each file was annotated with information of presence or absence of sperm whale clicks, and a flag added in case of identified anthropogenic noise (ship sonar, acoustic communication, acoustic trial). The whole dataset has been processed by the same operator. For quality control purposes, a second operator processed a randomly selected subset of each dataset, representing 20 % of the glider dives, using the same tool. The classifications from the two operators agreed for 95 % of the files (Table A.1).

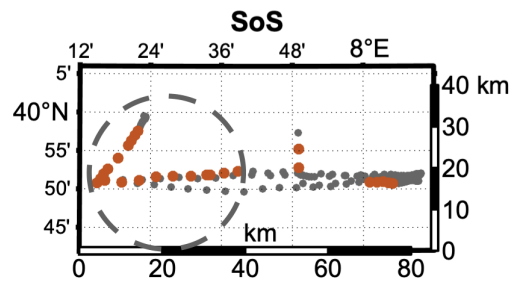


**Figure 3.5:** Schematic of footprint estimation, using as an example the first encounter with sperm whales during glider mission SoS. Glider dive locations are represented by orange dots when a sperm whale was detected, dark otherwise. The estimated footprint of the encounter is the diameter of the dashed circle, 39 km.

The files recorded between two successive glider surfacing phases were then regrouped as a single glider dive, annotated as containing sperm whale clicks if a dive contained at least one file with identified presence of sperm whale clicks. Finally, we defined as an encounter an uninterrupted succession of glider dives with identified sperm whale presence. For each encounter, the duration (in hours) of the event was noted, the footprint of the encounter was estimated as the largest distance between two glider positions during the encounter (Fig. 3.5), and a categorisation as an aggregation or single individual was made. As it is not possible to get bearing information from a single hydrophone, it is difficult to differentiate sounds from several animals. We decided to limit our analysis to the identification of a single whale or an aggregation of multiple individuals. We defined as an aggregation the simultaneous detection of multiple individuals, acoustically identified as the overlap of two or more distinct sperm whale *usual click* trains.

The detection range of sperm whale echolocation clicks has been estimated to be 4 to 20 km, from moored hydrophones or towed hydrophones (Gannier *et al.*, 2002; Barlow and Taylor, 2005; Hildebrand *et al.*, 2013; André *et al.*, 2017; Miller and Miller, 2018). In the case of glider surveys, there are no independent observation data available to estimate the detection range. The limitations in weight, size and power necessitate the use of a hydrophone of reduced sensitivity that affects the detection capacity of the system. We can therefore estimate our detection range to be no greater than the observed range from moored and towed instruments. This uncertainty does not affect our observation of the spatial and temporal distribution of sperm whale detections.

Underwater sound propagation is affected by variations in sound velocity, driven by

temperature, salinity and pressure changes. Long-range propagation can occur in the deep sound channel, with sounds being refracted around the depth of minimum sound velocity without reflection loss on the seabed or the surface (Munk, 1974). Measurements taken by the gliders provide contemporaneous knowledge of the local sound speed profile (0 – 1000 m), allowing estimation of its effects on sound propagation. We linearly extrapolated the sound speed profile to the full depth of the basin (2300 m) to model the refraction of acoustic rays. We modelled the propagation across depth layers of varying sound speed for acoustic rays emitted at multiple angles by sources at depths of 300 m and 1000 m (Jensen *et al.*, 2011). The average sound speed profile observed during our winter surveys is characterised by a continuous positive gradient, refracting sounds towards the surface (Fig. 3.6). Within the estimated detection range of sperm whale echolocation clicks (<20 km), we expect no observable effect of the recording depth on the detection range of sperm whale clicks (Fig. 3.6). The sound speed profile observed in June shows a strong negative gradient near the surface, a minimum around 100 m, then a continuous positive gradient to 1000 m, hence refracting up and down all sound emitted within 0 – 1000 m depth and possibly extending the detection range of sperm whale clicks (Fig. 3.6).

### 3.3.3 Estimation of the mixed layer depth

Mixed layer depth is a metric commonly used in physical oceanography studies to quantify vertical homogeneity of the water column. Estimation of the mixed layer depth was made from measurements of potential temperature collected by the gliders, detecting strong temperature gradients along each vertical profile. We used a double criterion, looking for gradients greater than  $\Delta T1 = 0.1$  °C with the reference temperature at 10 m in the upper 300 m of the water column, and gradients greater than  $\Delta T2 = 0.01$  °C with the reference temperature at 300 m when the mixed layer depth exceeds 300 m, to account for smaller temperature gradients in the deeper layers. This method was described in a previous study using some of the same glider data sets, focusing on deep convection events in the Gulf of Lion during 2007 – 2013 (Houpert *et al.*, 2016).

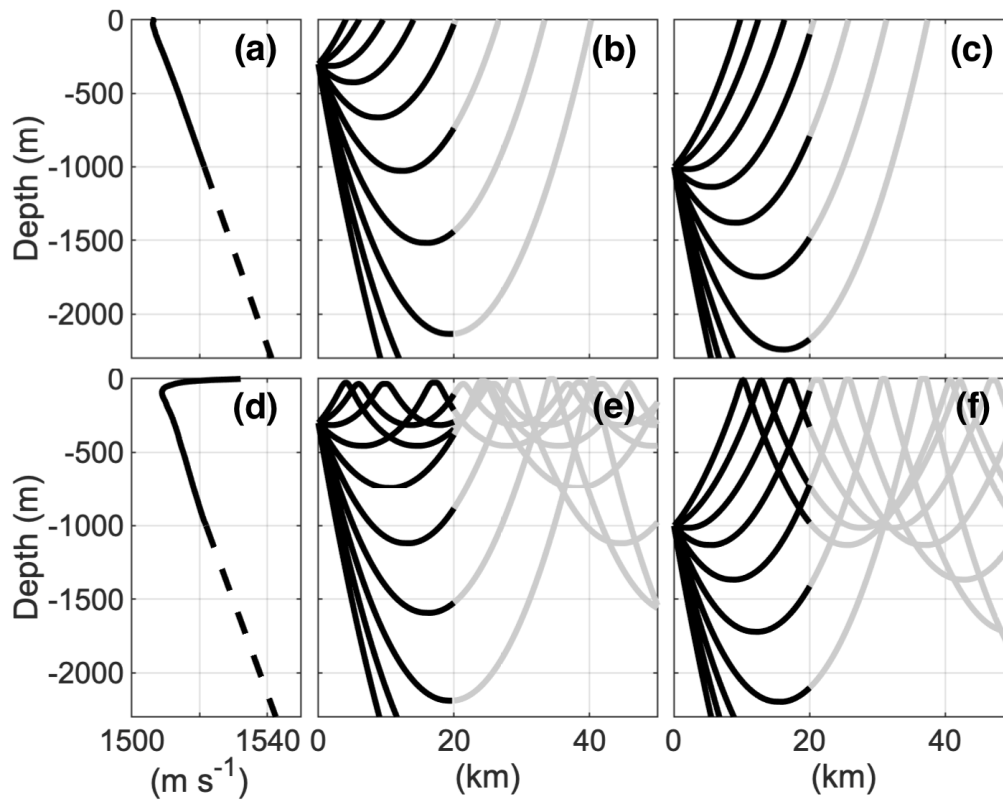


**Figure 3.6:** Average sound velocity profiles calculated from glider temperature and salinity profiles in winter (a) and summer (d), and associated effects on the refraction of sounds emitted at 300 m (b, e) and 1000 m (c, f). Only the direct paths are shown (no reflection). The linear extrapolation of the sound velocity profile at depth greater than 1000 m is shown as a dashed line. The acoustic rays are in black within the empirical sperm whale detection range (<20 km) and grey outside (>20 km).

### 3.3.4 Definition of detection ratios

Observation effort was not evenly distributed with regards to location, time of day or depth, due to specificities of the mission design and glider behaviour. The GoL and LS glider surveys were specifically designed with an increased sampling effort at the oceanographic mooring Azur and Lion locations for calibration purposes. When surveying waters shallower than 1000 m, gliders need to interrupt their dives before reaching their usual dive depth (1000 m), which results in a number of recorded samples decreasing with depth.

To analyse the spatial distribution of sperm whale detections with regards to distance travelled along a glider track, we defined a detection ratio corrected for uneven geographic sampling, as the ratio between the number of dives with sperm whale detected and the total number of dives in each 5-kilometre distance bin. To analyse distribution of sperm whale

acoustic presence with regards the time of day, we defined the detection ratio as the ratio between the number of files with detected sperm whale acoustic presence and the total number of samples recorded in glider quiet gliding phases in each 1-hour bin. To analyse the distribution of sperm whale click detection with regards to measurement depth, we defined the detection ratio as the ratio between the number of files with detected sperm whale acoustic presence and the total number of files recorded in glider quiet gliding phases in each 100 m depth bin. We considered only the samples collected during a sperm whale encounter.

### 3.3.5 Statistical analysis

We used generalised additive models (GAM) to assess the statistical significance of our observations. We used R version 3.6.1 (R Core Team, 2019) and the package *geepack* (Halekoh *et al.*, 2006), to fit binomial GAMs, with logit link function and working independence model (Pirodda *et al.*, 2011). For the analysis of the distribution sperm whale presence at the scale of a glider dive, we considered each encounter as an independent block. For the analysis of sperm whale presence at the scale of an acoustic file (1 minute), we considered each glider dive as an independent block. Statistical significance of each variable was assessed using a Wald's test.

### 3.3.6 Glider mission SoS

Glider mission SoS was part of the wider REP-14MED experiment (Onken *et al.*, 2018). Acoustic trials were conducted during the REP14-MED experiment, overlapping with the glider mission and in the same geographical area. Acoustic sources, emitting repeated multi-tonal continuous wave pulses and linear frequency modulation pulses in the 300 – 4000 Hz frequency range, were towed from 12 to 20 June 2014 by NATO Research Vessel Alliance (Jiang, 2016). These can be detected on the glider acoustic recordings. Our observations do not provide enough information to study the behavioural response of sperm whale to the acoustic trials. Such a study would require measurement of the sound level received by an individual whale, and the ability to track the individual before, during and after exposure, usually obtained by tagging the whale with a PAM sensor (Curé *et al.*, 2016). However, sperm whale behaviour is likely to be affected by such a nearby

**Table 3.2:** Number of files and dives available for analysis and with identified sperm whale click detected, for glider missions GoL1, GoL2, LS1, LS2 and SoS.

	GoL1	GoL2	LS1	LS2	SoS
Number of available files	1970	4350	6088	4114	5130
Files with click detection	55	214	54	102	586
Files with click detection (%)	2.8	4.9	0.9	2.5	11.4
Number of dives	139	276	560	456	168
Dives with click detection	13	32	22	35	27
Dives with click detection (%)	9.4	11.6	3.9	7.7	16.1

contemporaneous acoustic trial. We considered our sperm whale observation as corrupted from 12 June 2014 onward.

PAM glider mission SoS is reduced to three days before the start of the acoustic trial and is our only dataset in summer season and in the Sea of Sardinia. We therefore kept it separated from other glider missions in our analysis.

## 3.4 Results

### 3.4.1 Opportunistic observations

The addition of PAM sensors to five opportunistic oceanographic glider campaigns in the north-western Mediterranean Sea allowed us to successfully detect sperm whale acoustic presence. Over the whole dataset, we identified 39 sperm whale encounters, five of which were aggregations of two or more individuals. These detections were made during 129 glider dives out of 1599, resulting in 1011 audio recordings containing sperm whale clicks (Fig. 3.7, Table 3.2, Table 3.3). These data confirm the widespread presence of sperm whales in the area (Gannier *et al.*, 2002; Drouot *et al.*, 2004c; Frantzis *et al.*, 2011; Notarbartolo-Di-Sciara, 2014; Carpinelli *et al.*, 2014). Sperm whales were encountered during 9.4 % and 11.6 % of glider dives during missions GoL1 and GoL2 in the Gulf of Lion, 3.9 % and 7.7 % of glider dives during missions LS1 and LS2 in the Ligurian Sea, and 16.1 % of glider dives during missions SoS in the Sea of Sardinia (Table 3.2).

**Duration** and footprint of the encounters were highly variable (Table 3.3), depending on the mobility and speed of both the whales and the glider. At an average whale transit speed of 3 km h<sup>-1</sup> (Drouot *et al.*, 2004b), a sperm whale would cross the acoustic



detection range (10 – 40 km diameter) in 3 – 13 h, which was the case for most of our encounters with single individuals (4.2 h average). In the case of stationary whales, a glider at a typical horizontal speed of  $0.8 \text{ km h}^{-1}$  would cross the detection range in 12 – 50 h. Encounters with aggregations tended to last longer (25.4 h on average) than encounters with single individuals, suggesting that sperm whale aggregations were less mobile or spread out over a wider area. Our definition of aggregation includes the simultaneous presence of several isolated animals in the same area, within the detection range of the PAM glider. This configuration would necessarily explain encounters of longer duration and larger footprint. In the specific case of encounter #3 of glider mission GoL1 (Table 3.3), the glider kept its position for 60 h, performing 'virtual mooring' dives, and was able to detect an aggregation of sperm whales for 11 h with a glider footprint of only 1 km (Table 3.3). The encounter #1 of glider mission SoS had a footprint of 53 km (Table 3.3), larger than our estimated detection range, which suggests that the aggregation was either scattered over a wide area or was moving along with the glider. We cannot eliminate the possibility that the whales were curious about the glider and followed it.

### **3.4.2 Repeated glider transects**

Our gliders repeatedly followed cross-shelf transects, providing information about sperm whale presence relative to the slope, defined as the closest -2000 m isobath. In the Gulf of Lion, glider missions GoL1 and GoL2 followed two cross-shelf transect lines, between the middle of the Gulf of Lion, and alternatively the northern and western slopes. Our observations show two modes of increased sperm whale presence, around  $\sim 30 \text{ km}$  and  $\sim 100 \text{ km}$  away from the slopes (Fig. 3.7, Fig. 3.8, Fig. 3.9). In the Ligurian Sea, glider missions LS1 and LS2 followed a cross-shelf transect line between two slopes, France to the north and the island of Corsica to the south. Our observations suggest an increased sperm whale presence within  $\sim 25 \text{ km}$  from the northern slope. Sperm whales were also found in the open ocean and along the southern slope (Fig. 3.7, Fig. 3.8, Fig. 3.9). Glider mission SoS followed a cross-shelf transect between the western coast of Sardinia and the open ocean. Our observations are reduced to one long-encounter with a large sperm whale aggregation, spread from the slope to the open ocean (Fig. 3.7, Fig. 3.8, Fig. 3.9). Predictions of the distribution of sperm whale presence with respect to distance

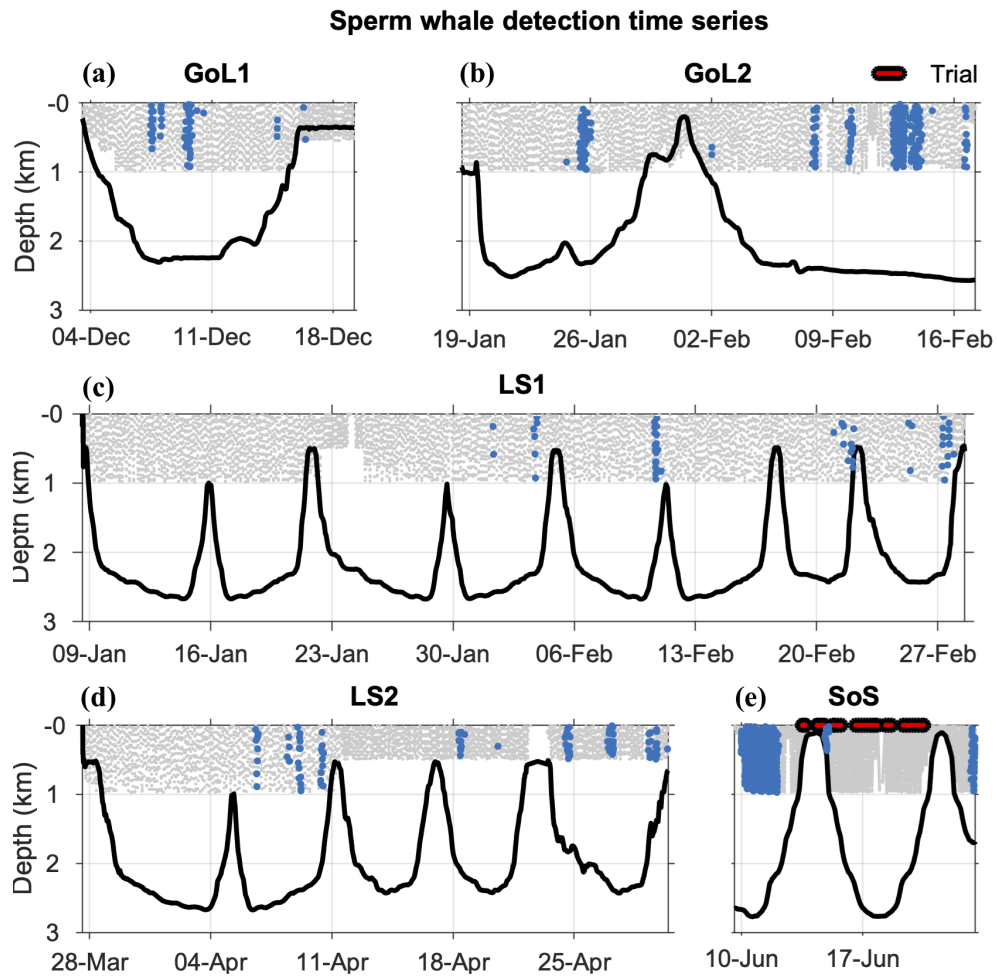


**Figure 3.8:** Time series of sperm whale click detections along each glider section, according to the depth of the detection and bathymetry. The time and depth of each recorded file is shown in grey when no whale is detected, in blue when a whale is detected. The bathymetry is shown, with the slope angle colour coded when the glider is on the slope. Detection of the REP14-MED acoustic trial activity is shown at the surface in red.

to the slope and associated  $p$  values for each of the three geographical areas studied are provided in the appendix (Fig. A.3).

### 3.4.3 Temporal patterns

Uninterrupted monitoring over weeks to months permits fine-scale observation of sperm whale acoustic activity. We studied the distribution of sperm whale presence with time of day, for each 1-minute file recorded by the gliders. In the Ligurian Sea, sperm whale clicks were detected at all times of day during both glider missions LS1 (Jan – Feb 2013) and LS2 (Apr 2013). In the Sea of Sardinia, sperm whale clicks were detected at all times of day during the glider mission (Jun 2014). In the Gulf of Lion, sperm whale acoustic

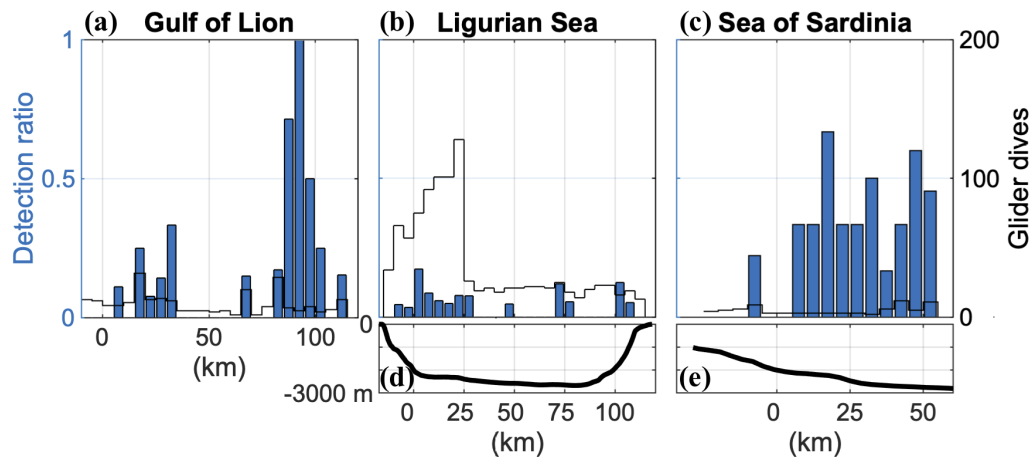


**Figure 3.9:** Number of glider dives with acoustic recording available for analysis (black line, black vertical axis) as a function of the distance to the slope in the Gulf of Lion (a), and along the repeated glider transect line in the Ligurian Sea (b) and the Sea of Sardinia (c). The bars (blue vertical axis) show the detection ratio (dives with sperm whale detection / total number of glider dives) in each 5-km distance bin. The bathymetry along the glider transect lines is shown for the Ligurian sea (d) and the Sea of Sardinia (e).

activity showed a clear circadian pattern, with decreased detection ratio at dawn, for both glider missions GoL1 (Dec 2012) and GoL2 (Jan – Feb 2013) (Fig. 3.10). Predictions of the distribution of sperm whale presence with respect to time of day and associated *p* values for each of the three geographical areas studied are provided in the appendix (Fig. A.4).

### 3.4.4 Large scale monitoring

Gliders are often deployed as a coordinated fleet, offering contemporaneous observations in multiple geographic areas. In the winter 2013 season, such monitoring was possible during the overlap between glider missions GoL2 and LS1 in Jan – Feb 2013 (Fig. 3.2). Aggregations of two or more individuals were encountered four times in the Gulf of Lion (Dec 2012 – Feb 2013) and only lone individuals were detected in the Ligurian Sea (Jan, Feb and April 2013) (Fig. 3.7, Table 3.3). It is worth noting that no sperm whales were detected during the three weeks sampled in January 2013.

### 3.4.5 Collocated oceanographic measurements

Temperature profiles collected from the gliders enable estimation of the mixed layer depth for each glider dive, used as an index to describe homogenisation of the water column.

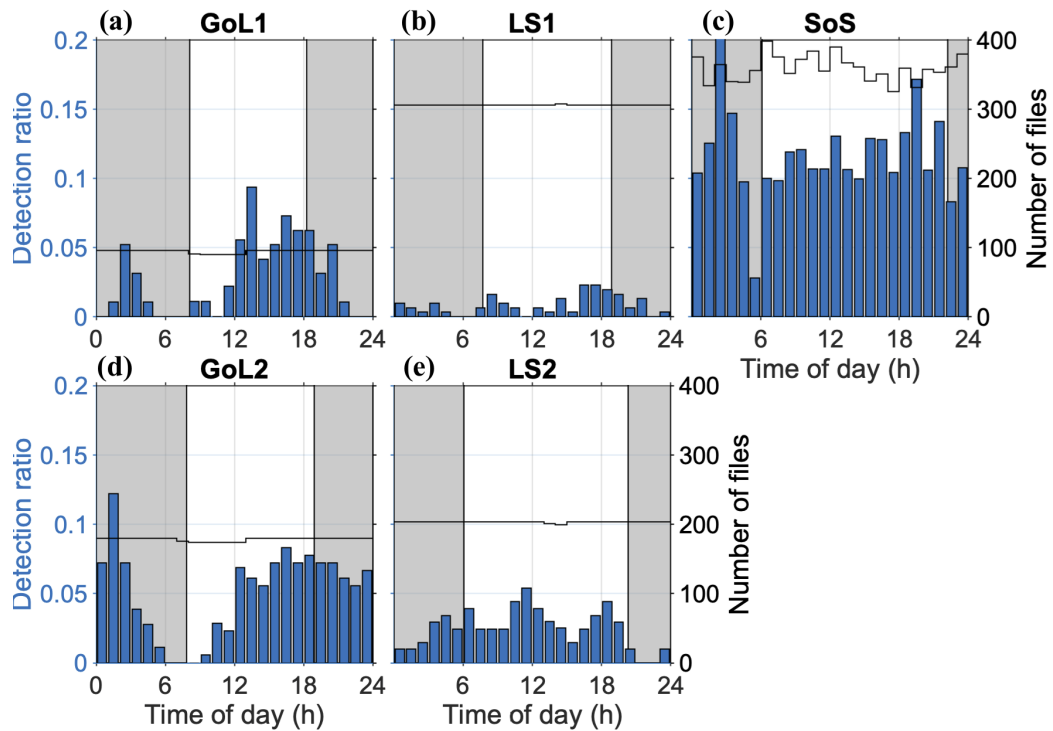


**Figure 3.10:** Number of acoustic files available for analysis (black line, right axis) per 1-hour bin. The bars (left axis) show the detection ratio (files with sperm whale detection / available files) in each 1-hour bin. Each panel represents one glider mission, arranged so that each column covers one deployment site: (a, d) Gulf of Lion, (b, e) Ligurian Sea, (c) Sea of Sardinia.

Observation during glider missions GoL2, LS1 and LS2 suggest an apparent increased sperm whale presence with deeper mixed layers (Fig. 3.11). Glider missions GoL1 and SoS only sampled stratified water masses (i.e shallow mixed layer). Predictions of the distribution of sperm whale presence with respect to mixed layer depth obtain from the GAM and associated p values for each of the three geographical areas studied are provided in the appendix (Fig. A.5).

### 3.4.6 Observation from varying depth

The vertical profiling of the glider allows for observation of sperm whale acoustic presence from varying depths. Distribution of sperm whale detection ratio with regards to measurement depth was highly variable between the different deployments and showed no clear signal over the whole dataset (Fig. 3.12a). However, the SoS glider mission showed a detection ratio increasing with depth. This dataset was dominated by one long duration encounter with a large aggregation (encounter #1: 53 hours), which was also analysed separately (Fig. 3.12b).

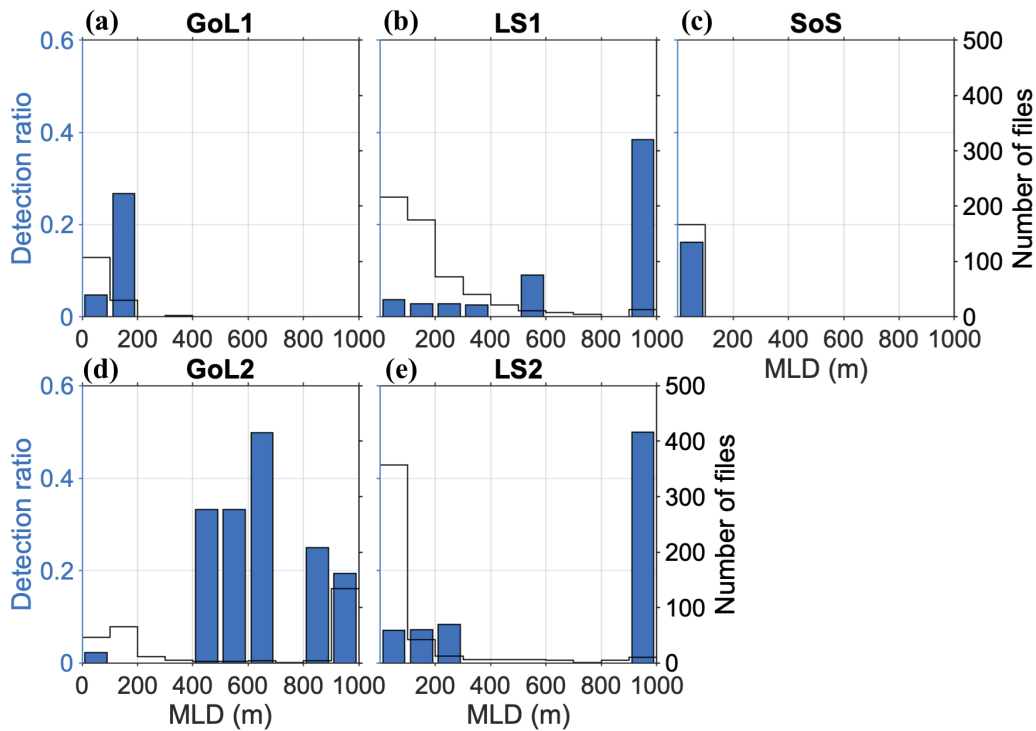


**Figure 3.11:** Number of glider dives with acoustic recording available for analysis (black line, right axis) per 100 m MLD bin. The bars (left axis) show the detection ratio (dives with sperm whale detection / total number of glider dives) in each 100 m MLD bin. Each panel represents one glider mission, arranged so that each column covers one deployment site: (a, d) Gulf of Lion, (b, e) Ligurian Sea, (c) Sea of Sardinia.

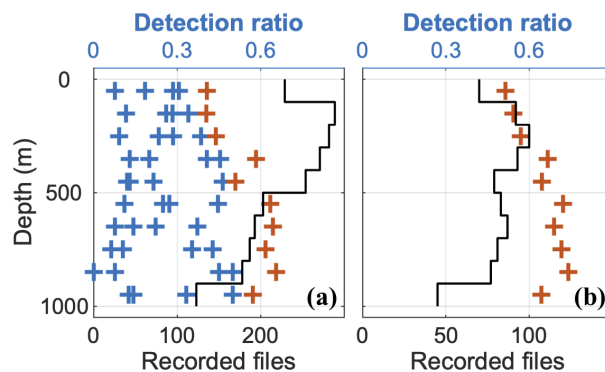


**Figure 3.12:** Number of acoustic files available for analysis (black line, lower axis) as a function of the depth of the glider. Panel (a) shows the detection ratio (files with sperm whale detection / available files) for the four winter (blue crosses) and summer (red crosses) glider deployment (upper axes). A specific focus on encounter #1 of glider mission SoS is shown in panel (b).

## 3.5 Discussion

### 3.5.1 Sperm whale observation from opportunistic glider surveys

We deployed our PAM sensors on gliders of opportunity, whose missions were designed to collect oceanographic observations. We successfully detected sperm whale presence along the surveyed tracks. The PAM glider missions considered in this study offer a trial framework for PAM gliders as a tool for sperm whale observations and a preview of the monitoring capabilities of purposefully designed PAM glider surveys. Oceanographic gliders have been routinely deployed in the northwestern Mediterranean Sea since 2005, with a specific focus on the winter season. In a near future, a similar coverage with PAM equipped glider surveys can be adapted for sperm whale population monitoring, providing long-term basin-wide observations. Repeated observation of sperm whale distribution along predefined glider transect lines can provide useful information about their habitat use (Verfuss *et al.*, 2019). Intensive PAM glider observation during winter season can fill observational gaps such as the winter period or adverse weather conditions (Mannocci *et al.*, 2018). Deployment of PAM gliders as a coordinated fleet can provide contemporaneous observations in multiple geographic areas to study geographical patterns.

### 3.5.2 Collocated oceanographic measurements

Oceanographic features (e.g. fronts, stratification, mixing, primary production) are a key parameter of sperm whale habitat models (Gannier and Praca, 2007; Praca and Gannier, 2008; Praca *et al.*, 2009; Pirotta *et al.*, 2011). PAM glider surveys provide collection of oceanographic profiles collocated with sperm whale detection. Deep convection events, such as the one starting in February 2013 in the middle of the Gulf of Lion (Testor *et al.*, 2018), are associated with small scale convective plumes (<1 km diameter) characterised by significant vertical velocities (up to  $18 \text{ cm s}^{-1}$ ) (Margirier *et al.*, 2017). The surface signature of such events, cooling of surface waters, and the observed upwelling and downwelling (Margirier *et al.*, 2017) are consistent with habitat use models made using sea surface temperature data (Praca *et al.*, 2009; Pirotta *et al.*, 2011).

Our observations in the Gulf of Lion covered only one winter season. We are therefore unable to conclude on the effect of the intensity of the mixing event on sperm whale

distribution, nor on inter-annual variability. Our glider missions were primarily designed to monitor deep convection events, and therefore introduce a sampling bias towards an increased observation effort in deep mixed layer waters. Significance of the statistical model would benefit from correcting this bias and covering a wider variety of water column homogenisation.

### 3.5.3 Spatial distribution

The spatial distribution pattern we observed in the winter 2013 season, from contemporaneous glider missions in the Gulf of Lion and the Ligurian Sea, suggests a geographical segregation between the Ligurian Sea, where distant single individuals only were detected, and the Gulf of Lion where sperm whale aggregations were found. Sporadic encounters of single individuals in every area surveyed highlight sperm whale mobility in this part of the Mediterranean basin. Longer term observations are needed to better describe their complex distribution and migration pattern, such as their relative low presence in the Ligurian Sea in January, and the necessary regrouping between males and females for mating.

Cross shelf repeated observations in the Ligurian Sea suggest possible increased sperm whale concentration along the northern slope, not confirmed by the statistical model. This area is a well-known favourable sperm whale habitat, both for its topographic (steep slopes and canyons) and hydrographic (permanent front, upwellings) features (Gannier and Praca, 2007; Laran and Drouot-Dulau, 2007).

In the Gulf of Lion, the observed patches of increased sperm whale presence are not confirmed by the statistical model. The glider observations are designed to monitor an oceanographic hotspot ( $\sim 2500 \text{ km}^2$ ) of intense deep mixing events occurring in winter, that are likely to favour prey availability and therefore favourable sperm whale habitats. Prey availability plays a key role in sperm whale distribution, as they adapt their distribution and group size to the size of prey patches (Relini *et al.*, 2000; Jaquet and Gendron, 2002; Drouot *et al.*, 2004c; Soria *et al.*, 2009).

### 3.5.4 Circadian pattern

Distribution of sperm whale click detection ratio with regards to time of day showed a significant circadian pattern ( $p\text{-value} = 6.9 \times 10^{-7}$ ) in the Gulf of Lion (Fig. 3.10). Such

a clear circadian pattern may suggest an adaptation of sperm whale foraging strategy to local prey behaviour (Stanistreet *et al.*, 2018). Tag surveys have found evidence of diurnal variations of sperm whale foraging depth, linked to jumbo squid (*Dosidicus gigas*) migrating deeper during daytime in the Gulf of California (Davis *et al.*, 2007), and warty squid (*Onykia ingens*) migrating from mid water during daytime to the bottom during nighttime in the Kaikōura submarine canyon (New Zealand) (Guerra *et al.*, 2017). During long-term time series from passive acoustic moorings in the northwestern Mediterranean Sea, various diurnal patterns have been observed. A daytime peak in sperm whale acoustic presence was reported in the north of the Gulf of Lion in all twelve months of 2012 (André *et al.*, 2017). A seasonal shift from a constant foraging effort over day and night in summer to a nighttime peak in winter was observed in the Ligurian Sea (Giorli *et al.*, 2016), supporting the idea that sperm whale foraging strategy is very flexible and adapts locally to environmental characteristics and prey behaviour (Stanistreet *et al.*, 2018).

Limited time coverage of the PAM glider missions available in each geographical area does not allow us to conclude on the seasonality of the observed patterns. However, the contemporaneous glider missions GoL2 and LS1 (Fig. 3.2) suggest a geographical pattern in the winter season. Further observation of circadian patterns would provide valuable information on local variations of sperm whale diet and its seasonal and inter-annual variability.

### 3.5.5 Seasonal to inter-annual variations

No sperm whales were encountered in the Ligurian Sea during the three weeks sampled in January (Fig. 3.2, Fig. 3.8). This does not allow us to conclude on the absence of sperm whales but adds to similar observations previously reported for this month in the same region (Laran and Drouot-Dulau, 2007). It is worth noting that the sperm whale detection range from passive acoustic monitoring can be affected by local phenomena increasing the background noise (e.g. ship traffic, storms). The glider surveys GoL1, GoL2, LS1 and LS2 have been previously used in a wind speed measurement study (Cauchy *et al.*, 2018). There was no remarkable storm in January 2013 that could explain the absence of sperm whale detection.

The time coverage of the PAM glider surveys available for this study, one month in

the Sea of Sardinia, three months in the Gulf of Lion and four months in the Ligurian Sea, do not exceed the intra-seasonal scale. Long-term monitoring via successive PAM glider surveys is needed to determine how the observations we made in this study vary with the seasons and through the years.

### **3.5.6 Depth distribution**

We found no clear dependence of the sperm whale click detection ratio on the depth of the recording made by the glider. This result is consistent with the highly variable foraging depth of sperm whales, their constant click production throughout the dive, and the limited influence of the sound velocity profile on the detection range of sperm whale echolocation clicks. However, in the case of the SoS mission, focusing on the long duration encounter with a large aggregation (encounter #1: 53 hours), we observed an increased detection ratio with depth of the measurement (Fig. 3.12b). This could be due to increased prey availability at depth, which would influence the foraging pattern of observed sperm whale aggregations. Specific analysis of such a large aggregation encounter, with measurement of the number of clicks detected with regards to depth, may provide more information about the foraging depth, and therefore diet, of an aggregation of whales at a certain time. The data available for this study does not allow us to conclude whether this observed behaviour would be specific to this particular time and location, or representative of the general sperm whale behaviour in summer or in this region.

### **3.5.7 Sampling strategy**

The PAM glider sampling strategy was not optimised for a sperm whale population monitoring activity. The speed and trajectory of our glider missions differ from the usual marine mammal survey design, introducing sampling bias that could not be corrected to estimate the sperm whale population or model its habitat. The spatial-temporal coverage of our observations was sparse, making it impossible in general to conclude on whether observed patterns were geographical or seasonal and leading to large uncertainties in the statistical models. Observations from glider mission SoS must be taken with a particular care, as it was the only glider mission in its area and in a summer month (Fig. 3.2). It was also partially corrupted by contemporaneous acoustic trial activities occurring in the

area and reduced to three encounters with sperm whales, twice with single individuals and once with a large aggregation (Table 3.3).

### 3.5.8 Acoustic detection

In this study, we limited our acoustic processing effort to visual detection of sperm whale usual click trains, and to a simple classification between the presence of a single individual and the simultaneous detection of several individuals. We were only interested in presence/absence of sperm whales during 1-minute samples, to demonstrate the opportunity to use PAM gliders to collect valuable data on sperm whales.

Use of onboard data processing systems is now possible on marine autonomous platforms, allowing for real time transmission of the observations. Development of an adapted automatic detection/classification system on PAM glider data would also allow to further investigate each acoustic file, to extract the number of detected clicks, number, gender and size of individuals (Caruso et al. 2015), to look for social interactions via detection of *coda* sequences.

It is worth noting that using two or more acoustic sensors would enable collection of bearing information, critical in counting, identifying and tracking individuals, analysing inter pulse interval variations (Caruso *et al.*, 2015; Kusel *et al.*, 2017).

## 3.6 Conclusion

This study demonstrates that the addition of PAM sensors to existing oceanographic glider missions, with mission design adjustments, offers a possible opportunity for sustained monitoring of the Mediterranean sperm whale subpopulation over the winter months for which there is clear lack of crucial data for conservation. Our ability to observe the population distribution in different geographic areas of the north-western Mediterranean Sea, across the slopes and the open ocean, highlighted the complexity of sperm whale behaviour, foraging strategy and habitat use.

We detected isolated animals in the three areas monitored both on the slopes and in the open ocean. We observed areas in the open ocean, in the Gulf of Lion, where sperm whales were less distant and were detected at the same time from the PAM glider. The collocated collection of oceanographic measurements allowed us to identify vertically

mixed waters as possible hotspots for sperm whale habitat. Continuous day and night monitoring over several months allowed identification of a circadian pattern in sperm whale acoustic presence in the Gulf of Lion, possibly linked to a specific diet or prey availability pattern.

The use of PAM sensors can expand the observation range of existing oceanographic infrastructure. Such sustained multi-disciplinary observations would allow better description of the oceanographic parameters of sperm whale preferred habitat. The opportunity for sustained long-term monitoring of cetacean populations would improve behaviour description, identification of key habitat and potentially harmful interaction with anthropic activities.

## **Chapter 4**

# **Use of ocean gliders for passive acoustic monitoring applications**

The northwestern Mediterranean basin benefited from an exceptional PAM glider observation intensity in this project, four PAM glider missions being carried out in the area between December 2012 and April 2013. Access to auxiliary in-situ wind speed measurements from meteorological buoys along the glider tracks enabled the WOTAN study presented in Chapter 2. Observation along repeated transect lines, with a focus on an area of interest for the Mediterranean sperm whale population, enabled the specific study presented in Chapter 3. However, many other PAM glider experiments have been carried out during this project, often opportunistic and for experimental purposes, as listed in Table 1.1. They provided valuable knowledge about technical and strategic aspects of PAM glider observation. This Chapter summarises the knowledge gathered during these PAM glider experiments.

### **4.1 Platform noise, limitations**

Ocean gliders are extremely quiet ocean observing platforms. They move through water without emitting either engine or propeller noise, unlike ships. They do not emit structural noise due to vibration or mobile parts, unlike moored structures. They spend most of their time silently gliding, away from the noisy air-sea interface. However, ocean gliders can generate platform noise when performing manoeuvres, interacting with their environment and collecting scientific measurements. Platform noise received level on the PAM system

is high, due to the close proximity between the noise source and the receiver, masking most of the usual oceanic soundscape. An ocean glider's usual diving pattern is composed of repeated cycles of three successive steady phases, described in Figure 1.7: Two profiling phases, descent and ascent, where the glider is collecting scientific measurements along a pseudo vertical trajectory, and a communication phase, where the glider stays afloat communicating with land via satellite communication and updating its location using GPS. Most of a glider's manoeuvres, hence platform noise generation, occur during the transition between two successive steady phases, as illustrated in Figure 4.1, where the spectrograms correspond to a full dive cycle, similar to the presented in Figure 1.7. Each of the steady phases and transitions presents a specific platform noise regime, due to the glider's behaviour and combination of systems in use, summarised in Table 4.1.

Analysis of past glider missions from the UEA glider group (11 missions using Seaglid-ers) and the MOOSE network (26 missions using Slocum gliders) provided quantitative observations of the relative importance of each of these phases and transitions, and the implications for PAM applications. These glider missions did not include acoustic recordings. Information contained in mission log files was used to identify the dive phases and transitions. Time spent at surface was detected using a depth threshold (20 m). Such criterion includes surface manoeuvre, communication phase and start dive transition. Apogee phase was detected focusing on volume bladder change around the depth maximum. Descent and ascent profiles were defined as the phases between the surface and the apogee, as described in the dive cycle schematics (Fig. 1.7). The time spent at surface, descending, in apogee transition and ascending was extracted for each glider mission. Average and 25<sup>th</sup> and 75<sup>th</sup> percentiles of the time ratio spent in each phase are summarised in Table 4.1.

#### 4.1.1 Profiling phases

Descent and ascent profiling phases are the quietest phases of a glider's mission. The glider is (pseudo-) vertically profiling in a relatively steady state (Fig. 1.7). The recorded soundscape can however be affected by flow noise, mid-profile adjustments of the gliders navigation (pump, pitch, roll or rudder), use of the altimeter and some instruments from the scientific payload.

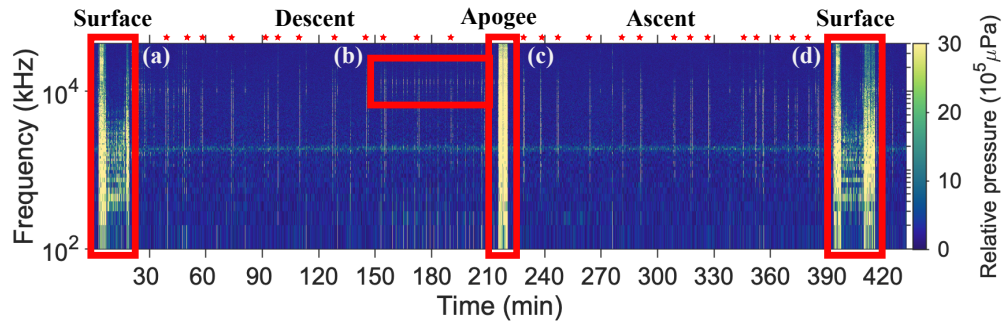


**Figure 4.1:** Spectrogram of a typical Seaglider dive cycle, recorded using an Acousonde during glider mission PERLE. (a, d) Succession of surface manoeuvre, communication phase and start dive transition. (b) Train of 13 kHz altimeter pings. (c) Pump noise during apogee phase. The red stars at the top show the mid-profile adjustments of the glider’s attitude (pitch, roll and/or pump). The constant 2 kHz noise throughout is an electrical noise from the Acousonde

**Table 4.1:** Sources of platform noise impact on the recorded soundscape for each phase of a dive, and average time ratio spent in each phase. 25<sup>th</sup> and 75<sup>th</sup> percentiles are given in brackets.

Dive phase	Acoustic monitoring conditions	Time ratio
Descent	Constant flow noise throughout (<100 Hz)	42 % (37–47)
	Mid-profile pump, pitch and roll adjustments (<1 s)	
	Altimeter	
	Scientific payload	
<b>Good acoustic monitoring conditions</b>		
Apogee	Pump noise dominates the recorded soundscape	1.8 %
	<b>No acoustic monitoring possible</b>	
Ascent	Constant flow noise throughout (<100 Hz)	42 % (36–45)
	Mid-profile pump, pitch and roll adjustments (<1 s)	
	Scientific payload	
	<b>Good acoustic monitoring conditions</b>	
Surface manoeuvre	Pump noise dominates the recorded soundscape	15 % (13–17)
<b>No acoustic monitoring possible</b>		
Communication	Splash noise and air-sea oscillations	15 % (13–17)
	Integrated payload turned off	
<b>Challenging acoustic monitoring conditions</b>		
Start dive	Pump noise dominates the recorded soundscape	15 % (13–17)
<b>No acoustic monitoring possible</b>		

Flow noise is generated by the water flow around the glider's hull. Slow speed through water ( $\sim 0.25 \text{ m s}^{-1}$ ) and optimised hydrodynamic profile lead to reduced flow noise compared to PAM systems towed from ships. Flow noise has however been shown to be a possible issue for PAM applications focusing on weak and low frequency ( $< 100 \text{ Hz}$ ) signal (Dos Santos *et al.*, 2016; Fregosi *et al.*, 2020). It is possible to reduce the glider's speed through water to reduce flow noise, as shown in a recent study (Fregosi *et al.*, 2020). However, reduced glider speed may have adverse effects on manoeuvrability, ability to cope with currents and reliability of some scientific measurements from instruments such as un-pumped CTD or turbulence sensors. It is also worth noting that reducing a glider's speed is a well known way to increase its endurance, therefore usually optimised by pilots whether or not the glider operates a PAM system. Recent developments of ocean gliders enable promising behaviours for PAM applications. Seagliders can adjust their buoyancy to become neutrally buoyant at a predefined depth, then loiter like a profiling float as described in Section 1.3.3, generating no flow noise. SeaExplorer gliders can be programmed to land and rest on the seabed, behaving like a mooring, with possible flow noise and noise from benthic life depending on the landing site as described in Section 1.3.2). These new behaviours are still in development and have not been tested during this PhD project.

Mid-profile adjustments of the glider's buoyancy, pitch and roll or rudder may happen, for steering and control of the vertical speed, generating platform noise as illustrated in Figure 4.1. Such adjustments are of short duration ( $< 10 \text{ s.}$ ) and their occurrences are logged in the glider's log file. It is therefore easy to detect and remove the samples corrupted by the associated platform noise from the acoustic analysis, to avoid artificial increase of sound levels or false detections of events. The implied reduction of the overall monitoring time is marginal. In the example dive shown in Figure 1.7, mid-profile adjustments represent  $\sim 1 \%$  of the recorded time (26 10-second segments out of a  $\sim 400$ -minute dive). The occurrence rate of mid-profile adjustments can be modified by the pilots, or even deactivated, with obvious effects on the navigation accuracy however.

The altimeter is used during the descent, to detect the seabed and trigger the apogee transition as shown in Figure 4.1, avoiding collision. Recently developed under-ice navigation capability activates the altimeter during the ascent, to detect and avoid ice. The

acoustic characteristics of the altimeter ping (central frequency, duration, intensity) are known and constant throughout the mission. The central frequency depends on glider type and configuration, 10–25 kHz for Seagliders and 200 kHz for Slocum gliders. It is therefore easy to assess whether an acoustic analysis is likely to be affected by altimeter noise and mitigate the effects. When studying echolocation clicks, altimeter ping parameters can be given to the classification software, or the operator, then identified and removed from the analysis to avoid false detections. When studying sound level in a frequency band affected by altimeter noise, altimeter pings can be detected and corrupted samples removed from the analysis. It is also possible to deactivate the altimeter, during descent when the bathymetry is well known or much deeper than the glider's profiling depth, or during ascent in ice free conditions.

No interfering noise has been identified from the usual sensors equipping the PAM gliders during this PhD project (un-pumped CTD, optical backscatter sensors, O<sub>2</sub> sensor). However, some sensors available on gliders are likely to generate noise, such as pumped ctd, water samplers and active acoustic systems. The sound level, bandwidth and occurrence of each noise must be taken into account when planning a PAM glider mission, as discussed in the following examples. Pumped ctd systems can be used to generate a constant flow through the sensor and improve the measurement quality. The pump generated noise needs to be accounted for, as it will be continuously present throughout the mission. Water samplers have recently been developed to be integrated on ocean gliders but are limited to collecting up to 16 water samples. The associated noise will therefore be rare, hence having very limited impact on the PAM observations. Echosounders and acoustic doppler current profilers (ADCP) are now available on gliders, with frequencies as low as 125 kHz for echosounders and 600 kHz or 1 MHz for ADCP. In the case of a PAM system recording in these frequencies, care must be taken to avoid interferences. Synchronised duty cycles can be used to activate active and passive acoustic systems at different times.

Thrusters have recently been added to ocean gliders as an option, increasing traveling speed when necessary (coping with strong currents, or simply being late) and allowing horizontal motion. Thrusters have been used on a Slocum glider equipped with an Acousonde during the MASSMO5 mission (Tab. 1.1). The contribution of thruster noise to the measured soundscape is shown on a spectrogram in Figure 4.2. The glider was

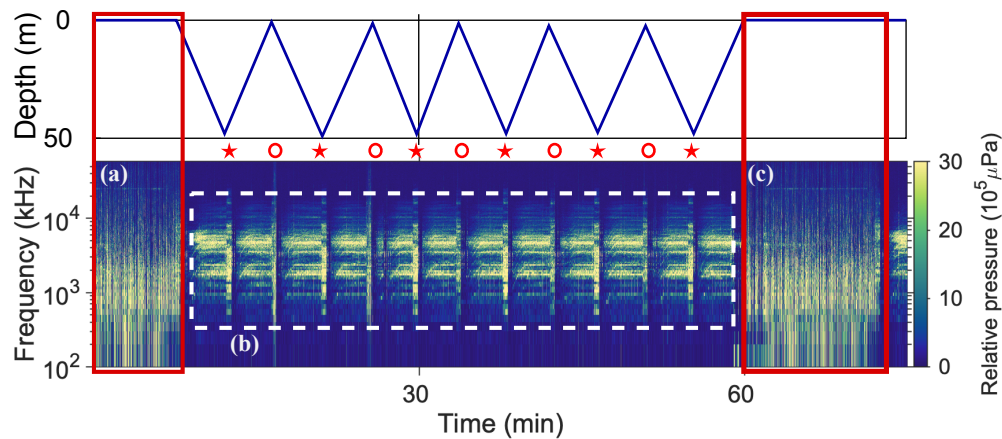


**Figure 4.2:** Thruster noise recorded with an Acousonde mounted on a Slocum during the MASSMO5 mission. Top panel shows the diving pattern of the glider, performing 6 successive 50-m dives between each communication phase (a, c). Bottom panel shows the spectrogram of the recordings. Bottom and surface inflexion noise are identified by red stars and circles on the top of the spectrogram. (b) Thruster noise is continuously recorded in the 200 Hz – 20 kHz frequency band.

configured to perform multiple (6) shallow dives (50 m) between the communications phases (Fig. 4.2a and c), with continuous use of thrusters, to escape strong coastal currents. Thrusters generated constant broadband noise, masking most of the soundscape in the 200 Hz – 20 kHz frequency band, as shown in Figure 4.2b. It is clear that the use of thrusters is not compatible with most PAM glider applications and should therefore be avoided when possible on PAM gliders.

Descent and ascent profiles are mainly similar. However, minor imperfections and asymmetries in weight and buoyancy balance, drag or drift of the glider can lead to different vertical speed during ascent and descent, leading to different flow noise levels as reported in previous studies (Matsumoto *et al.*, 2015; Fregosi *et al.*, 2020). Such asymmetries are usually consistent throughout a glider mission, but vary randomly from one mission to another, which explains the two opposites observations from two single deployment studies (Matsumoto *et al.*, 2015; Fregosi *et al.*, 2020). Descent and ascent have the same time ratio (42 %) when averaged over the 37 missions considered in this chapter. Large asymmetries can however be observed on an individual mission, as illustrated by the 10 % gap between the 25<sup>th</sup> and 75<sup>th</sup> percentiles in Table 4.1. This variability highlights the importance of fine tuning of the piloting parameters, with a specific focus on slow and constant vertical speed to control flow noise variations. Profiling phases are the

main phases of a glider's mission, covering on average 84 % of the time spent at sea (Tab. 4.1) in our dataset.

#### 4.1.2 Apogee

The apogee, at the end of the descent phase (negative buoyancy, downward pitch), requires activation of the buoyancy engine and the pitch motor to initiate the ascent phase (positive buoyancy, upward pitch) (Fig. 1.7). Noise generated by the buoyancy pump covers the whole recorded spectrum (1 Hz – 62 kHz), completely masking the underwater soundscape as shown in Figure 4.1c. The apogee represents on average 1.8 % of the time spent at sea by the glider (Tab. 4.1) during the 37 missions considered in this chapter.

#### 4.1.3 Surface

The surface phase, identified using a 20 m depth threshold in this Chapter, is the succession of a surface manoeuvre, a communication phase and a start dive transition, as described in the schematic in Figure 1.7. The succession of 3 different soundscapes can be seen on the spectrogram in both the surface phases on Figure 4.1a and d. The surface manoeuvre sets the glider in position for the communication phase, sticking the antenna high above the sea surface (highly positive buoyancy, downward pitch) (Fig. 1.7). Noise production during this transition is similar to the apogee, described in Section 4.1.2, dominated by the broadband loud noise of the buoyancy pump as shown in Figure 4.1a and d. During the communication phase, the glider stays afloat at the surface. Noise is generated by the interaction of the glider with the sea surface. Splash sounds of waves hitting the hull and the PAM sensor oscillating between in-air and underwater positions generate a mix of multiple broadband, impulsive sounds as shown in Figure 4.1a and d, making the use of automatic processing tools extremely challenging for detection / classification of sources or quantification of ambient noise levels. The communication phase is therefore considered unsuitable for most PAM glider applications. Finally, the start dive transition modifies the glider's navigation parameters from the communication phase (highly positive buoyancy, downward pitch) to the descent phase (negative buoyancy, downward pitch) as shown in Figure 1.7. Noise production during this transition is similar to the apogee, described in Section 4.1.2, dominated by the broadband loud noise of the buoyancy pump

as shown in Figure 4.1a and d.

Time spent at surface is the main source of acoustic monitoring time loss, representing an average of 15 % of the time spent by the glider at sea (Tab. 4.1). It is however necessary for the glider to receive piloting instruction, transfer data to land and acquire its GPS location. It is worth adding that ocean glider pilots usually intend to reduce the time spent at surface, as the glider is in danger of getting hit by a boat or covered in ice, the glider is not manoeuvrable and drifts with the surface currents, and the glider is not collecting any scientific data. Time spent at surface is directly affected by the quality of the communication, dependent on antenna performance, sea state and weather. Time spent at surface can be reduced by limiting the amount of data transmitted. Piloting files, transmitted from the pilot to the glider, should be reduced to the bare minimum to reduce their size. The amount of scientific data transmitted from the glider to the pilot can be adjusted. Scientific data files can be downsampled before transmission.

#### **4.1.4 Influence of profiling depth**

It seems obvious that the diving depth has a direct impact on the ratio of time spent in each phase (surface, profiling, apogee), performing shallower dives necessarily implying more frequent apogee and surface phases. The time ratio spent in each phase (surface, profiling, apogee) was plotted against the average dive depth for each of the 37 glider missions in Figure 4.3. There were no notable differences between Seaglider and Slocum missions. The glider missions studied here were all carried out in deep water, hence diving to 1000 m most of the time. One shallow glider mission was added to this analysis, to illustrate the influence of dive depth. The Slocum glider "Crate" was deployed off the Rhone river mouth in the Gulf of Lion during 3 weeks, diving in 50 to 150 m deep water. The average profiling time ratio was 66 % of the total time spent at sea during this mission (descent phase – 35 %, ascent phase – 31 %). The average surface time ratio was 35 %, and the apogee time ratio 2.1 %. The profiling average for each mission of the time ratio spent in descent, ascent and surface phases are shown on Figure 4.3, illustrating the influence of the dive depth.

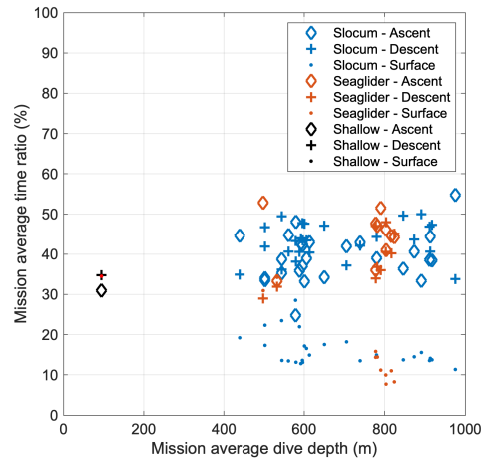


**Figure 4.3:** Influence of average dive depth on the ratio of time spent by the glider in each of the three main phases of the dive cycle (surface, descent, ascent). Slocum glider missions are shown in blue, Seaglider missions in orange. One shallow mission was added (in black and red) for contrast.

## 4.2 PAM systems

### 4.2.1 Self-contained PAM systems

Self-contained PAM systems are autonomous recorders equipped with their own battery and memory and which follow a programmed sampling mission. Raw data are accessed and processed after recovery of the instrument. They have been designed to be deployed on moorings for long-duration missions, as described in Section 1.3.2. They are usually composed of a main pressure housing, containing the electronics, memory and battery, with one or several tethered hydrophones and optional external battery packs. They can record continuously for months to years, collecting terabytes of data. Multiple versions are available, with depth ratings ranging from 100 to 3000 metres (Table 4.2). Such systems have been designed without constraints regarding their size, weight and power consumption, focusing on offering high sensitivity and low self-noise acoustic measurements. Many manufacturers have developed compact self-contained PAM systems, to be deployed on small moorings, from a small boat or handheld by divers. Downsized versions of the previous PAM systems mentioned, compact PAM systems offer continuous recording for 3 to 13 days according to the manufacturers (Table 4.3), with simplified electronics and reduced sensitivity. They can be used with an external battery pack for extended deployment duration. Miniaturised self-contained PAM systems have been specifically developed to study marine mammal behaviour, such as Acousonde (Burgess,

**Table 4.2:** Usual self-contained PAM systems. Endurance is given for continuous recording. The Orca and Ocean Observer are available with different housing and battery versions but no size or endurance information are given.

	Orca	ST500	Resea	Ocean Observer
Manufacturer	Turbulent Research	Ocean Instruments	RTSYS	Jasco
Diam x length	-	10 x 35 cm	12 x 32 cm	-
Weight in water	-	2 kg	2 kg	-
Depth rating	3000 m	500 m	750 m	-
Endurance	-	180 days	-	-
Consumption	0.9 – 3 W	0.035 W	0.6 – 2 W	2.5 W
Channels	5+	1	4	16
Sampling	24 – 384 kHz	24 – 576 kHz	39 – 1000 kHz	8 – 2048 kHz
Bits	16 – 24	16	24	24
Memory	6 TB	1 TB	2 TB	10 TB

2010) and D-Tag (Johnson and Tyack, 2003) (Table 4.4). They have been designed to be attached on marine mammals, with reduced size and weight for an easier tagging process and increased pressure rating to be used on deep diving animals (up to 3000 m). The drastic miniaturisation constraints lead to limited endurance and sensitivity. They are attached to cetaceans using suction cups for up to 20 hours (Johnson and Tyack, 2003; Burgess, 2010) or glued on a seal's fur and recovered after the moulting season (Cazau *et al.*, 2017). The primary use of such systems is behavioural response studies, tracking the reaction of the tagged animal to external acoustic stimuli, such as predator sounds or anthropogenic noise (Johnson and Tyack, 2003). Acousonde glued on southern elephant seals, recording 4 hours a day for up to 1 month, have been used for a soundscape study in the Southern Indian Ocean (Cazau *et al.*, 2017).

When considering adding a self-contained PAM system externally to an ocean glider, weight is the critical constraint. The buoyancy propulsion relies on small buoyancy changes, requiring the glider to be carefully ballasted at the same density than seawater at the mission's location. Therefore, any weight added needs to be compensated for, by addition of high-density foam of the equivalent buoyancy inside the glider's fairing. The maximum total payload weight is around 4, 5 and 8 kg for Seaglider, Slocum and Seaexplorer respectively (Rudnick *et al.*, 2004) and can vary between glider versions. Secondary constraints are the pressure rating of the sensor, which must survive the numerous dive cycles of the glider, and the size and shape, for easy attachment onto the

**Table 4.3:** Compact self-contained PAM systems. Endurance is given for continuous recording. The Amar G4 is available with different housing and battery versions but no size or endurance information are given. \*icListen Kayak needs to be cabled, to receive power and stream audio data. It is however targeting the same applications as the compact self-contained PAM systems.

	Porpoise	ST300	Amar G4	icListen Kayak*
Manufacturer	Turbulent Research	Ocean Instruments	Jasco	Ocean Sonics
Diam x length	7 x 23 cm	6 x 20 cm	-	2.3 x 21 cm
Weight in water	500 g	180 g	-	130 g
Depth rating	2000 m	500 m	-	3500 m
Endurance	2 days	13 days	-	No batteries
Consumption	-	-	0.5 W	0.2 W
Channels	1	1	4	1
Sampling	24 – 384 kHz	24 – 576 kHz	8 – 512 kHz	1 – 480 kHz
Bits	16 – 24	16	24	16 – 24
Memory	4 TB	256 GB	10 TB	No memory

**Table 4.4:** Self-contained PAM systems designed to be attached on marine mammals.

	Acousonde	D-Tag
Manufacturer	Cetacean Research Technology	Woods Hole Oceanographic Institution
Diam x length	3.5 x 22 cm	-
Weight in water	86 g	-
Depth rating	3000 m	2000 m
Endurance	4 days	<1 day
Consumption	-	0.15 W
Channels	1	1 – 4
Sampling	1 – 464 kHz	48 – 192 kHz
Bits	16	16
Memory	128 GB	6.6 GB

glider's fairing. For this project, two Acousonde were used during most of the glider missions (Table 1.1, Fig. 1.9) as described in Section 2.3. The Acousonde weighs 86 g in seawater, can operate up to 3000 m deep and is small enough to be externally attached to a glider without adding excessive drag (Table 4.4). Addition of an Acousonde onto a glider requires fairly simple mechanical engineering and ballasting. Simple fixation brackets can be used to attach the Acousonde onto the hull of any ocean glider (mounted on a Seaglider Fig. 4.4 and on a Slocum Fig. 2.2) and the added weight can easily be adjusted during ballasting of the glider. An external battery pack can be added, requiring significantly more ballasting effort due to its weight (~500 g in water). It has been used on Slocum gliders during the missions presented in Section 2.3 in the north western



**Figure 4.4:** Acousonde mounted on a Seaglider during glider mission ELO. Existing fairing attachment screws have been used to affix plastic brackets holding the Acousonde.

Mediterranean Sea, using alkaline batteries and recording for the continuous equivalent of 3.8 – 5.4 days, and on a Seaglider during the PERLE mission presented in Section 1.4 (Table 1.1) in the eastern Mediterranean Sea, using lithium batteries and recording for the continuous equivalent of 8 days, limited by memory rather than power.

Self-contained PAM systems run on their own batteries, leaving the glider's endurance unaffected. The success of many oceanographic glider missions relies on the ability to sustain observations over long periods, to monitor intra-seasonal variability, to be able to travel to and back from remote locations or across oceanic basins and to reduce logistical costs. Such missions can only afford to run a limited number of sensors, to limit power consumption, but can accommodate a self-contained, energy self-sufficient, PAM systems. Most of the PAM glider missions described in this thesis were opportunistic, the PAM system being added to a pre-organised glider mission, sometimes even hosted by the glider of a partner organisation such as the University of Gothenburg (glider mission Orchestra) and the Marine Autonomous Robotic Systems facility (glider mission MASSMO5) (Table 1.1). In such conditions, the self-contained PAM sensor has often been the only acceptable solution.

Compact self-contained PAM systems have limited endurance (Table 4.3). However, they offer the opportunity to configure a duty cycle, spreading the available recording time over a larger period to match the glider's endurance. For WOTAN applications (Table 1.1), the Acousonde was setup to record 1 minute every 10 minutes, as described in Section

2.3. For application to soundscape analysis, longer samples were recorded to improve understanding of the context. The Acousonde was setup to record 20 minutes every 1 or 6 hours, depending on the expected mission duration. A delayed start mode allows configuration of a future date and time for the recording cycle to start. This opportunity was used during the PERLE mission (Table 1.1, Fig. 1.9), to start recording after the glider has navigated out of Cyprus waters, where acoustic recording was not allowed.

#### 4.2.2 Integrated PAM systems

Integrated PAM systems have been recently developed for ocean gliders. They are powered by the glider's batteries and controlled by the glider's operating system. They can communicate data back to the glider, enabling a level of real-time data transmission, and can receive sampling instructions from the pilot. The choice of commercially available integrated PAM sensor is very limited. At the time of writing, each of the 3 glider manufacturers offer one unique integrated PAM system, adapted from the Ocean Observer (Table 4.2), developed by Jasco. The current observed trend in integrated PAM systems development is a focus on acoustic recording and processing performance. The current integrated PAM systems offer multi-channel and high-sensitivity acoustic recordings, with real-time processing capability. This choice from the manufacturers is following the needs of military applications, enabling detection and localisation of weak signals, and real-time classification and communication of the results to the pilots.

At the start of this PhD project, we purchased a Seaglider integrated PAM sensor, provided by Kongsberg and developed by Embedded Ocean Systems, described in Section 3.3, now discontinued. This system was used during PAM glider missions in the Mediterranean Sea, the north Atlantic Ocean, and the Indian Ocean (Fig. 1.9). This integrated PAM system was recording continuously for 15 and 4 days, during the MED-REP14 and MASSMO4 mission respectively (Table 1.1).

Integrated PAM systems allow up to ~30 days glider mission with continuous acoustic recording. However, they are powered from the glider's batteries, considerably reducing the glider's mission duration. According to glider manufacturers' figures, a glider running on primary lithium batteries has an endurance of up to 6 months running usual sensors, reduced to 30 days when running an integrated PAM system. Acceptability of

such a 6-fold reduction of duration depends on the location and primary objective of a glider mission. The ELO mission (Fig. 1.9, Table 1.1) illustrates this endurance issue. One Seaglider was deployed with an integrated PAM sensor, for a long-duration mission (3+ month) including return transit between its deployment and survey locations, 100 km apart. This mission resulted in the collection of only 20 h of acoustic data, due to unexpectedly high-power consumption and fear of draining the batteries and risking losing the glider. Some glider missions are adapted to integrated PAM system operation: short duration oceanographic glider missions, such as in polar regions where accessibility is limited during a short summer season (e.g. PROVOCCAR mission, 2 weeks, Table 1.1), and missions along repeated coastal transect lines, with easy and cheap deployment and recovery opportunities such as the repeated sections of the MOOSE network in the northwestern Mediterranean Sea (Fig. 1.9, Table 1.1).

Integrated PAM systems can be controlled remotely, benefitting from satellite connection through the glider. Acoustic sampling can therefore be adapted to the location of the glider, the battery usage and the observed conditions. During the ELO mission (Table 1.1, Fig. 1.9), the integrated PAM system was kept off during the 6 days transit, until the glider reached its survey location to save energy. An integrated PAM system can be automatically turned off when the glider is at surface, or during the bottom inflexion phase, known to be unsuitable for PAM applications (See Section 4.1). However, our version of the Seaglider integrated PAM system does not permit to subsample at a finer resolution than a glider profile (descent or ascent). The only sampling pattern offered is continuous recording, above or below a depth threshold. It is therefore impossible to reproduce the sampling pattern described previously for WOTAN applications. A similar 1/10 recording ratio, assuming 1000 m dives, can be obtained recording above 100 m (or below 900 m) during each profile, i.e. approximately 12 minutes of recordings every 2 hours. It is worth noting that the addition of a duty cycle ability, similar to a self-contained PAM system, is not a technical challenge and will be easily corrected in future versions.

### 4.2.3 Desirable hardware developments

This project focused on adapting PAM techniques to ocean gliders, to expand their observational capability and benefit from their wide-spread presence and coverage. The PAM

glider experiments described in this study were carried out during glider missions with a primary focus on oceanographic research. For such missions, choice of the sensor suite equipping the glider depends on the scientific importance of each measurement, space and weight available for the payload, and power consumption. These experiments highlighted the critical importance of preserving glider endurance and limiting payload size and weight. Self-contained PAM sensors do not affect the autonomy of the glider hosting them. They are easily added to and removed from any type of ocean glider, increasing deployment opportunities. Their relatively low cost suggests they can be used in fleets, widely deployed on multiple glider missions, increasing acoustic monitoring coverage. Such characteristics seem adapted to widespread use on ocean gliders.

Currently available glider integrated PAM systems are powerful acoustic monitoring tools, collecting low noise recordings for detection of weak signals, using multiple channels for source localisation, with onboard processing ability for real-time transmission of the information and reaction to event detection. Such characteristics are particularly adapted to military applications, such as maritime surveillance. However, power consumption of integrated PAM systems significantly reduces gliders' endurance, limiting their coverage to short durations and small distances, compared to the usual oceanographic glider coverage.

Desirable future development of glider integrated PAM systems should focus on solutions that could be routinely used on ocean gliders. Low power consumption, versatile programmable recording patterns and mechanical resistance to repeated 1000 m dives are achievable without great development effort. The manufacturer of the SoundTrap ST500 announces a 35 mW power consumption, which is comparable to an un-pumped ctd (45 mW for the RBR*legato*<sup>3</sup> sampling at 2 Hz, [www.rbr-global.com/products/oem/rbrlegato](http://www.rbr-global.com/products/oem/rbrlegato)) and much lower than a pumped ctd (175 mW for the Seabird Glider Payload CTD when sampling at 1 Hz (Janzen and Creed, 2011)). Simple duty cycles, as available for each self-contained PAM system presented, could be completed by a glider piloted on/off switch for each dive, as offered by the current integrated systems. Mechanical resistance to repeated deep dives is a challenge that glider and sensor manufacturers have already solved on multiple occasions.

Real-time data access is not critical for most ocean monitoring applications. However,

simple detection / classification systems exist, that could be integrated to commercially available integrated PAM sensor. The custom made DMON system, developed at the Woods Hole Oceanographic Institution from the D-TAG, has been integrated in Slocum gliders, for real-time detection and transmission of baleen whale calls (Baumgartner *et al.*, 2013). It is operationally used on ocean gliders as part of the Ocean Tracking Network for real-time mapping of baleen whale presence on the Canadian Atlantic coast (Davis *et al.*, 2016). The gListen board has been developed by Cyprus Subsea Consulting and services (<https://cyprus-subsea.com/glisten-board>), creating an interface between an iCListen smart hydrophone (Table 4.3) and a Seaglider, enabling real time transmission of click detections and third-octave levels. Such demonstrations of interest from the relevant communities should trigger development effort from the manufacturers.

# Chapter 5

## Conclusion

In this chapter, the methods developed during this PhD project and their limitations are discussed. Pathways to improvement are suggested. The main challenge identified is described. Good practices and usual constraints are summarised, aiming to facilitate future PAM glider experiments and improve the quality of the observation.

### 5.1 Lessons learnt - Going further

#### 5.1.1 Weather observation

The opportunity to apply the WOTAN technique to PAM glider measurements was investigated in Chapter 2. The novelty of the study was the use of acoustic recordings made from vertically profiling platforms, introducing differences with previous studies using moored PAM systems (Vagle *et al.*, 1990; Nystuen and Ma, 2002), or drifting at fixed depth on a profiling float (Riser *et al.*, 2008). Operational meteorological buoys at the glider's location in the open ocean allowed for recurrent access to in-situ wind speed measurements. The duration and geographic area of the survey allowed for observation of higher wind speed conditions than any of the previous studies, as summarised in Table 2.2, leading to documentation of a different relationship between background noise and wind speed above  $\sim 11 \text{ m s}^{-1}$ . This study was carried out in a geographic area with limited fetch, preventing the observation of fully developed sea state at high wind speed. We were therefore not able to investigate the influence of sea state on the dependence of underwater background noise to surface wind speed. Further work with that dataset

might include analysis of other parameters critical to air-sea interaction modelling, such as energy flux and wave height. Finally, this study highlighted the challenge of repeating such surveys without access to in-situ wind speed measurements for calibration of the system. Acoustic characterisation of the full system (PAM system + glider), as described in Section 5.2, could be the way forward to measure absolute wind speed without access to any nearby in-situ observation for calibration. Analysis of the underwater background noise also enables monitoring of rainfall rate (Riser *et al.*, 2008; Black *et al.*, 1997; Ma and Nystuen, 2005) and ice shelf calving (Dziak *et al.*, 2019) using similar approaches to the study presented in Chapter 2. Such techniques can be adapted to monitoring from PAM glider surveys, allowing for data acquisition during monsoon events and in near ice environments, collocated with usual oceanographic measurements.

**Duty cycle:** Applications based on analysis of the background noise do not need continuous sampling, as they do not focus on individual acoustic events. The extraction of acoustic features of wind or rain noise has been shown to need only 15-s long samples (Nystuen and Ma, 2002). Energy and memory usage can be optimised by spreading the recording of short samples throughout the glider mission. High time resolution is obtained by reducing the time separating the consecutive samples.

**Frequency resolution:** The spectra of wind- rain- or ice-generated noise are smooth, as illustrated by the Wenz curves (Fig. 2.1). Analysis on TOL reduces computation costs while providing sufficient information about the spectral slope, critical to classify noise sources contributing to the background noise (e.g. distant traffic, rainfall types, wind). Monitoring a wide range of frequencies can be useful to improve the analysis, as different frequency bands are not affected in the same way by external contributions. High frequencies remain unaffected by distant shipping noise and low frequencies are less affected by the subsurface bubble layer forming at high wind speeds.

**Real-time transmission:** On-board extraction of information from acoustic recordings, such as TOL time series, can generate meaningful information that is small enough to be transmitted in real-time, via satellite communication. In the near future, products such as the recently developed gListen board ([www.cyprus-subsea.com/glisten-board](http://www.cyprus-subsea.com/glisten-board)) will be available on PAM gliders, enabling real-time access to acoustic-based observations of surface wind speed, rainfall rate or ice calving activity.

### 5.1.2 Marine life monitoring

The opportunity to study sperm whale populations from PAM glider observation was investigated in Chapter 3. The novelty of the study was the opportunistic use of PAM glider surveys designed for WOTAN applications along repeated transect lines of hydrographic interest. The PAM gliders repeated 3-days to 2-weeks long transect lines, providing sperm whale observations on unusual time and space scales. Repeated observations highlighted time variability of the sperm whale activity, on daily (Fig. 3.10a and d) and intra-seasonal (Fig. 3.8c) scales. Collocated observation of oceanographic features provided valuable information on sperm whale habitat use. Further work with that dataset might include automatic click detection, enabling estimation of the number of clicks hence quantification of the foraging effort. Further analysis with a focus on social sounds might provide identification of social structures and observation of social interaction. This study highlighted the challenge of converting sperm whale detections along glider trajectories into estimates of population distribution or density. Statistical methods have been developed for observation from fixed locations-, or ship-borne surveys that need to be adapted to PAM glider observations. The low speed of the platform relative to the whale's speed raises issues about an individual being detected multiple times. The non-uniform coverage of the oceanic basin raises questions about the extrapolation of the observations. The detection range, detection probability, and possible avoidance or attraction effects on marine animals is unknown. The possible contribution of autonomous vehicles, including ocean gliders, for acoustic detection and monitoring of the marine life has been reviewed (Verfuss *et al.*, 2019), demonstrating the interest of the scientific community for these new platforms. PAM gliders were found adapted for short-term and long-term population monitoring. It is worth adding that the design of the PAM glider surveys could be adapted to increase the impact of the observations for both the oceanography and marine biology communities. PAM glider surveys can similarly enable monitoring of other cetacean species producing echolocation clicks (e.g. dolphins, beaked whales, pilot whales) or low frequency calls (e.g. fin whale, right whale). Other soniferous species including seals, fish and crustacean can also be studied through their acoustic activity.

**Duty cycle:** Continuous recording is not necessary to marine life monitoring applications. Such applications usually rely on extrapolation from sparse observation (in space

and time). Frequent collection of acoustic samples is necessary to observe short term patterns, such as the daily pattern observed in Section 3.4.3. The samples collected must be long enough to provide the opportunity to observe trains of clicks or calls, detect the presence of multiple animals and collect contextual information.

**Multi channel:** Use of multichannel recordings would increase the performance of automatic detection software and enable animal tracking (Kusel et al. 2017), hence counting individuals and better description of groups.

**Real-time:** On-board detection/classification of acoustic signals can be used, to transmit the detections via satellite communication after each dive.

## 5.2 Absolute sound level measurements

### 5.2.1 Challenge

Data presented in Chapter 2 highlighted the challenge of collecting calibrated acoustic measurements from PAM gliders. The PAM glider missions MooseT00.23 and 25 were carried out using the same PAM system (Acousonde #A040) but measured different levels of wind noise in comparable wind speed conditions, as shown in Table 2.5. Such a difference might be explained by variations in the mounting of the Acousonde on the glider's hull, as explained in Section 2.6, generating different reflection/shielding patterns between the glider's hull and the hydrophone. The observed peak dynamic response at 3 kHz, described in Section 2.5 and shown in Figure 2.7b, did not match the observations illustrated by the Wenz curves (Fig. 2.1 and has not been described in any other WOTAN study. This characteristic of the wind noise observed from PAM glider measurements is therefore not inherent to wind noise, but rather a characteristic of PAM glider measurements. Such amplification of sound levels in the 3 kHz third-octave band may result from an effect of resonance of the glider's body.

The presence of the glider's body modifies the acoustic field, through scattering and resonance effects, generating complex patterns in the nearby acoustic field that affect the measurements. The main contributor to such acoustic interactions is the dry section of the glider, containing the batteries and the electronics, which can be modelled as an air-filled cavity encapsulated in a pressure hull. Acoustic characterisation of the whole PAM glider

system, including the glider's body, is therefore necessary to collect calibrated acoustic measurements. Such acoustic characterisation has been carried out in a previous study, with an autonomous underwater vehicle composed of two spherical pressure hulls and a specific focus on source localisation (Lepper and D'Spain, 2007). This study demonstrated the feasibility of such characterisation, provided a methodology for the acoustic modelling of an autonomous underwater vehicle and evaluated the relative importance of the mechanical characteristics of the hull (e.g. thickness, elasticity). In addition to correcting the effects caused by interference with the hulls on the measurements, the study showed the potential benefit from the knowledge of the diffraction pattern to improve acoustic source characterisation based on a similar effect as the concept of head related transfer function, used in human acoustic perception (Middlebrooks, 1991).

Ocean gliders are composed of only one main air-filled cavity, which would simplify the modelling. However, the characteristics of the pressure hull relevant to the acoustic monitoring (shape, size, material) are more complex and vary with each glider manufacturer. The non-spherical shape of the pressure hull implies variations of the response pattern with source – glider – hydrophone geometry. A method for acoustic characterisation of PAM gliders needs to be developed that could be adapted to each PAM glider system. The relative small size of ocean gliders allows for in-situ acoustic measurements to be carried out in a controlled environment, such as the National Physics Laboratory's open water test facility at Wraybury, for validation / improvement of the acoustic model.

### 5.2.2 Outcomes

The data presented in this thesis have been collected using uncalibrated PAM glider systems. Absolute sound levels were unknown and the spectral slope was modified by interactions with the glider's body. In such conditions, it is possible to detect and identify acoustic signals such as the sperm whale echolocation clicks considered in Chapter 3. It is also possible to rely on access to ancillary observations, such as the wind speed measurements provided by the meteorological buoys in Chapter 2, to calibrate a posteriori acoustic based observations. However, collection of calibrated absolute sound levels is necessary to use PAM gliders for WOTAN applications in areas with no access to ancillary in-situ observations, as highlighted in Section 2.7. For marine life monitoring, comparison of

received level to known source level can provide ranging, as demonstrated in a previous study on blue whale calls (Samaran *et al.*, 2010).

More generally, the ability to collect calibrated sound level measurements will broaden the observation spectrum of PAM gliders. Monitoring of the anthropogenic noise and its effects on the marine life requires quantification of the received levels to quantify cumulative exposure over time. The need for anthropogenic underwater noise monitoring has been expressed by the European Union via the European Marine Strategy Framework Directive (Van der Graaf *et al.*, 2012). Qualifying PAM gliders for such monitoring activity would widely increase the PAM glider coverage, providing new observation opportunities.

## 5.3 Take home messages

### 5.3.1 Recommendations for a first PAM glider deployment

**Sampling frequency:** The choice of the sampling frequency should be adapted to the application. Keeping the sampling frequency low allows reduction of the power consumption and memory usage. It is however necessary to use a sampling frequency at least twice as high as the maximum frequency of the observed signal, usually referred to as the Nyquist frequency. Collection of wide band recordings also provides contextual information, often useful for robust classification and estimation of the possible noise sources.

**Duty cycle:** The duty cycle (and delayed start) should be used to optimise the monitoring coverage. Data collection should be evenly spread over the area / period of interest. Depending on the application, wide spread discontinuous sampling is often the most valuable option.

**Measurement depth:** Measuring at multiple depths can provide useful information. The subsurface layer is often considered noisy and avoided, as deep as 200 m in some studies (Fregosi *et al.*, 2020). Surface noise, such as wind and rain generated noise, can be detected as deep as 6000 m (Barclay and Buckingham, 2013)!

**Flow noise:** Acoustic measurement from glider have been shown to contain flow noise (Dos Santos *et al.*, 2016; Fregosi *et al.*, 2020). It is however very small compared to other mobile platforms, due to the low speed of the glider through water. Flow noise is also limited to frequencies below 100 Hz.

**Drag:** The question of the added drag caused by addition of a sensor on a glider's hull is not specific to PAM systems. Other sensors are routinely attached on gliders such as PAR sensors (measuring photosynthetically active radiation), Microrider (measuring turbulences) and Suna (measuring nitrates). Excessive added drag can hamper the flight of the glider, therefore increase its power consumption and reduce its manoeuvrability. During the PAM glider missions presented in the thesis, no effects of the added drag have been noted on glider piloting or endurance.

**Piloting:** The dataset of 37 glider missions presented in Chapter 4 was chosen without specific criterion other than depth of deployment (deep water deployments  $>1000$  m). 84 % of the monitoring time was free of platform noise, without any specific effort on platform noise reduction. Piloting aim for these missions was focused on endurance, performing deep slow dives to limit power consumption. Such behaviour is particularly adapted to reduction of flow noise and platform noise. If the glider mission allows, the use of loitering and bottom landing functions offered by some gliders could be interesting.

**Data processing:** Platform noise can be removed without signal processing efforts. Gliders provide log files from which activity of the buoyancy pump and pitch and roll motors can be monitored easily. Glider temperature and salinity profiles can be used to calculate the local sound velocity profile. Glider varying depth must be taken into account when processing the acoustic observations, as described in Section 2.4 to correct propagation loss.

### 5.3.2 Key successes of the project

Ocean gliders were successfully used as platforms for experimental development of PAM applications. Gliders performing usual oceanographic survey missions were used to host PAM systems. Their ability to navigate along predefined trajectories provided the opportunity to carry out the experiment in controlled areas. In Chapter 2, repeated passages in the vicinity of meteorological buoys were used to calibrate the acoustic measurements against in-situ wind speed measurements. The ability to recover the glider at the end of each mission provided access to the raw acoustic data and recovery of the PAM system for later use.

A unique PAM glider dataset was used to carry out two studies focusing on different

aspects of the oceanic environment. WOTAN application, described in Chapter 2, contributes to improved observation of the air-sea interactions. Sperm whale observation, described in Chapter 3, contributes to improved understanding of the population, critical to its conservation. These two case studies, presented in Chapters 2 and 3, demonstrated the opportunity to broaden the spectrum of glider-based observation using PAM techniques of interest for the physical oceanography and marine biology communities. They highlighted the potential benefits of a wide addition of PAM systems to routine ocean glider deployments.

It is worth noting that the datasets described in Chapters 2 and 3 were composed of only  $\sim 4$  and  $\sim 5$  months of observation, respectively, in the NW Mediterranean Sea. In this specific area, ocean gliders have been routinely deployed since 2010, cumulating annual glider presence at sea of 6 to 12 months. Such coverage with PAM glider observations would provide great information on sperm whale population behaviour, expanding the results presented in Chapter 3 on inter-seasonal and inter-annual scales. In the future, PAM applications developed, validated and promoted using PAM gliders can be transferred to profiling floats. Provided that the technical challenges of on-board processing and satellite data transmission without access to raw acoustic data are solved, key PAM applications can be selected for integration to the ARGO float program, and benefit from its great time and space coverage.

## Appendix A

# Supplementary Material

**Table A.1:** Confusion matrix of the presence – absence classification from the two independent operators, showing number and percentage of acoustic files. Classification from operator 'O' was used in this study. Operator 'E' processed a randomly selected subset representing 20 % of each glider mission, for evaluation purposes. 95 % of the test files were correctly classified.

	O-Absence	O-Presence
E-Absence	3943 – 89 %	163 – 4 %
E-Presence	23 – 1 %	285 – 6 %

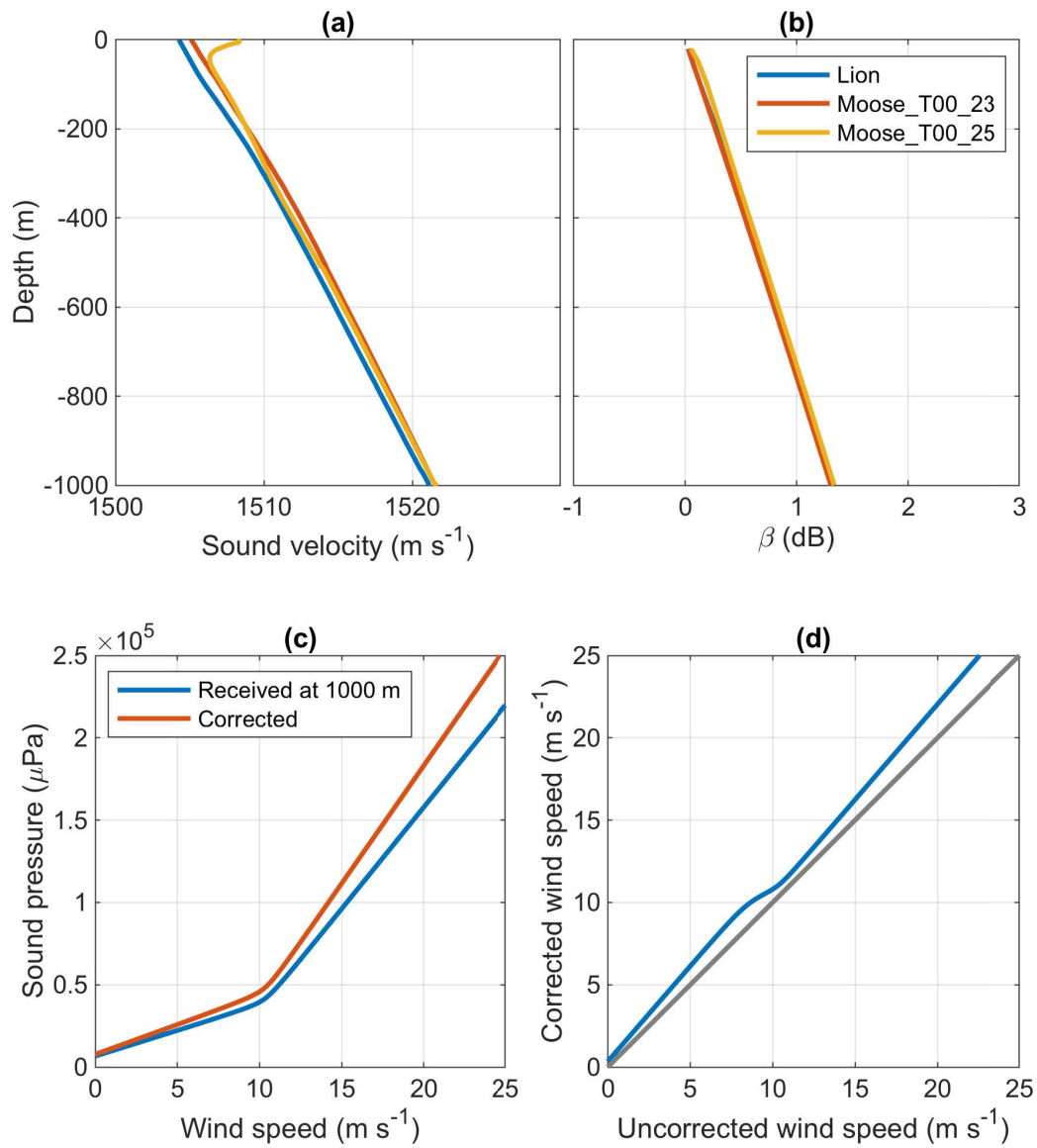


**Figure A.1:** (a) Average sound velocity profiles, and (b) the associated  $\beta$  profiles at 3 kHz for the datasets Lion, MooseT00.23, and MooseT00.25. (c) Effects of the correction on sound pressure measurements at a 1000-m depth, and (d) the associated wind speed estimation correction.

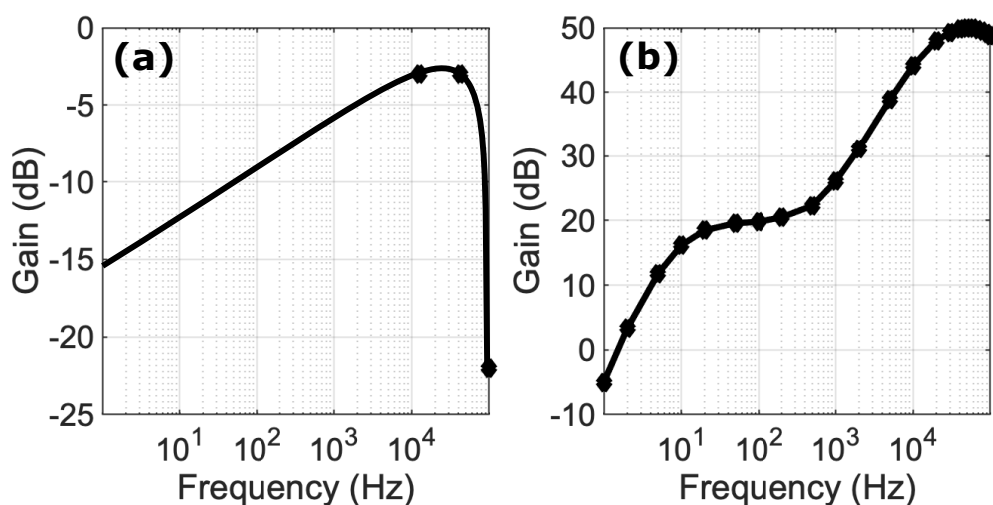


**Figure A.2:** (a) Acousonde pre-amp filter gain as a function of frequency. Data from (Burgess, 2010). (b) WISPR pre-amp filter gain as a function of frequency, approximately equal to the inverse of typical deep-water ambient noise. Data from [http://embeddedocean.com/wp-content/uploads/2015/03/EOS\\_HM1\\_users\\_guide.pdf](http://embeddedocean.com/wp-content/uploads/2015/03/EOS_HM1_users_guide.pdf) (Accessed 26/11/2019).

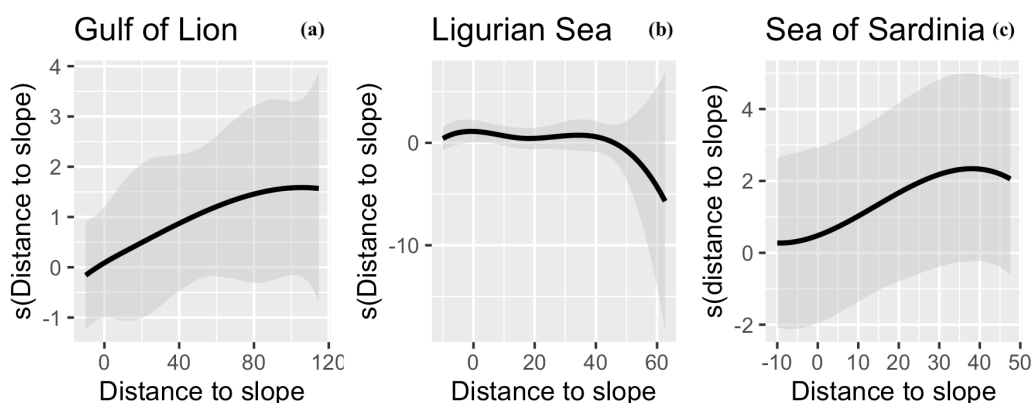


**Figure A.3:** Sperm whale presence modelled as a smooth function of distance to the slope in (a) the Gulf of Lion ( $p = 0.18$ ), (b) the Ligurian Sea ( $p = 0.35$ ) and (c) the Sea of Sardinia ( $p = 2.9 \times 10^{-6}$ ). Shaded areas represent 95 % confidence intervals.

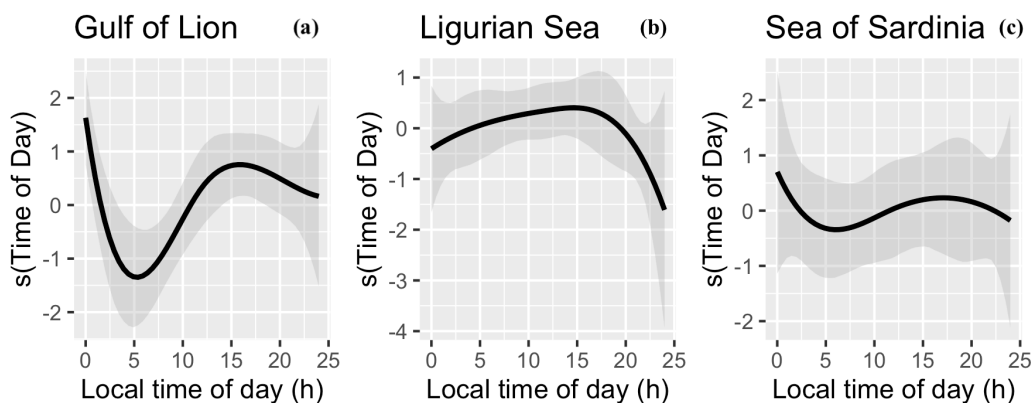


**Figure A.4:** Sperm whale presence modelled as a smooth function of local time of day in (a) the Gulf of Lion ( $p = 6.9 \times 10^{-7}$ ), (b) the Ligurian Sea ( $p = 0.22$ ) and (c) the Sea of Sardinia ( $p = 0.89$ ). Shaded areas represent 95 % confidence intervals.

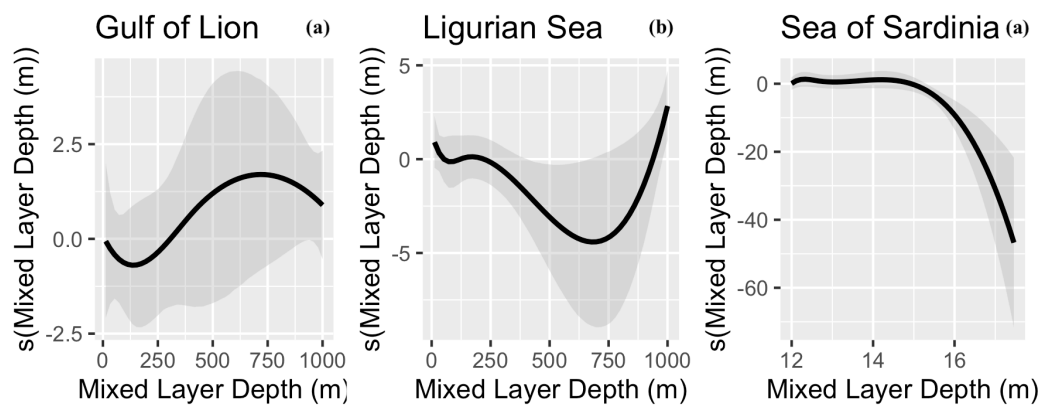


**Figure A.5:** Sperm whale presence modelled as a smooth function of mixed layer depth in (a) the Gulf of Lion ( $p = 0.08$ ), (b) the Ligurian Sea ( $p = 0.018$ ) and (c) the Sea of Sardinia ( $p = 2 \times 10^{-16}$ ). Shaded areas represent 95 % confidence intervals.

# Bibliography

Accobams (2019), *ACCOBAMS Survey Initiative Progress Report*, Tech. rep., ACCOBAMS-MOP7/2019/Inf 11.

Ageron, M., J. A. Aguilar, I. Al Samarai, A. Albert, F. Ameli, M. André, M. Anghinolfi, G. Anton, S. Anvar, M. Ardid, K. Arnaud, E. Aslanides, A. C. Assis Jesus, T. Astraatmadja, J. J. Aubert, R. Auer, E. Barbarito, B. Baret, S. Basa, M. Bazzotti, Y. Becherini, J. Beltramelli, A. Bersani, V. Bertin, S. Beurthey, S. Biagi, C. Bigongiari, M. Billault, R. Blaes, C. Bogazzi, N. De Botton, M. Bou-Cabo, B. Boudahef, M. C. Bouwhuis, A. M. Brown, J. Brunner, J. Busto, L. Caillat, A. Calzas, F. Camarena, A. Capone, L. Caponetto, C. Cârloganu, G. Carminati, E. Carmona, J. Carr, P. H. Carton, B. Cassano, E. Castorina, S. Cecchini, A. Ceres, T. Chaleil, P. Charvis, P. Chautot, T. Chiarusi, M. Circella, C. Compère, R. Coniglione, X. Coppolani, A. Cosquer, H. Costantini, N. Cottini, P. Coyle, S. Cuneo, C. Curtil, C. Damato, G. Damy, R. Van Dantzig, G. De Bonis, G. Decock, M. P. Decowski, I. Dekeyser, E. Delagnes, F. Desages-Ardellier, A. Deschamps, J. J. Destelle, F. Di Maria, B. Dinkespiler, C. Distefano, J. L. Dominique, C. Donzaud, D. Dornic, Q. Dorosti, J. F. Drogou, D. Drouhin, F. Druillolle, D. Durand, R. Durand, T. Eberl, U. Emanuele, J. J. Engelen, J. P. Ernenwein, S. Escoffier, E. Falchini, S. Favard, F. Fehr, F. Feinstein, M. Ferri, S. Ferry, C. Fiorello, V. Flaminio, F. Folger, U. Fritsch, J. L. Fuda, S. Galatá, S. Galeotti, P. Gay, F. Gensolen, G. Giacomelli, C. Gojak, J. P. Gómez-González, P. Goret, K. Graf, G. Guillard, G. Halladjian, G. Hallewell, H. Van Haren, B. Hartmann, A. J. Heijboer, E. Heine, Y. Hello, S. Henry, J. J. Hernández-Rey, B. Herold, J. Hößl, J. Hogenbirk, C. C. Hsu, J. R. Hubbard, M. Jaquet, M. Jaspers, M. De Jong, D. Jourde, M. Kadler, N. Kalantar-Nayestanaki, O. Kalekin, A. Kappes, T. Karg, S. Karkar, M. Karolak, U. Katz, P. Keller, P. Kestener, E. Kok, H. Kok, P. Kooijman, C. Kopper, A. Kouchner, W. Kretschmer, A. Kruijjer, S. Kuch, V. Kulikovskiy, D. Lachartre, H. Lafoux, P. Lagier, R. Lahmann, C. Lahonde-Hamdoun, P. Lamare, G. Lambard, J. C. Languillat, G. Larosa, J. Lavalle, Y. Le Guen, H. Le Provost, A. Levansuu, D. Lefèvre, T. Legou, G. Lelaizant, C. Lévêque, G. Lim, D. Lo Presti, H. Loehner, S. Loucatos, F. Louis, F. Lucarelli, V. Lyashuk, P. Magnier, S. Mangano, A. Marcel, M. Marcelin, A. Margiotta, J. A. Martinez-Mora, R. Masullo, F. Mazéas, A. Mazure, A. Meli, M. Melissas, E. Migneco, M. Mongelli, T. Montaruli, M. Morganti, L. Moscoso, H. Motz, M. Musumeci, C. Naumann, M. Naumann-Godo, M. Neff, V. Niess, G. J. Nooren, J. E. Oberski, C. Olivetto, N. Palanque-Delabrouille, D. Palioselitis, R. Papaleo, G. E. Pvlá, K. Payet, P. Payre, H. Peek, J. Petrovic, P. Piattelli, N. Picot-Clemente, C. Picq, Y. Piret, J. Poinsignon, V. Popa, T. Pradier, E. Presani, G. Prono, C. Racca, G. Raia, J. Van Randwijk, D. Real, C. Reed, F. Réthoré, P. Rewiersma, G. Riccobene, C. Richardt, R. Richter, J. S. Ricol, V. Rigaud, V. Roca, K. Roensch, J. F. Rolin, A. Rostovtsev, A. Rottura, J. Roux, M. Rujoiu, M. Ruppi, G. V. Russo, F. Salesa, K. Salomon, P. Sapienza, F. Schmitt, F. Schöck, J. P. Schuller, F. Schüssler, D. Sciliberto, R. Shanidze, E. Shirokov, F. Simeone, A. Sottoriva, A. Spies, T. Spona, M. Spurio, J. J.

- Steijger, T. Stolarczyk, K. Streeb, L. Sulak, M. Taiuti, C. Tamburini, C. Tao, L. Tasca, G. Terreni, D. Tezier, S. Toscano, F. Urbano, P. Valdy, B. Vallage, V. Van Elewyck, G. Vannoni, M. Vecchi, G. Venekamp, B. Verlaat, P. Vernin, E. Virique, G. De Vries, R. Van Wijk, G. Wijnker, G. Wobbe, E. De Wolf, Y. Yakovenko, H. Yepes, D. Zaborov, H. Zacccone, J. D. Zornoza, and J. Zúñiga (2011), ANTARES: The first undersea neutrino telescope, *Nuclear Instruments and Methods in Physics Research, Section A: Accelerators, Spectrometers, Detectors and Associated Equipment*, 656(1), 11–38.
- Aguilar de Soto, N. (2016), Peer-Reviewed Studies on the Effects of Anthropogenic Noise on Marine Invertebrates: From Scallop Larvae to Giant Squid, in: *The Effects of Noise on Aquatic Life II*, Unit 16, pp. 17–26, Springer Science+Business Media.
- Ainslie, M. (2010), *Principles of Sonar Performance Modelling*, Springer, Berlin, Heidelberg.
- Alappattu, D. P., Q. Wang, R. Yamaguchi, R. J. Lind, M. Reynolds, and A. J. Christman (2017), Warm layer and cool skin corrections for bulk water temperature measurements for air-sea interaction studies, *Journal of Geophysical Research: Oceans*, 122(8), 6470–6481.
- André, M., A. Caballé, M. van der Schaar, A. Solsona, L. Houégnigan, S. Zaugg, A. M. Sánchez, J. V. Castell, M. Solé, F. Vila, D. Djokic, S. Adrián-Martínez, A. Albert, M. Anghinolfi, G. Anton, M. Ardid, J.-J. Aubert, T. Avgitas, B. Baret, J. Barrios-Martí, S. Basa, V. Bertin, S. Biagi, R. Bormuth, M. C. Bouwhuis, R. Bruijn, J. Brunner, J. Busto, A. Capone, L. Caramete, J. Carr, S. Celli, T. Chiarusi, M. Circella, A. Coleiro, R. Coniglione, H. Costantini, P. Coyle, A. Creusot, A. Deschamps, G. De Bonis, C. Distefano, I. Di Palma, C. Donzaud, D. Dornic, D. Drouhin, T. Eberl, I. El Boddaini, D. Elsässer, A. Enzenhöfer, K. Fehn, I. Felis, L. A. Fusco, S. Galatà, P. Gay, S. Geißelsöder, K. Geyer, V. Giordano, A. Gleixner, H. Glotin, R. Gracia-Ruiz, K. Graf, S. Hallmann, H. van Haren, A. J. Heijboer, Y. Hello, J. J. Hernandez-Rey, J. Höbl, J. Hofestädt, C. Hugon, G. Illuminati, C. W. James, M. de Jong, M. Jongen, M. Kadler, O. Kalekin, U. Katz, D. Kießling, A. Kouchner, M. Kreter, I. Kreykenbohm, V. Kulikovskiy, C. Lachaud, R. Lahmann, D. Lefèvre, E. Leonora, S. Loucatos, M. Marcelin, A. Margiotta, A. Marinelli, J. A. Martínez-Mora, A. Mathieu, K. Melis, T. Michael, P. Migliozi, A. Moussa, C. Mueller, E. Nezri, G. E. Pvlá, C. Pellegrino, C. Perrina, P. Piattelli, V. Popa, T. Pradier, C. Racca, G. Riccobene, K. Roensch, M. Saldaña, D. F. E. Samtleben, M. Sanguineti, P. Sapienza, J. Schnabel, F. Schüssler, T. Seitz, C. Sieger, M. Spurio, T. Stolarczyk, A. Sánchez-Losa, M. Taiuti, A. Trovato, M. Tselengidou, D. Turpin, C. Tönnis, B. Vallage, C. Vallée, V. Van Elewyck, D. Vivolo, S. Wagner, J. Wilms, J. D. Zornoza, and J. Zúñiga (2017), Sperm whale long-range echolocation sounds revealed by ANTARES, a deep-sea neutrino telescope, *Scientific Reports*, 7(April), 45,517.
- André, M., M. van der Schaar, S. Zaugg, L. Houégnigan, A. M. Sánchez, and J. V. Castell (2011), Listening to the Deep: Live monitoring of ocean noise and cetacean acoustic signals, *Marine Pollution Bulletin*, 63(1-4), 18–26.
- Andreas, E. L., L. Mahrt, and D. Vickers (2015), An improved bulk air-sea surface flux algorithm, including spray-mediated transfer, *Quarterly Journal of the Royal Meteorological Society*, 141(687), 642–654.
- Au, W. W. L., G. Giorli, J. Chen, A. Copeland, M. O. Lammers, M. Richlen, S. Jarvis,

- R. Morrissey, and D. Moretti (2014), Presence and seasonal variation of deep diving foraging odontocetes around Kauai, Hawaii using remote autonomous acoustic recorders, *The Journal of the Acoustical Society of America*, 135(1), 521–530.
- Bailey, H., B. Senior, D. Simmons, J. Rusin, G. Picken, and P. M. Thompson (2010), Assessing underwater noise levels during pile-driving at an offshore windfarm and its potential effects on marine mammals, *Marine Pollution Bulletin*, 60(6), 888–897.
- Barclay, D. R., and M. J. Buckingham (2013), Depth dependence of wind-driven, broadband ambient noise in the Philippine Sea, *The Journal of the Acoustical Society of America*, 133(1), 62–71.
- Barlow, J., and B. L. Taylor (2005), Estimates of Sperm Whale Abundance in the Northeastern Temperate Pacific From a Combined Acoustic and Visual Survey, *Marine Mammal Science*, 21(3), 429–445.
- Barnes, C. R., M. M. R. Best, F. R. Johnson, and B. Pirenne (2010), Final installation and initial operation of the world's first regional cabled ocean observatory (NEPTUNE Canada), *Canadian Meteorological and Oceanographic Society Bulletin*, 38(3), 89–96.
- Baumgartner, M. F., and D. M. Fratantoni (2008), Diel periodicity in both sei whale vocalization rates and the vertical migration of their copepod prey observed from ocean gliders, *Limnology and Oceanography*, 53(5-part\_2), 2197–2209.
- Baumgartner, M. F., D. M. Fratantoni, T. P. Hurst, M. W. Brown, T. V. N. Cole, S. M. Van Parijs, and M. Johnson (2013), Real-time reporting of baleen whale passive acoustic detections from ocean gliders, *The Journal of the Acoustical Society of America*, 134(3), 1814–1823.
- Benoit-Bird, K. J., and G. L. Lawson (2016), Ecological Insights from Pelagic Habitats Acquired Using Active Acoustic Techniques, *Annual Review of Marine Science*, 8(1), 463–490.
- Black, P. G., J. R. Proni, J. C. Wilkerson, and C. E. Samsury (1997), Oceanic Rainfall Detection and Classification in Tropical and Subtropical Mesoscale Convective Systems Using Underwater Acoustic Methods, *Monthly Weather Review*, 125(9), 2014–2042.
- Boisseau, O., C. Lacey, T. Lewis, A. Moscrop, M. Danbolt, and R. McLanaghan (2010), Encounter rates of cetaceans in the Mediterranean Sea and contiguous Atlantic area, *Journal of the Marine Biological Association of the United Kingdom*, 90(8), 1589–1599.
- Bolgan, M., M. C. P. Amorim, P. J. Fonseca, L. Di Iorio, and E. Parmentier (2018), Acoustic complexity of vocal fish communities: A field and controlled validation, *Scientific Reports*, 8(1).
- Bolgan, M., A. Crucianelli, C. Mylonas, S. Henry, J. Falguière, and E. Parmentier (2020), Calling activity and calls' temporal features inform about fish reproductive condition and spawning in three cultured Sciaenidae species, *Aquaculture*, p. 735243.
- Bourassa, M., S. Gille, D. Jackson, J. B. Roberts, and G. Wick (2010), Ocean Winds and Turbulent Air-Sea Fluxes Inferred From Remote Sensing, *Oceanography*, 23(4), 36–51.
- Burgess, W. C. (2010), *Development of a Wideband Acoustic Recording Tag to Assess the Acoustic Behavior of Marine Wildlife*, Tech. Rep. January, Greeneridge Sciences.

- Butler, J. L., and C. H. Sherman (2016), Hydrophone Arrays, in: *Transducers and Arrays for Underwater Sound*, chap. 6, pp. 407–473, Springer.
- Callaghan, A., G. De Leeuw, L. Cohen, and C. D. O’Dowd (2008), Relationship of oceanic whitecap coverage to wind speed and wind history, *Geophysical Research Letters*, 35(23), 1–5.
- Cañadas, A., R. Sagarminaga, S. Garca-Tiscar, and S. García-Tiscar (2002), Cetacean distribution related with depth and slope in the Mediterranean waters off southern Spain, *Deep Sea Research Part I: Oceanographic Research Papers*, 49(11), 2053–2073.
- Carey, W. M., J. W. Fitzgerald, E. C. Monahan, and Q. Wang (1993), Measurement of the sound produced by a tipping trough with fresh and salt water, *The Journal of the Acoustical Society of America*, 93(6), 3178–3192.
- Carpinelli, E., P. Gauffier, P. Verborgh, S. Airoidi, L. David, N. Di-Méglia, A. Cañadas, A. Frantzis, L. Rendell, T. Lewis, B. Mussi, D. S. Pace, R. De Stephanis, C. Eva, G. Pauline, V. Philippe, A. Sabina, D. Léa, D. Nathalie, C. Ana, F. Alexandros, R. Luke, L. Tim, M. Barbara, P. D. Silvia, and D. S. Renaud (2014), Assessing sperm whale (*Physeter macrocephalus*) movements within the western Mediterranean Sea through photo-identification, *Aquatic Conservation: Marine and Freshwater Ecosystems*, 24(SUPPL.1), 23–30.
- Carrillo, M., and F. Ritter (2010), Increasing numbers of ship strikes in the Canary Islands : proposals for immediate action to reduce risk of vessel-whale collisions, *Journal of Cetatean Research Management*, 11(2), 131–138.
- Caruso, F., V. Sciacca, G. Bellia, E. De Domenico, G. Larosa, E. Papale, C. Pellegrino, S. Pulvirenti, G. Riccobene, and F. Simeone (2015), Size distribution of sperm whales acoustically identified during long term deep-sea monitoring in the Ionian Sea, *PLoS one*, 10(12), e0144503.
- Cauchy, P., K. J. Heywood, N. D. Merchant, B. Y. Queste, and P. Testor (2018), Wind Speed Measured from Underwater Gliders Using Passive Acoustics, *Journal of Atmospheric and Oceanic Technology*, 35(12), 2305–2321.
- Cazau, D., J. Bonnel, and M. Baumgartner (2019), Wind Speed Estimation Using Acoustic Underwater Glider in a Near-Shore Marine Environment, *IEEE Transactions on Geoscience and Remote Sensing*, 57(4), 2097–2106.
- Cazau, D., J. Bonnel, J. Jouma’a, Y. le Bras, and C. Guinet (2017), Measuring the Marine Soundscape of the Indian Ocean with Southern Elephant Seals Used as Acoustic Gliders of Opportunity, *Journal of Atmospheric and Oceanic Technology*, 34(1), 207–223.
- Charrier, I., S. Marchesseau, P. Dendrinis, E. Tounta, and A. A. Karamanlidis (2017), Individual signatures in the vocal repertoire of the endangered Mediterranean monk seal: New perspectives for population monitoring, *Endangered Species Research*, 32(1), 459–470.
- Clausen, K. T., M. Wahlberg, K. Beedholm, S. Deruiter, and P. T. Madsen (2011), Click communication in harbour porpoises *phocoena phocoena*, *Bioacoustics*, 20(1), 1–28.
- Cleator, H. J., I. Stirling, and T. G. Smith (1989), Underwater vocalizations of the bearded seal (*Erignathus barbatus*), *Canadian Journal of Zoology*, 67(8), 1900–1910.

- Coquereau, L., J. Grall, L. Chauvaud, C. Gervaise, J. Clavier, A. Jolivet, and L. Di Iorio (2016), Sound production and associated behaviours of benthic invertebrates from a coastal habitat in the north-east Atlantic, *Marine Biology*, 163(5), 1–13.
- Crouch, W. W. (1972), The Logarithmic Dependence of Surface-Generated Ambient-Sea-Noise Spectrum Level on Wind Speed, *The Journal of the Acoustical Society of America*, 51(3B), 1066.
- Curé, C., S. Isojunno, F. Visser, P. J. Wensveen, L. D. Sivle, P. H. Kvaldsheim, F. P. A. Lam, and P. J. Miller (2016), Biological significance of sperm whale responses to sonar: Comparison with anti-predator responses, *Endangered Species Research*, 31(1), 89–102.
- Davis, R., M. Baumgartner, A. Comeau, D. Cunningham, K. Davies, A. Furlong, H. Johnson, S. L'Orsa, T. Ross, C. Taggart, and F. Whoriskey (2016), Tracking whales on the Scotian Shelf using passive acoustic monitoring on ocean gliders, *OCEANS 2016 MTS/IEEE Monterey, OCE 2016*, pp. 1–4.
- Davis, R. E., L. A. Regier, J. Dufour, and D. C. Webb (1992), The Autonomous Lagrangian Circulation Explorer (ALACE), *Journal of Atmospheric and Oceanic Technology*, 9(3), 264–285.
- Davis, R. E., J. T. Sherman, and J. Dufour (2001), Profiling ALACEs and other advances in autonomous subsurface floats, *Journal of Atmospheric and Oceanic Technology*, 18(6), 982–993.
- Davis, R. W., N. Jaquet, D. Gendron, U. Markaida, G. Bazzino, and W. Gilly (2007), Diving behavior of sperm whales in relation to behavior of a major prey species, the jumbo squid, in the Gulf of California, Mexico, *Marine Ecology Progress Series*, 333, 291–302.
- de Stephanis, R., J. Giménez, E. Carpinelli, C. Gutierrez-Exposito, and A. Cañadas (2013), As main meal for sperm whales: Plastics debris, *Marine Pollution Bulletin*, 69(1), 206–214.
- Di Iorio, L., C. Gervaise, V. Jaud, A. A. Robson, and L. Chauvaud (2012), Hydrophone detects cracking sounds: Non-intrusive monitoring of bivalve movement, *Journal of Experimental Marine Biology and Ecology*, 432-433, 9–16.
- Di Iorio, L., X. Raick, E. Parmentier, P. Boissery, C.-A. Valentini-Poirier, and C. Gervaise (2018), Posidonia meadows calling': a ubiquitous fish sound with monitoring potential, *Remote Sensing in Ecology and Conservation*, 4(3), 248–263.
- Dolman, S. J., P. G. Evans, G. Notarbartolo-di Sciara, and H. Frisch (2011), Active sonar, beaked whales and European regional policy, *Marine Pollution Bulletin*, 63(1-4), 27–34.
- Dos Santos, F. A., P. M. São Thiago, A. L. S. De Oliveira, R. Barmak, J. A. M. Lima, F. G. De Almeida, and T. P. Paula (2016), Investigating flow noise on underwater gliders acoustic data, *The Journal of the Acoustical Society of America*, 140(4), 3409–3409.
- Drouot, V., M. Berube, A. Gannier, J. C. Goold, R. J. Reid, and P. J. Palsboll (2004a), A note on genetic isolation of Mediterranean sperm whales (*Physeter macrocephalus*) suggested by mitochondrial DNA, *Journal of Cetacean Research and Management*, 6(1), 29–32.

- Drouot, V., A. Gannier, and J. C. Goold (2004b), Diving and Feeding Behaviour of Sperm Whales (*Physeter macrocephalus*) in the Northwestern Mediterranean Sea, *Aquatic Mammals*, 30(3), 419–426.
- Drouot, V., A. Gannier, and J. C. Goold (2004c), Summer social distribution of sperm whales (*Physeter macrocephalus*) in the Mediterranean Sea, *Journal of the Marine Biological Association of the United Kingdom*, 84(3), 675–680.
- Dziak, R. P., W. S. Lee, J. H. Haxel, H. Matsumoto, G. Tepp, T.-K. Lau, L. Roche, S. Yun, C.-K. Lee, J. Lee, and S.-T. Yoon (2019), Hydroacoustic, Meteorologic and Seismic Observations of the 2016 Nansen Ice Shelf Calving Event and Iceberg Formation, *Frontiers in Earth Science*, 7(July), 1–12.
- Engelhaupt, D., A. Rus Hoelzel, C. Nicholson, A. Frantzis, S. Mesnick, S. Gero, H. Whitehead, L. Rendell, P. Miller, and R. de Stephanis (2009), Female philopatry in coastal basins and male dispersion across the North Atlantic in a highly mobile marine species, the sperm whale (*Physeter macrocephalus*), *Molecular Ecology*, 18(20), 4193–4205.
- Erbe, C. (2002), Underwater noise of whale-watching boats and potential effects on killer whales (*Orcinus orca*), based on an acoustic impact model, *Marine Mammal Science*, 18(2), 394–418.
- Erbe, C., A. Verma, R. McCauley, A. Gavrilov, and I. Parnum (2015), The marine soundscape of the Perth Canyon, *Progress in Oceanography*, 137, 38–51.
- Everest, F. a. (1947), Acoustical Characteristics of Noise Produced by Snapping Shrimp, *The Journal of the Acoustical Society of America*, 19(4), 726.
- Farmer, D. M., and D. D. Lemon (1984), The Influence of Bubbles on Ambient Noise in the Ocean at High Wind Speeds, *Journal of Physical Oceanography*, 14(11), 1762–1778.
- Foreman, R. J., and S. Emeis (2010), Revisiting the Definition of the Drag Coefficient in the Marine Atmospheric Boundary Layer, *Journal of Physical Oceanography*, 40(10), 2325–2332.
- Francois, R. E., and G. R. Garrison (1982), Sound absorption based on ocean measurements. Part II: Boric acid contribution and equation for total absorption, *Journal of the Acoustical Society of America*, 72(6), 1879–1890.
- Frantzis, A., S. Airoidi, G. Notarbartolo-di Sciara, C. Johnson, and S. Mazzariol (2011), Inter-basin movements of Mediterranean sperm whales provide insight into their population structure and conservation, *Deep Sea Research Part I: Oceanographic Research Papers*, 58(4), 454–459.
- Frantzis, A., P. Alexiadou, and K. C. Gkikopoulou (2014), Sperm whale occurrence, site fidelity and population structure along the Hellenic Trench (Greece, Mediterranean Sea), *Aquatic Conservation: Marine and Freshwater Ecosystems*, 24(S1), 83–102.
- Frantzis, A., P. Alexiadou, G. Paximadis, E. Politi, A. Gannier, and M. Corsini-Foka (2003), Current knowledge of the cetacean fauna of the Greek Seas, *Journal of Cetacean Research and Management*, 5(3), 219–232.

- Frantzis, A., R. Leaper, P. Alexiadou, A. Prospathopoulos, and D. Lekkas (2019), Shipping routes through core habitat of endangered sperm whales along the Hellenic Trench, Greece: Can we reduce collision risks?, *PLOS ONE*, *14*(2), e0212,016.
- Fregosi, S., D. V. Harris, H. Matsumoto, D. K. Mellinger, C. Negretti, D. J. Moretti, S. W. Martin, B. Matsuyama, P. J. Dugan, and H. Klinck (2020), Comparison of fin whale 20 Hz call detections by deep-water mobile autonomous and stationary recorders, *The Journal of the Acoustical Society of America*, *147*(2), 961–977.
- Gallo-Reynoso, J. P., J. Égido-Villarreal, and G. L. Martínez-Villalba (2011), Reaction of fin whales balaenoptera physalus to an earthquake, *Bioacoustics*, *20*(3), 317–329.
- Gannier, A., V. Drouot, and J. C. Goold (2002), Distribution and relative abundance of sperm whales in the Mediterranean Sea, *Marine Ecology Progress Series*, *243*, 281–293.
- Gannier, A., and E. Praca (2007), SST fronts and the summer sperm whale distribution in the north-west Mediterranean Sea, *Journal of the Marine Biological Association of the United Kingdom*, *87*(1), 187–193.
- Garbe, C. S., A. Rutgersson, J. Boutin, G. D. Leeuw, B. Delille, C. W. Fairall, N. Gruber, J. Hare, D. T. Ho, M. T. Johnson, P. D. Nightingale, H. Pettersson, J. Piskozub, E. Sahle, W.-t. Tsai, B. Ward, D. K. Woolf, and C. J. Zappa (2014), Transfer Across the Air-Sea Interface, in: *Ocean-Atmosphere Interactions of Gases and Particles* (Liss, P. S., and M. T. Johnson, eds.), chap. 2, pp. 55–112, Springer, Berlin, Heidelberg.
- Giorli, G., W. W. L. Au, and A. Neuheimer (2016), Differences in foraging activity of deep sea diving odontocetes in the Ligurian Sea as determined by passive acoustic recorders, *Deep Sea Research Part I: Oceanographic Research Papers*, *107*, 1–8.
- Glenn, S. M., T. N. Miles, G. N. Seroka, Y. Xu, R. K. Forney, F. Yu, H. Roarty, O. Schofield, and J. Kohut (2016), Stratified coastal ocean interactions with tropical cyclones, *Nature Communications*, *7*(May 2015).
- Gordon, J., R. Leaper, F. G. Hartley, and O. Chappell (1992), Effects of whale-watching vessels on the surface and underwater acoustic behaviour of sperm whales off Kaikoura, New Zealand, *Science & Research Series*, *52*.
- Grist, J. P., S. A. Josey, Z. L. Jacobs, R. Marsh, B. Sinha, and E. Van Sebille (2016), Extreme airsea interaction over the North Atlantic subpolar gyre during the winter of 2013/2014 and its sub-surface legacy, *Climate Dynamics*, *46*(11-12), 4027–4045.
- Guan, S., J. Vignola, J. Judge, and D. Turo (2015), Airgun inter-pulse noise field during a seismic survey in an Arctic ultra shallow marine environment, *The Journal of the Acoustical Society of America*, *138*(6), 3447–3457.
- Guerra, M., L. Hickmott, J. van der Hoop, W. Rayment, E. Leunissen, E. Slooten, and M. Moore (2017), Diverse foraging strategies by a marine top predator: Sperm whales exploit pelagic and demersal habitats in the Kaikura submarine canyon, *Deep-Sea Research Part I: Oceanographic Research Papers*, *128*(July), 98–108.
- Guerra, M., A. M. Thode, S. B. Blackwell, and A. Michael Macrander (2011), Quantifying seismic survey reverberation off the Alaskan North Slope, *The Journal of the Acoustical Society of America*, *130*(5), 3046–3058.

- Halekoh, U., S. Højsgaard, and J. Yan (2006), The R package geepack for generalized estimating equations, *Journal of Statistical Software*, 15(2), 1–11.
- Harris, S. A., N. T. Shears, and C. A. Radford (2016), Ecoacoustic indices as proxies for biodiversity on temperate reefs, *Methods in Ecology and Evolution*, 7(6), 713–724.
- Harrison, C. H., and D. G. Simons (2002), Geoacoustic inversion of ambient noise: A simple method, *The Journal of the Acoustical Society of America*, 112(4), 1377–1389.
- Hatcher, M. G. (2017), *Ambient Noise From Turbidity Currents in Howe Sound*, Ph.D. thesis, Dalhousie University.
- Haver, S. M., H. Klinck, S. L. Nieuwkerk, H. Matsumoto, R. P. Dziak, and J. L. Miksis-Olds (2017), The not-so-silent world: Measuring Arctic, Equatorial, and Antarctic soundscapes in the Atlantic Ocean, *Deep-Sea Research Part I: Oceanographic Research Papers*, 122(February), 95–104.
- Hawkins, A. D., A. E. Pembroke, and A. N. Popper (2014), Information gaps in understanding the effects of noise on fishes and invertebrates, *Reviews in Fish Biology and Fisheries*, 25(1), 39–64.
- Hildebrand, J. A., Z. E. Gentes, S. C. Johnson, K. E. Frasier, K. Merckens, B. J. Thayre, and S. M. Wiggins (2013), *Acoustic Monitoring of Cetaceans in the Northern Gulf of Mexico using Wave Gliders equipped with High-Frequency Acoustic Recording Packages*, Tech. Rep. March, Scripps Institution of Oceanography.
- Hoegh-Guldberg, O., R. Cai, E. S. Poloczanska, P. G. Brewer, S. Sundby, K. Hilmi, V. J. Fabry, and S. Jung (2014), The ocean, in: *Climate Change 2014: Impacts, Adaptation, and Vulnerability. Part B: Regional Aspects. Contribution of Working Group II to the Fifth Assessment Report of the Intergovernmental Panel on Climate Change* (Barros, V. R., C. B. Field, D. J. Dokken, M. D. Mastrandrea, K. J. Mach, T. E. Bilir, M. Chatterjee, K. L. Ebi, Y. O. Estrada, R. C. Genova, B. Girma, E. Kissel, A. Levy, S. MacCracken, P. Mastrandrea, and L. L. White, eds.), chap. 30, pp. 1655–1731, Cambridge University Press, Cambridge, United Kingdom and New York, NY, USA.
- Houpert, L., X. Durrieu de Madron, P. Testor, A. Bosse, F. D’Ortenzio, M. N. Bouin, D. Dausse, H. Le Goff, S. Kunesch, M. Labaste, L. Coppola, L. Mortier, and P. Raimbault (2016), Observations of open-ocean deep convection in the northwestern Mediterranean Sea: Seasonal and interannual variability of mixing and deep water masses for the 2007–2013 Period, *Journal of Geophysical Research: Oceans*, 121(11), 8139–8171.
- IOC (2019), *The global ocean observing system 2030 strategy*, Tech. Rep. 239, IOC, Paris.
- Janzen, C. D., and E. L. Creed (2011), Physical oceanographic data from Seaglider trials in stratified coastal waters using a new pumped payload CTD, *OCEANS’11 - MTS/IEEE Kona, Program Book*.
- Jaquet, N., and D. Gendron (2002), Distribution and relative abundance of sperm whales in relation to key environmental features, squid landings and the distribution of other cetacean species in the Gulf of California, Mexico, *Marine Biology*, 141(3), 591–601.
- Jensen, F. B., W. A. Kuperman, M. B. Porter, and H. Schmidt (2011), *Fundamentals of Ocean Acoustics. In: Computational Ocean Acoustics. Modern Acoustics and Signal Processing*, Springer, New York, NY.

- Jensen, F. H., M. Johnson, M. Ladegaard, D. M. Wisniewska, and P. T. Madsen (2018), Narrow Acoustic Field of View Drives Frequency Scaling in Toothed Whale Biosonar, *Current Biology*, 28(23), 3878–3885.e3.
- Jiang, Y.-m. (2016), *Capability of the direction of arrival estimation using a 3D acoustic compact array*, Tech. rep., CMRE.
- Johnson, M. P., and P. L. Tyack (2003), A digital acoustic recording tag for measuring the response of wild marine mammals to sound, *IEEE Journal of Oceanic Engineering*, 28(1), 3–12.
- Johnson, M. W., F. A. Everest, and R. W. Young (1947), The Role of Snapping Shrimp (Crangon and Synamphus) in the Production of Underwater Noise in the Sea, *Biological Bulletin*, 93(2), 122–138.
- Kent, E. C. (1998), A comparison of ship- and scatterometer-derived wind speed data in open ocean and coastal areas, *International Journal of Remote Sensing*, 19(17), 3361–3381.
- Klinck, H., D. K. Mellinger, K. Klinck, N. M. Bogue, J. C. Luby, W. A. Jump, G. B. Shilling, T. Litchendorf, A. S. Wood, G. S. Schorr, and R. W. Baird (2012), Near-real-time acoustic monitoring of beaked whales and other cetaceans using a Seaglider, *PLoS ONE*, 7(5).
- Krause, B. (2008), Anatomy of the soundscape: Evolving perspectives, *AES: Journal of the Audio Engineering Society*, 56(1-2), 73–80.
- Kuperman, W. (2001), Acoustics, Deep Ocean, in: *Encyclopedia of Ocean Sciences*, pp. 101–111, Elsevier.
- Kusel, E. T., T. Munoz, M. Siderius, D. K. Mellinger, and S. Heimlich (2017), Marine mammal tracks from two-hydrophone acoustic recordings made with a glider, *Ocean Science*, 13(2), 273–288.
- Ladich, F. (2013), Effects of Noise on Sound Detection and Acoustic Communication in Fishes, in: *Animal Communication and Noise*, vol. 2, chap. 4, pp. 65–90, Springer.
- Laran, S., and V. Drouot-Dulau (2007), Seasonal variation of striped dolphins, fin-and sperm whales' abundance in the Ligurian Sea (Mediterranean Sea), *Journal of the Marine Biological Association of the United Kingdom*, 87(1), 345–352.
- Large, W. G., and S. Pond (1981), Open Ocean Momentum Flux Measurements in Moderate to Strong Winds, *Journal of Physical Oceanography*, 11(3), 324–336.
- Lasky, M., R. D. Doolittle, B. D. Simmons, and S. G. Lemon (2004), Recent progress in towed hydrophone array research, *IEEE Journal of Oceanic Engineering*, 29(2), 374–387.
- Lee, C., J. Gobat, and L. Rainville (2012), *An Autonomous Investigation of Kuroshio and Mesoscale Impacts on Upper Ocean Response to Typhoon Forcing*, Tech. rep., Washington University Seattle Applied Physics Lab.
- Lee, C. M., J. Thomson, K. H. Cho, S. Cole, M. Doble, L. Freitag, H. Graber, B. Hwang, S. Jayne, S. H. Kang, J. H. Kim, R. Krishfield, C. Lee, T. Maksym, W. Maslowski, B. Owens, M. J. Perry, P. Posey, L. Rainville, J. Richter-Menge, A. Roberts, A. Schweiger, W. Shaw, T. Stanton, M. Steele, M. L. Timmermans, J. Toole,

- P. Wadhams, J. Wilkinson, E. J. Yang, J. Zhang, S. Ackley, F. Arduin, F. G. Arduin, A. Babanin, T. Collins, C. Fairall, J. Gemmrich, P. Guest, B. Holt, S. Lehner, M. Meylan, F. Montiel, W. Perrie, O. Persson, E. Rogers, H. Shen, H. Shen, V. Squire, S. Stammerjohn, J. Stopa, P. Sutherland, and T. Williams (2017), An autonomous approach to observing the seasonal ice zone in the western arctic, *Oceanography*, 30(2), 56–68.
- Lemon, D. D., D. M. Farmer, and D. R. Watts (1984), Acoustic Measurements of Wind Speed and Precipitation Over a Continental Shelf, *Journal of Geophysical Research*, 89(20), 3462–3472.
- Lemon, S. (2004), Towed-Array History, 19172003, *IEEE Journal of Oceanic Engineering*, 29(2), 365–373.
- Lepper, P. A., and G. L. D’Spain (2007), Measurement and modeling of the acoustic field near an underwater vehicle and implications for acoustic source localization, *The Journal of the Acoustical Society of America*, 122(2), 892–905.
- Lewis, E. R., and S. E. Schwartz (2004), Sea salt aerosol production: mechanisms, methods, measurements, and models-A critical review, in: *Geophysical Monograph*, vol. 152, pp. A–408, American Geophysical Union.
- Lewis, T., O. Boisseau, R. McLanaghan, A. Moscrop, D. Gillespie, C. Lacey, J. Matthews, M. Danbolt, and R. Leaper (2018), Abundance estimates for sperm whales in the Mediterranean Sea from acoustic line-transect surveys, *Journal of Cetacean Research and Management*, 18, 103–117.
- Ma, B. B., and J. A. Nystuen (2005), Passive Acoustic Detection and Measurement of Rainfall at Sea, *Journal of Atmospheric and Oceanic Technology*, 22(8), 1225–1248.
- Madsen, P. T., R. Payne, N. U. Kristiansen, M. Wahlberg, I. Kerr, and B. Møhl (2002), Sperm whale sound production studied with ultrasound time/depth-recording tags, *Journal of Experimental Biology*, 205(13), 1899–1906.
- Malanotte-Rizzoli, P. (1985), Long-range inversions for ocean acoustic tomography, *Journal of Geophysical Research*, 90(C4), 7098.
- Mannocci, L., J. J. Roberts, P. N. Halpin, M. Authier, O. Boisseau, M. N. Bradai, A. Cañadas, C. Chicote, L. David, N. Di-Méglio, C. M. Fortuna, A. Frantzis, M. Gazo, T. Genov, P. S. Hammond, D. Holcer, K. Kaschner, D. Kerem, G. Lauriano, T. Lewis, G. Notarbartolo-di Sciara, S. Panigada, J. A. Raga, A. Scheinin, V. Ridoux, A. Vella, and J. Vella (2018), Assessing cetacean surveys throughout the Mediterranean Sea: a gap analysis in environmental space, *Scientific Reports*, 8(1), 3126.
- Many, G., F. Bourrin, X. Durrieu de Madron, A. Ody, D. Doxaran, and P. Cauchy (2018), Glider and satellite monitoring of the variability of the suspended particle distribution and size in the Rhône ROFI, *Progress in Oceanography*, 163, 123–135.
- Margirier, F., A. Bosse, P. Testor, B. L’Hévéder, L. Mortier, and D. Smeed (2017), Characterization of Convective Plumes Associated With Oceanic Deep Convection in the Northwestern Mediterranean From High-Resolution In Situ Data Collected by Gliders, *Journal of Geophysical Research: Oceans*, 122(12), 9814–9826.
- Marques, T. A., L. Thomas, S. W. Martin, D. K. Mellinger, J. A. Ward, D. J. Moretti, D. Harris, and P. L. Tyack (2013), Estimating animal population density using passive acoustics, *Biological Reviews*, 88(2), 287–309.

- Matsumoto, H., J. Haxel, A. Turpin, S. Fregosi, D. Mellinger, M. Fowler, S. Bauman-Pickering, R. Dziak, H. Klinck, K. Klinck, A. Erofeev, J. Barth, R. Shearman, and C. Jones (2015), Simultaneous operation of mobile acoustic recording systems off the Washington coast for cetacean studies, in: *OCEANS 2015 - MTS/IEEE Washington*, October, pp. 1–7, IEEE.
- Matsumoto, H., J. H. Haxel, R. P. Dziak, D. R. Bohnenstiehl, and R. W. Embley (2011), Mapping the sound field of an erupting submarine volcano using an acoustic glider, *The Journal of the Acoustical Society of America*, 129(3), EL94–EL99.
- Matsumoto, H., C. Jones, H. Klinck, D. K. Mellinger, R. P. Dziak, and C. Meinig (2013), Tracking beaked whales with a passive acoustic profiler float, *The Journal of the Acoustical Society of America*, 133(2), 731–740.
- McGuire, J. J., M. S. Boettcher, and T. H. Jordan (2005), Erratum: Foreshock sequences and short-term earthquake predictability on East Pacific Rise transform faults, *Nature*, 435(7041), 528–528.
- McPhaden, M., K. Ando, B. Bourlès, H. P. Reitag, R. Lumpkin, Y. Masumoto, V. S. N. Murty, P. Nobre, M. Ravichandran, J. Vialard, D. Vousden, and W. Yu (2010), The Global Tropical Moored Buoy Array, in: *Proceedings of OceanObs'09: Sustained Ocean Observations and Information for Society*, 1, pp. 668–682, European Space Agency.
- Mellinger, D. K. (2007), An Overview of Fixed Passive Acoustic Observation Methods for Cetaceans, *Oceanography*, 20(4), 36 – 45.
- Merchant, N. D., P. Blondel, D. T. Dakin, and J. Dorocicz (2012), Averaging underwater noise levels for environmental assessment of shipping, *The Journal of the Acoustical Society of America*, 132(4), EL343–EL349.
- Merchant, N. D., K. L. Brookes, R. C. Faulkner, A. W. J. Bicknell, B. J. Godley, and M. J. Witt (2016), Underwater noise levels in UK waters, *Scientific Reports*, 6(1), 36,942.
- Merchant, N. D., R. C. Faulkner, and R. Martinez (2018), Marine Noise Budgets in Practice, *Conservation Letters*, 11(3), 1–8.
- Merchant, N. D., K. M. Fristrup, M. P. Johnson, P. L. Tyack, M. J. Witt, P. Blondel, and S. E. Parks (2015), Measuring acoustic habitats, *Methods in Ecology and Evolution*, 6(3), 257–265.
- Middlebrooks, J. (1991), Sound Localization By Human Listeners, *Annual Review of Psychology*, 42(1), 135–159.
- Miller, B. S., and E. J. Miller (2018), The seasonal occupancy and diel behaviour of Antarctic sperm whales revealed by acoustic monitoring, *Scientific Reports*, 8(1), 1–12.
- Miller, P. J. O., M. P. Johnson, and P. L. Tyack (2004), Sperm whale behaviour indicates the use of echolocation click buzzes creaks' in prey capture, *Proceedings of the Royal Society of London B: Biological Sciences*, 271(1554), 2239–2247.
- Milne, P. H. (1983), *Underwater acoustic positioning systems*, E & FN Spon, United States.

- Moat, B. I., M. J. Yelland, R. W. Pascal, and A. F. Molland (2005), An overview of the airflow distortion at anemometer sites on ships, *International Journal of Climatology*, 25(7), 997–1006.
- Møhl, B., M. Wahlberg, P. T. Madsen, A. Heerfordt, and A. Lund (2003), The monopulsed nature of sperm whale clicks, *The Journal of the Acoustical Society of America*, 114(2), 1143–1154.
- Møhl, B., M. Wahlberg, P. T. Madsen, L. A. Miller, and A. Surlykke (2000), Sperm whale clicks: Directionality and source level revisited, *The journal of the acoustical society of America*, 107(1), 638–648.
- Monahan, E. C., and H. G. Dam (2001), Bubbles: An estimate of their role in the global oceanic flux of carbon, *Journal of Geophysical Research: Oceans*, 106(C5), 9377–9383.
- Monahan, E. C., C. W. Fairall, K. L. Davidson, and P. J. Boyle (1983), Observed interrelations between 10m winds, ocean whitecaps and marine aerosols, *Quarterly Journal of the Royal Meteorological Society*, 109(460), 379–392.
- Monahan, E. C., and I. G. O’Muircheartaigh (1986), Whitecaps and the passive remote sensing of the ocean surface, *International Journal of Remote Sensing*, 7(5), 627–642.
- Monahan, E. C., A. Staniec, and P. Vlahos (2017), Spume Drops: Their Potential Role in Air-Sea Gas Exchange, *Journal of Geophysical Research: Oceans*, 122(12), 9500–9517.
- Moore, S. E., B. M. Howe, K. M. Stafford, and M. L. Boyd (2007), Including Whale Call Detection in Standard Ocean Measurements: Application of Acoustic Seagliders, *Marine Technology Society Journal*, 41(4), 53–57.
- Moors, H. B., and J. M. Terhune (2004), Repetition patterns in Weddell seal ( *Leptonychotes weddellii* ) underwater multiple element calls , *The Journal of the Acoustical Society of America*, 116(2), 1261–1270.
- Munk, W. H. (1974), Sound channel in an exponentially stratified ocean, with application to SOFAR, *The Journal of the Acoustical Society of America*, 55(2), 220–226.
- Munk, W. H., P. Worcester, and C. Wunsch (1995), Ocean acoustic tomography, Cambridge Univ, Pr., Cambridge UK.
- Northrop, J., and J. G. Colborn (1975), Sofar Channel Axial Sound Speed and Depth in the Atlantic Ocean, *The Journal of the Acoustical Society of America*, 57(2), 522–522.
- Notarbartolo-di Sciara, G. (1990), A note on the cetacean incidental catch in the Italian driftnet swordfish fishery, 1986-1988, *Report of the International Whaling Commission*, 40, 459–460.
- Notarbartolo-Di-Sciara, G. (2014), Sperm whales, *Physeter macrocephalus*, in the Mediterranean Sea: A summary of status, threats, and conservation recommendations, *Aquatic Conservation: Marine and Freshwater Ecosystems*, 24(SUPPL.1), 4–10.
- Notarbartolo-di Sciara, G., T. Agardy, D. Hyrenbach, T. Scovazzi, and P. Van Klaveren (2008), The Pelagos sanctuary for Mediterranean marine mammals, *Aquatic Conservation: Marine and Freshwater Ecosystems*, 18(4), 367–391.

- Notarbartolo-di Sciara, G., G. Bearzi, A. Canadas, and A. Frantzis (2004), *High mortality of sperm whales in the north-western Mediterranean, 1971-2003*, Tech. rep., Scientific Committee of the International Whaling Commission.
- Notarbartolo-di Sciara, G., A. Frantzis, G. Bearzi, and R. Reeves (2012), *Physeter macrocephalus (Mediterranean subpopulation)*, Tech. rep., The IUCN Red List of Threatened Species 2012: e.T16370739A16370477.
- Nott, B. J. (2015), *Long-Endurance Maritime Surveillance With Ocean Glider Networks*, Master's thesis, Monterey, California: Naval Postgraduate School.
- Nowacek, D. P., C. W. Clark, D. Mann, P. J. Miller, H. C. Rosenbaum, J. S. Golden, M. Jasny, J. Kraska, and B. L. Southall (2015), Marine seismic surveys and ocean noise: time for coordinated and prudent planning, *Frontiers in Ecology and the Environment*, 13(7), 378–386.
- Nuret, M., and N. Fourrié (2011), AROME.WMED. GAME/ CNRM, Météo-France, accessed 19 February 2015, [https://doi.org/10.6096/hymex.arome\\_wmed.2012.02.20](https://doi.org/10.6096/hymex.arome_wmed.2012.02.20).
- Nystuen, J. A. (1996), Acoustical rainfall analysis: Rainfall drop size distribution using the underwater sound field, *Journal of Atmospheric and Oceanic Technology*, 13(1), 74–84.
- Nystuen, J. A., and B. B. Ma (2002), Using Ambient Sound to Passively Monitor Sea Surface Processes, in: *Pan Ocean Remote Sensing Conference (PORSEC)*, pp. 3–6.
- Onken, R., H.-V. Fiekas, L. Beguery, I. Borrione, A. Funk, M. Hemming, J. Hernandez-Lasheras, K. J. Heywood, J. Kaiser, M. Knoll, B. Mourre, P. Oddo, P.-M. Poulain, B. Y. Queste, A. Russo, K. Shitashima, M. Siderius, and E. T. Küsel (2018), High-resolution observations in the western Mediterranean Sea: the REP14-MED experiment, *Ocean Sci.*, 14(2), 321–335.
- Pace, D. S., B. Mussi, J. C. D. Gordon, M. Würtz, M. Aïssi, A. Ouammi, C. Fiori, and J. Alessi (2014), Sperm whales in the Mediterranean are classified as Endangered by the IUCN. They are apparently isolated from adjacent Atlantic populations, and subject to anthropogenic pressures including interactions with illegal driftnet fisheries, ship strikes, in: *Aquatic Conservation: Marine and Freshwater Ecosystems*, 24(S1), 103–118.
- Parmentier, E., and M. L. Fine (2016), Fish Sound Production: Insights, in: *Vertebrate Sound Production and Acoustic Communication*, chap. 2, pp. 19–49, Springer International Publishing.
- Pavan, G., G. La Manna, F. Zardin, E. Internullo, S. Kloeti, G. Cosentino, F. Speziale, G. Riccobene, and B. Skripten (2008), Short term and long term bioacoustic monitoring of the marine environment. Results from NEMO ONDE experiment and way ahead, in: *Computational bioacoustics for assessing biodiversity. Proceedings of the International Expert meeting on IT-based detection of bioacoustical patterns. Published by Federal Agency for Nature Conservation, Bonn, Germany*, pp. 7–14.
- Piggott, C. L. (1964), Ambient sea noise at low frequencies in shallow water of the Scotian shelf, *The Journal of the Acoustical Society of America*, 36(11), 2152–2163.
- Pirotta, E., J. Matthiopoulos, M. MacKenzie, L. Scott-Hayward, and L. Rendell (2011), Modelling sperm whale habitat preference: a novel approach combining transect and follow data, *Marine Ecology Progress Series*, 436, 257–272.

- Pirotta, V., A. Grech, I. D. Jonsen, W. F. Laurance, and R. G. Harcourt (2019), Consequences of global shipping traffic for marine giants, *Frontiers in Ecology and the Environment*, 17(1), 39–47.
- Praca, E., and A. Gannier (2008), Ecological niches of three teuthophageous odontocetes in the northwestern Mediterranean Sea, *Ocean Science*, 4(1), 49–59.
- Praca, E., A. Gannier, K. Das, and S. Laran (2009), Modelling the habitat suitability of cetaceans: example of the sperm whale in the northwestern Mediterranean Sea, *Deep Sea Research Part I: Oceanographic Research Papers*, 56(4), 648–657.
- Quijano, J. E., S. E. Dosso, J. Dettmer, L. M. Zurk, M. Siderius, and C. H. Harrison (2012), Bayesian geoacoustic inversion using wind-driven ambient noise, *The Journal of the Acoustical Society of America*, 131(4), 2658–2667.
- R Core Team (2019), R: A Language and Environment for Statistical Computing. R Foundation for Statistical Computing. Vienna.
- Radford, C. A., A. Jeffs, C. Tindle, and J. C. Montgomery (2008a), Resonating sea urchin skeletons create coastal choruses, *Marine Ecology Progress Series*, 362, 37–43.
- Radford, C. A., A. G. Jeffs, C. T. Tindle, and J. C. Montgomery (2008b), Temporal patterns in ambient noise of biological origin from a shallow water temperate reef, *Oecologia*, 156(4), 921–929.
- Rainaud, R., C. Lebeau-pin Brossier, V. Ducrocq, H. Giordani, M. Nuret, N. Fourrié, M. N. Bouin, I. Taupier-Letage, and D. Legain (2016), Characterization of air-sea exchanges over the Western Mediterranean Sea during HyMeX SOP1 using the AROMEWMED model, *Quarterly Journal of the Royal Meteorological Society*, 142(August), 173–187.
- Relini, G., M. Relini, and M. Montanari (2000), An offshore buoy as a small artificial island and a fish-aggregating device (FAD) in the Mediterranean, *Hydrobiologia*, 440, 65–80.
- Rendell, L. E., and A. Frantzis (2016), Chapter two - Mediterranean Sperm Whales, *Physeter macrocephalus: The Precarious State of a Lost Tribe*, *Advances in Marine Biology*, 75, 37–74.
- Ricks, R., D. Grimmett, and C. Wakayama (2012), Passive acoustic tracking for cueing a multistatic active acoustic tracking system, in: *Program Book - OCEANS 2012 MTS/IEEE Yeosu: The Living Ocean and Coast - Diversity of Resources and Sustainable Activities*, pp. 1–7, IEEE.
- Riesch, R., J. K. B. Ford, and F. Thomsen (2008), Whistle sequences in wild killer whales (*Orcinus orca*), *The Journal of the Acoustical Society of America*, 124(3), 1822–1829.
- Riser, S. C., J. A. Nystuen, and A. Rogers (2008), Monsoon effects in the Bay of Bengal inferred from profiling float-based measurements of wind speed and rainfall, *Limnology and Oceanography*, 53(5\_part\_2), 2080–2093.
- Roemmich, D., M. H. Alford, H. Claustre, K. S. Johnson, B. King, J. Moum, P. R. Oke, W. B. Owens, S. Pouliquen, S. Purkey, M. Scanderbeg, T. Suga, S. E. Wijffels, N. Zilberman, D. Bakker, M. O. Baringer, M. Belbeoch, H. C. Bittig, E. Boss, P. Calil, F. Carse, T. Carval, F. Chai, D. O. Conchubhair, F. D’Ortenzio, G. Dall’Olmo, D. Desbruyères, K. Fennel, I. Fer, R. Ferrari, G. Forget, H. Freeland, T. Fujiki, M. Gehlen,

- B. Greenan, R. Hallberg, T. Hibiya, S. Hosoda, S. Jayne, M. Jochum, G. C. Johnson, K. R. Kang, N. Kolodziejczyk, A. Koertzing, P. Y. Le Traon, Y. D. Lenn, G. Maze, K. A. Mork, T. Morris, T. Nagai, J. Nash, A. N. Garabato, A. Olsen, R. R. Pattabhi, S. Prakash, S. C. Riser, C. Schmechtig, E. Shroyer, A. Sterl, P. Sutton, L. Talley, T. Tanhua, V. Thierry, S. Thomalla, J. Toole, A. Troisi, T. Trull, J. D. Turton, P. J. Velez-Belchi, W. Walczowski, H. Wang, R. Wanninkhof, A. Waterhouse, A. Watson, C. Wilson, A. P. Wong, J. Xu, and I. Yasuda (2019), On the future of Argo: A global, full-depth, multi-disciplinary array, *Frontiers in Marine Science*, 6(JUL), 1–28.
- Rossong, M. A., and J. M. Terhune (2009), Source levels and communication-range models for harp seal (*Pagophilus groenlandicus*) underwater calls in the gulf of St. Lawrence, Canada, *Canadian Journal of Zoology*, 87(7), 609–617.
- Rudnick, D. L. (2016), Ocean Research Enabled by Underwater Gliders, *Annual Review of Marine Science*, 8(1), 519–541.
- Rudnick, D. L., R. E. Davis, C. C. Eriksen, D. M. Fratantoni, and M. J. Perry (2004), Underwater Gliders for Ocean Research, *Marine Technology Society Journal*, 38(2), 73–84.
- Salon, S., A. Crise, P. Picco, E. de Marinis, and O. Gasparini (2003), Sound speed in the Mediterranean Sea: An analysis from a climatological data set, *Annales Geophysicae*, 21(3), 833–846.
- Samaran, F., O. Adam, and C. Guinet (2010), Detection range modeling of blue whale calls in Southwestern Indian Ocean, *Applied Acoustics*, 71(11), 1099–1106.
- Schmidt, K. M., S. Swart, C. Reason, and S. Nicholson (2017), Evaluation of satellite and reanalysis wind products with in situ Wave Glider wind observations in the Southern Ocean, *Journal of Atmospheric and Oceanic Technology*, pp. JTECH–D–17–0079.1.
- Shaw, P. T., D. R. Watts, and H. T. Rossby (1978), On the estimation of oceanic wind speed and stress from ambient noise measurements, *Deep-Sea Research*, 25(12), 1225–1233.
- Simmonds, M. P., S. J. Dolman, M. Jasny, E. C. Parsons, L. Weilgart, A. J. Wright, and R. Leaper (2014), Marine noise pollution - increasing recognition but need for more practical action, *Journal of Ocean Technology*, 9(1), 71–90.
- Širović, A., J. A. Hildebrand, S. M. Wiggins, M. A. McDonald, S. E. Moore, and D. Thiele (2004), Seasonality of blue and fin whale calls and the influence of sea ice in the Western Antarctic Peninsula, *Deep-Sea Research Part II: Topical Studies in Oceanography*, 51(17-19), 2327–2344.
- Soria, M., L. Dagorn, G. Potin, and P. Fréon (2009), First field-based experiment supporting the meeting point hypothesis for schooling in pelagic fish, *Animal Behaviour*, 78(6), 1441–1446.
- Stafford, K. M., C. G. Fox, and D. S. Clark (1998), Long-range acoustic detection and localization of blue whale calls in the northeast Pacific Ocean, *The Journal of the Acoustical Society of America*, 104(6), 3616–3625.
- Stafford, K. M., D. K. Mellinger, S. E. Moore, and C. G. Fox (2007), Seasonal variability and detection range modeling of baleen whale calls in the Gulf of Alaska, 19992002, *The Journal of the Acoustical Society of America*, 122(6), 3378–3390.

- Stanistreet, J. E., D. P. Nowacek, J. T. Bell, D. M. Cholewiak, J. A. Hildebrand, L. E. W. Hodge, S. M. Van Parijs, and A. J. Read (2018), Spatial and seasonal patterns in acoustic detections of sperm whales *Physeter macrocephalus* along the continental slope in the western North Atlantic Ocean, *ENDANGERED SPECIES RESEARCH*, 35, 1–13.
- Sukhovich, A., S. Bonnieux, Y. Hello, J. O. Irisson, F. J. Simons, and G. Nolet (2015), Seismic monitoring in the oceans by autonomous floats, *Nature Communications*, 6, 1–6.
- Tesei, A., R. Been, D. Williams, B. Cardeira, D. Galletti, D. Cecchi, B. Garau, and A. Marguer (2015), Passive acoustic surveillance of surface vessels using tridimensional array on an underwater glider, in: *OCEANS 2015 - Genova*, pp. 1–8, IEEE.
- Testor, P., A. Bosse, L. Houpert, F. Margirier, L. Mortier, H. Legoff, D. Dausse, M. Labaste, J. Karstensen, D. Hayes, A. Olita, A. Ribotti, K. Schroeder, J. Chiggiato, R. Onken, E. Heslop, B. Mourre, F. D'ortenzio, N. Mayot, H. Lavigne, O. de Fommervault, L. Coppola, L. Prieur, V. Taillandier, X. Durrieu de Madron, F. Bourrin, G. Many, P. Damien, C. Estournel, P. Marsaleix, I. Taupier-Letage, P. Raimbault, R. Waldman, M.-N. Bouin, H. Giordani, G. Caniaux, S. Somot, V. Ducrocq, and P. Conan (2018), Multiscale Observations of Deep Convection in the Northwestern Mediterranean Sea During Winter 2012-2013 Using Multiple Platforms, *Journal of Geophysical Research: Oceans*, 123(3), 1745–1776.
- Testor, P., G. Meyers, C. B. Pattiaratchi, R. Bachmeyer, D. Hayes, S. Pouliquen, L. Petit de la Villeon, T. Carval, A. Ganachaud, L. Gourdeau, L. Mortier, H. Claustre, V. Taillandier, P. Lherminier, T. Terre, M. Visbeck, J. Kartensen, G. Krahmman, A. Alvarez, M. Rixen, P. M. Poulain, S. Osterhus, J. Tintore, S. Ruiz, B. Garau, D. Smeed, G. Griffiths, L. Merckelbach, T. Sherwin, C. Schmid, J. A. Barth, O. Schofield, S. M. Glenn, J. T. Kohut, M. J. Perry, C. C. Eriksen, U. Send, R. W. E. Davis, D. L. Rudnick, J. Sherman, C. Jones, D. C. Webb, C. M. Lee, and B. Owens (2010), Gliders as a Component of Future Observing Systems, in: *Proceedings of OceanObs'09: Sustained Ocean Observations and Information for Society*, 1, pp. 961–978, European Space Agency.
- Testor, P., V. Turpin, B. DeYoung, D. L. Rudnick, S. Glenn, J. Kohut, T. Miles, G. Saba, D. Hayes, C. Lee, B. Curry, L. Rainville, C. B. Pattiaratchi, K. L. Hill, E. Heslop, C. Toro, P. Alenius, C. Barrera, J. Barth, N. Beaird, R. E. Todd, G. Becu, E. Rehm, A. Bosse, I. Fer, P. Haugan, F. Bourrin, A. Brearley, S. Fielding, M. P. Meredith, H. Venables, Y. Chao, S. Chen, R. Crout, J. Cummings, P. Hogan, J. Chiggiato, K. Schroeder, L. Coppola, R. Curry, R. Davis, K. Desai, N. Rome, S. DiMarco, C. Edwards, E. Frajka-Williams, S. Hanson, M. Palmer, D. Smeed, H. Gildor, G. Goni, D. P. Snowden, D. Gutierrez, D. Hebert, T. Ross, J. Heiderich, K. J. Heywood, J. Kaiser, B. Y. Queste, L. Houpert, M. E. Inall, S. Huh, M. Ishii, S. ichi Ito, S. Itoh, S. Jan, J. Karstensen, G. Krahmman, B. Kirkpatrick, J. Klymak, M. Krug, S. Nicholson, S. McClatchie, F. Marin, E. Mauri, A. Mehra, J. Morell, L. Mortier, J. O'Callaghan, D. O'Conchubhair, P. R. Oke, E. P. Sanz, M. Tenreiro, J. J. Park, Y. Song, L. Perivoliotis, P. M. Poulain, R. Perry, M. Roughan, A. Schaeffer, S. Ruiz, M. Schonau, Y. Shimizu, B. M. Sloyan, S. Swart, A. F. Thompson, J. Tintore, S. Waterman, R. Watlington, and D. Wilson (2019), OceanGliders: A component of the integrated GOOS, *Frontiers in Marine Science*, 6(JUL), 1–32.
- Thode, A. (2004), Tracking sperm whale (*Physeter macrocephalus*) dive profiles using a towed passive acoustic array, *The Journal of the Acoustical Society of America*, 116(1), 245–253.

- Thompson, P. M., G. D. Hastie, J. Nedwell, R. Barham, K. L. Brookes, L. S. Cordes, H. Bailey, and N. Mclean (2013), Framework for assessing impacts of pile-driving noise from offshore wind farm construction on a harbour seal population, *Environmental Impact Assessment Review*, 43, 73–85.
- Tyack, P. L. (2008), Large-Scale Changes in the Marine Acoustic Environment, *Journal of Mammalogy*, 89(3), 549–558.
- Urick, R. J., and W. A. Kuperman (1989), Ambient Noise in the Sea, *The Journal of the Acoustical Society of America*, 86(4), 1626–1626.
- Vagle, S., W. G. Large, and D. M. Farmer (1990), An Evaluation of the WOTAN Technique of Inferring Oceanic Winds from Underwater Ambient Sound, *Journal of Atmospheric and Oceanic Technology*, 7(4), 576–595.
- Vakkayil, R., H. Graber, and W. Large (1996), Oceanic winds estimated from underwater ambient noise observations in SWADE, *OCEANS 96 MTS/IEEE Conference Proceedings. The Coastal Ocean - Prospects for the 21st Century*, 1, 45–51.
- Van der Graaf, A. J., M. A. Ainslie, M. André, K. Brensing, J. Dalen, R. P. A. Dekeling, S. Robinson, M. L. Tasker, F. Thomsen, and S. Werner (2012), *European Marine Strategy Framework Directive Good Environmental Status (MSFD-GES)*, Tech. rep., Technical Subgroup on Underwater noise and other forms of energy.
- Van Parijs, S. M., C. W. Clark, R. S. Sousa-Lima, S. E. Parks, S. Rankin, D. Risch, and I. C. Van Opzeeland (2009), Management and research applications of real-time and archival passive acoustic sensors over varying temporal and spatial scales, *Marine Ecology Progress Series*, 395, 21–36.
- Verfuss, U. K., A. S. Aniceto, D. V. Harris, D. Gillespie, S. Fielding, G. Jiménez, P. Johnston, R. R. Sinclair, A. Sivertsen, S. A. Solbø, R. Størvold, M. Biuw, and R. Wyatt (2019), A review of unmanned vehicles for the detection and monitoring of marine fauna, *Marine Pollution Bulletin*, 140(February 2018), 17–29.
- Virgili, A., M. Authier, O. Boisseau, A. Cañadas, D. Claridge, T. Cole, P. Corkeron, G. Dorémus, L. David, N. Di-Méglio, C. Dunn, T. E. Dunn, I. García-Barón, S. Laran, G. Lauriano, M. Lewis, M. Louzao, L. Mannocci, J. Martínez-Cedeira, D. Palka, S. Panigada, E. Pettex, J. J. Roberts, L. Ruiz, C. Saavedra, M. B. Santos, O. Van Canneyt, J. A. Vázquez Bonales, P. Monestiez, and V. Ridoux (2019), Combining multiple visual surveys to model the habitat of deep-diving cetaceans at the basin scale, *Global Ecology and Biogeography*, 28(3), 300–314.
- Visbeck, M. (2002), Deep velocity profiling using lowered acoustic Doppler current profilers: Bottom track and inverse solutions, *Journal of Atmospheric and Oceanic Technology*, 19(5), 794–807.
- Wahlberg, M. (2002), The acoustic behaviour of diving sperm whales observed with a hydrophone array, *Journal of Experimental Marine Biology and Ecology*, 281(1-2), 53–62.
- Wall, C., C. Lembke, and D. Mann (2012), Shelf-scale mapping of sound production by fishes in the eastern Gulf of Mexico, using autonomous glider technology, *Marine Ecology Progress Series*, 449, 55–64.

- Wall, C. C., D. A. Mann, C. Lembke, C. Taylor, R. He, and T. Kellison (2017), Mapping the Soundscape Off the Southeastern USA by Using Passive Acoustic Glider Technology, *Marine and Coastal Fisheries*, 9(1), 23–37.
- Wall, C. C., R. A. Rountree, C. Pomerleau, and F. Juanes (2014), Deep-Sea Research I An exploration for deep-sea fish sounds off Vancouver Island from the NEPTUNE Canada ocean observing system, *Deep-Sea Research Part I*, 83, 57–64.
- Wanninkhof, R. (2014), Relationship between wind speed and gas exchange over the ocean revisited, *Limnology and Oceanography: Methods*, 12(6), 351–362.
- Watkins, W. A., M. A. Daher, G. M. Reppucci, J. E. George, D. L. Martin, N. A. Di-Marzio, and D. P. Gannon (2000), Seasonality and distribution of whale calls in the North Pacific, *Oceanography*, 13(SPL.ISS. 1), 62–67.
- Watts, D. G., and D. W. Bacon (1974), Using an hyperbola as a transition model to fit two-regime straight-line data, *Technometrics*, 16(3), 369–373.
- Watwood, S. L., P. J. O. MILLER, M. JOHNSON, P. T. MADSEN, and P. L. TYACK (2006), Deep-diving foraging behaviour of sperm whales (*Physeter macrocephalus*), *Journal of Animal Ecology*, 75(3), 814–825.
- Weilgart, L. S. (2007), The impacts of anthropogenic ocean noise on cetaceans and implications for management, *Canadian Journal of Zoology*, 85(11), 1091–1116.
- Weilgart, L. S., and H. Whitehead (1988), Distinctive vocalizations from mature male sperm whales (*Physeter macrocephalus*), *Canadian Journal of Zoology*, 66(9), 1931–1937.
- Weilgart, L. S., and H. Whitehead (1990), Vocalizations of the North Atlantic pilot whale (*Globicephala melas*) as related to behavioral contexts, *Behavioral Ecology and Sociobiology*, 26(6), 399–402.
- Weilgart, L. S., and H. Whitehead (1993), Coda communication by sperm whales (*Physeter macrocephalus*) off the Galapagos Islands, *Canadian Journal of Zoology*, 71(4), 744–752.
- Weir, C. R. (2008), Overt responses of humpback whales (*Megaptera novaeangliae*), sperm whales (*Physeter macrocephalus*), and Atlantic spotted dolphins (*Stenella frontalis*) to seismic exploration off Angola, *Aquatic Mammals*, 34(1), 71.
- Weller, R., A., E. Bradley, J. Edson, C. Fairall, I. Brooks, M. Yelland, and R. Pascal (2008), Sensors for physical fluxes at the sea surface: energy, heat, water, salt, *Ocean Science*, 4(4), 247–263.
- Wenz, G. M. (1962), Acoustic Ambient Noise in the Ocean: Spectra and Sources, *The Journal of the Acoustical Society of America*, 34(12), 1936–1956.
- Whitehead, H. (2003), *Sperm whales: social evolution in the ocean*, University of Chicago press.
- Wiggins, S. M., M. A. McDonald, and J. A. Hildebrand (2012), Beaked whale and dolphin tracking using a multichannel autonomous acoustic recorder, *The Journal of the Acoustical Society of America*, 131(1), 156–163.

- Williams, R., A. J. Wright, E. Ashe, L. K. Blight, R. Bruintjes, R. Canessa, C. W. Clark, S. Cullis-Suzuki, D. T. Dakin, C. Erbe, P. S. Hammond, N. D. Merchant, P. D. O'Hara, J. Purser, A. N. Radford, S. D. Simpson, L. Thomas, and M. A. Wale (2015), Impacts of anthropogenic noise on marine life: Publication patterns, new discoveries, and future directions in research and management, *Ocean and Coastal Management*, 115, 17–24.
- Zhang, H. M., J. J. Bates, and R. W. Reynolds (2006), Assessment of composite global sampling: Sea surface wind speed, *Geophysical Research Letters*, 33(17), 1–5.
- Zimmer, W. M. X., P. L. Tyack, M. P. Johnson, and P. T. Madsen (2005), Three-dimensional beam pattern of regular sperm whale clicks confirms bent-horn hypothesis, *The Journal of the Acoustical Society of America*, 117(3), 1473–1485.